SHORT ANTENNA WITH ENHANCED RADIATION OR IMPROVED DIRECTIVITY

Ву

Chun-Ju Lin

AN ABSTRACT OF A THESIS

Submitted to
Michigan State University
in partial fulfillment of the requirements
for the degree of

DOCTOR OF PHILOSOPHY

Department of Electrical Engineering

1969

ABSTRACT

SHORT ANTENNA WITH ENHANCED RADIATION OR IMPROVED DIRECTIVITY

Ву

Chun-Ju Lin

A conventional electrically short, linear antenna has small radiated power and low directivity. Consequently, its practical applications are severely restricted. The purpose of this research is to investigate the feasibility of enhancing the radiated power or improving the directivity of a short antenna by a double impedance loading technique. This technique consists of mounting the appropriately chosen lumped impedances symmetrically along the antenna surface to implement a modification of its current distribution. The current is adjusted in such a way to achieve either enhancement of its radiated power or an improvement in the directivity of the short antenna.

In the theoretical study, King's modified method is applied to develop an approximate solution for the current distribution along the doubly loaded short antenna. From this solution, input impedances and typical current distributions of antennas loaded to obtain either enhanced radiation or improved directivity are determined. An expression for the optimum loading impedance to achieve improved directivity is established. For the enhanced radiation case, the area under the current distribution along the

antenna with optimum loading can be increased by a factor of four relative to than that of an unloaded antenna, and its input impedance has a significantly increased resistive component and a zero reactive component. Therefore, the radiated power is greatly enhanced compared with that of the unloaded antenna. For the improved directivity case, the current distribution has a phase reversal along the antenna and the directivity corresponding to such a current is improved significantly. In addition to the doubly loaded isolated antenna, an array of doubly loaded coupled antennas is also studied, the objective again being to achieve enhanced radiation or improved directivity.

An experimental study on the doubly loaded antennas, for both the enhanced radiation and improved directivity conditions, is conducted to verify the theoretical results. Enhanced radiation from a coupled short antenna is also investigated experimentally. It is shown that the experimental results are in good agreement with those of the theoretical predictions. In addition to the doubly loaded antennas, the characteristics of top-loaded antennas are also investigated experimentally for various types and sizes of end loadings.

SHORT ANTENNA WITH ENHANCED RADIATION OR IMPROVED DIRECTIVITY

Ву

Chun-Ju Lin

A THESIS

Submitted to
Michigan State University
in partial fulfillment of the requirements
for the degree of

DOCTOR OF PHILOSOPHY

Department of Electrical Engineering

1969

Copyright by

CHUN-JU LIN

1969

ACKNOWLEDGMENTS

The author wishes to express his sincere appreciation to his major professor, Dr. K.M. Chen, for his guidance and encouragement in the course of this research and for the inspiration he has given throughout the entire stage of the author's college education.

He also wishes to thank the committee member Dr. D.P. Nyquist for correcting the manuscript and giving valuable suggestions in the experimental part of this research, and to the other members, Dr. H.G. Hedges, Dr. Bong Ho and Dr. R. Hamelink, for reading the thesis.

Finally, the author wishes to express a special thanks to his wife, Lee-Whei, for the encouragement and understanding that only a wife can give.

The research reported in this thesis was supported by the Air Force Cambridge Research Laboratories under contract AF 19(628)-5732.

TABLE OF CONTENTS

			Page
	ACKN	OWLEDGMENTS	ii
	LIST	OF TABLES	v
	LIST	OF FIGURES	vi
1.	INTR	ODUCTION	1
2.	CURRI	ENT DISTRIBUTION ON A DOUBLY LOADED SHORT ANTENNA	4
	2.1 2.2	Geometry of the Doubly Loaded Short Antenna Boundary Conditions for Calculating the Antenna	4
	0 0	Current	6
	2.3	Integral Equation for the Antenna Current	7 12
	2.5	Input Impedance of Doubly Loaded Short Antenna	16
3.	SHOR	T ANTENNA WITH ENHANCED RADIATION	21
	3 1	Introduction	21
	3.2	Radiated Power and Radiation Resistance	22
	3.3	Doubly Loaded Short Antenna with Increased Input	0.5
		Resistance and Zero Input Reactance	25 25
		3.3.2 Input Impedance, Radiation Resistance, and	
		Optimum Loading Impedance	26
		Antenna	31
		3.3.4 Radiation Pattern	37
	3.4	Loaded Short Antenna with Increased Input Resistance	
		and Inductive Input Reactance	38
		3.4.1 Typical Current Distribution	38
		3.4.2 Input Impedance	39
	2 -	3.4.3 Radiated Power	39
	3.5	Conventional Top-Loaded (End-Loaded) Antenna	42
	3.6	Comparison of Doubly Loaded Antenna with Unloaded Base-Tuned Antenna for Radiated Power and Efficiency	42
	3.7	Bandwidth of Short Antenna with Enhanced Radiation	44
4.	SHOR	T ANTENNAS WITH IMPROVED DIRECTIVITY	50
	4.1	Introduction	50
	4.2	Radiation Field of a Short Antenna with Improved	5 1

			Page
	4.3 4.4	Optimum Loading Impedance for Improved Directivity Typical Current Distribution on Antenna with	61
	4.5	Optimum Loading	64
	4.6	Directivity	67
	,,,	Loading	73
5.	DOUBI	LY LOADED COUPLED SHORT ANTENNAS	75
	5.1 5.2	Geometry of the Doubly Loaded Short Array Boundary Conditions for Calculating the Antenna	75
		Current Distributions	78
	5.3	Integral Equations for Antenna Current Distributions	78
	5.4	Approximate Solutions for the Antenna Currents	84
	5.5	Input Impedance of the Antenna Coupled with a Doubly	
		Loaded Parasitic Element	96
	5.6	Radiation From Coupled Short Antenna	96
	5.7	Enhancement of Radiated Power	99
	5.8	Improved Directivity	105
	5.9	Discussion	108
6.	EXPE	RIMENTAL STUDY OF SHORT ANTENNA WITH HIGH DIRECTIVITY	
		NHANCED RADIATION	109
	6.1	Experimental Setup	109
	6.2	Doubly Loaded Short Antenna	115
		6.2.1 Enhanced Radiation Case	115
		6.2.2 Improved Directivity Case	118
	6.3	End-Loaded Short Antennas	121
		6.3.1 Current Distributions on the Antenna	121
		6.3.2 Input Impedances	128
	6.4	Short Antenna with Double Impedance and End Loadings	131
		6.4.1 Current Distribution	131
		6.4.2 Input Impedance	
	6.5	Doubly Loaded Coupled Antennas	
		P.T. VOTO	1/0

LIST OF TABLES

Table		Page
3.1	Input Impedance and Radiation Resistance of Short Antenna Doubly Loaded by Reactances X of Various Q. V = 1 volt, f = 200 MHz, a/λ = 0.00212, d/h = 0.7, h/λ_0 = 0.05, X = 145 Ω	32
3.2	Input Impedance and Radiation Resistance of Short Antenna Doubly Loaded by Reactances X of Various Q. V = 1 volt, f = 200 MHz, $a/\lambda_0 = 0.00212\lambda$, $d/h = 0.7$, $h/\lambda_0 = 0.075$, $X_L = 1080 \Omega$	33
3.3	Input Impedance and Radiation Resistance of Short Antenna Doubly Loaded by Reactances X, of Various Q. V = 1 volt, f = 200 MHz, a/λ = 0.00712 λ 0, d/h = 0.7, h/λ 0 = 0.1, XL = 850 Ω	34
5.1	Input Impedances of Driven Antenna Coupled with Loaded Parasitic Element and Phase Difference Between $I_{1z}(z)$ and $I_{2z}(z)$	106
6.1	Input Impedances of a Short Antenna End-Loaded with Rectangular Bars of Various Sizes (L(cm) x ½" x 1 mm thick)	129
6.2	Input Impedances of a Short Antenna End-Loaded with Cylindrical Bars of Various Sizes ();" in diameter)	129
6.3	Input Impedances of a Short Antenna End-Loaded with Circular Plates (1 mm thick) of Various Diameters	130
6.4	Input Impedances of a Short Antenna End Loaded with Helixes of Various Lengths (D = $3/4$ ")	130
6.5	Input Impedances of a Short Antenna End-Loaded with Helixes of Various Diameters (L = 37.5 cm)	130

LIST OF FIGURES

Figure		Page
2.1	The Doubly Loaded Short Antenna	5
3.1	Typical Current Distribution along Antenna with Optimum Reactance Loading to make $X_{in} = 0 \dots$	26
3.2	Theoretical Antenna Current Distribution Corresponding to Enhanced Radiation Condition Compared with that of Other Loadings (h = $0.1\lambda_0$, d = $0.5h$)	27
3.3	Theoretical Antenna Current Distribution Corresponding to Enhanced Radiation Condition Compared with that of Other Loadings (h = $0.1\lambda_0$, d = $0.7h$)	28
3.4	Theoretical Antenna Current Distribution Corresponding to Enhanced Radiation Condition Compared with that of Other Loadings (h = $0.1\lambda_0$, d = $0.9h$)	29
3.5	Theoretical Antenna Input Impedances for Zero and Optimum (enhancement) Reactive Loadings at Fixed Positions as Functions of Antenna Length	30
3.6	Theoretical Optimum Loading Reactance for Enhanced Radiation for Antennas of Various Lengths as a Function of Loading Position (h = $0.025\lambda_0 \sim 0.1\lambda_0$)	3 5
3.7	Theoretical Optimum Loading Reactance for Enhanced Radiation for Antennas of Various Lengths as a Function of Loading Position (h = $0.125\lambda_0 \sim 0.2\lambda_0$)	36
3.8	Radiation Pattern of the Short Antenna with Optimum Reactance Loading	37
3.9	Current Distribution along Antenna with Increased Input Resistance and Inductive Input Reactance	38
3.10	The Current Distributions on an Antenna with Increased Input Resistance and Input Inductive Reactance for Various Loading Reactances	40
3.11	Efficiencies of Optimum Reactively Loaded and Base- Tuned Antennas as Functions of Inductor Q	45

Fig

3

3

.

.

Figure		Page
3.12	The Ratio of Powers Radiated by Optimumly Loaded Antenna and Base-Tuned Antenna as a Function of Inductor Q	46
3.13	Theoretical Optimum Loading Reactance for Enhanced Radiation Compared with the Loading Reactance of a Fixed Inductor (L = 0.676µ henry)	47
3.14	Theoretical Input Impedances for Zero and Reactive Loading ($L = 0.676\mu$ henry) as Functions of Frequency	49
4.1	Theoretical Radiation Patterns of Short Antennas with K = 0, 1, and 2	54
4.2	Theoretical Radiation Patterns of Short Antennas with K = 2.33 and 3	55
4.3	Theoretical Radiation Patterns of Short Antennas with K = 10 and 46	56
4.4	Theoretical Radiation Pattern of Short Antennas with $K \rightarrow \infty$	57
4.5	Theoretical Optimum Loading Reactance for Improved Directivity (h = $0.025\lambda_0 \sim 0.1\lambda_0$)	65
4.6	Theoretical Optimum Loading Reactance for Improved Directivity (h = $0.125\lambda_0 \sim 0.2\lambda_0$)	66
4.7	Current Distribution on an Antenna with Optimum Loading for Improved Directivity	67
4.8	Theoretical Antenna Current Distribution Corresponding to Improved Directivity Condition Compared with that of Other Loadings (h = $0.1\lambda_0$, d = $0.5h$)	68
4.9	Theoretical Antenna Current Distribution Corresponding to Improved Directivity Condition Compared with that of Other Loadings (h = $0.1\lambda_0$, d = $0.7h$)	69
4.10	Theoretical Antenna Current Distribution Corresponding to Improved Directivity Condition Compared with that of Other Loadings (h = $0.1\lambda_0$, d = $0.9h$)	70
4.11	Theoretical Input Impedance for Zero and Optimum (Improved Directivity) Reactive Loadings with Various Loading Positions	71
4.12	Theoretical Input Resistance for Optimum Reactively Loaded Antennas with Various Loading Positions	72

Figure		Page
5.1	The Doubly Loaded Coupled Short Antennas	76
5.2	Geometry for Calculation of Radiation Field	97
5.3	Theoretical Current Distributions on Doubly Loaded Coupled Antennas Corresponding to Enhanced Radiation Condition Compared with that of Other Loadings (b = $0.01\lambda_0$)	101
5.4	Theoretical Current Distributions on Doubly Loaded Coupled Antennas Corresponding to Enhanced Radiation Condition Compared with that of Other Loadings (b = $0.03\lambda_0$)	102
5.5	Theoretical Current Distributions on Doubly Loaded Coupled Antennas Corresponding to Enhanced Radiation Condition Compared with that of Other Loadings (b = $0.05\lambda_0$)	103
5.6	Theoretical Current Distributions on Doubly Loaded Coupled Antennas Corresponding to Enhanced Radiation Condition Compared with that of Other Loadings (b = $0.08\lambda_0$)	104
5.7	Theoretical Radiation Patterns of Coupled Short Antennas with $K_1=0$, 1, 2 and ∞ , under Conditions of $K_1=K_2$ $K_3=1$ and $\alpha=\pi$ ($\phi=0$)	
6.1	Experimental Setup	110
6.2	The Inside View of Anechoic Chamber	111
6.3	The Outside View of Anechoic Chamber	111
6.4	Structure of Monopole Antenna	113
6.5	Structure of Current Probe	113
6.6	Experimental and Theoretical Reactance X_L as a Function of Loading Resistance R_L , $Q = \frac{1}{75}$	116
6.7	Experimental Antenna Current Distributions Corresponding to Enhanced Radiation Condition	117
6.8	Theoretical and Experimental Input Impedances of a Short Antenna as Functions of Loading Reactance X_L for the Cases of $Q = 100$ and $Q = \infty$	119

Figu

6.

6

6.

6

į

(

(

(

,

Figure		Page
6.9	Experimental Antenna Current Distributions Corresponding to Improved Directivity Condition	120
6.10	Various End Loadings	122
6.11	Experimental Current Distributions on an Antenna End-Loaded with Rectangular Bars of Various Sizes (L x ½" x 1 mm thick)	123
6.12	Experimental Current Distributions on an Antenna End-Loaded with Cylindrical Bars of Various Sizes (D = ½")	124
6.13	Experimental Current Distributions on an Antenna End-Loaded with Circular Plates of Various Diameters	125
6.14	Experimental Current Distributions on an Antenna with Helixes of Various Lengths (D = $3/4$ ")	126
6.15	Experimental Current Distributions on an Antenna End-Loaded with Helixes of Various Diameters (L = 37.5 cm)	127
6.16	Experimental Current Distributions on a Doubly Loaded Antenna End-Loaded by a Cylindrical Bar of 8 cm	132
6.17	Experimental Current Distributions on a Doubly Loaded Antenna End-Loaded by a Cylindrical Bar of 10 cm	133
6.18	Experimental Current Distributions on a Doubly Loaded Antenna End-Loaded by a Cylindrical Bar of 12 cm	134
6.19	Experimental Current Distributions on a Doubly Loaded Antenna End-Loaded by a Circular Plate of 8 cm diameter	135
6.20	Experimental Current Distributions on a Doubly Loaded Antenna End-Loaded by a Circular Plate of 10 cm diameter	136
6.21	Experimental Current Distributions on a Doubly Loaded Antenna End-Loaded by a Circular Plate of 12 cm diameter	137
6.22	Experimental Current Distribution on a Doubly Loaded Antenna End-Loaded by a Helix of 2.1 cm diameter	138

Figure		Page
6.23	Experimental Current Distribution on a Doubly Loaded Antenna End-Loaded by a Helix of 2.8 cm diameter	139
6.24	Experimental Current Distributions on Doubly Loaded Coupled Antennas	141

Sta

;à

a: be

> re ba

a

]

:

CHAPTER 1

INTRODUCTION

It is well known that a conventional short, linear antenna has small radiated power and low directivity. Therefore, much research has been conducted on improving the directivity or enhancing the radiated power of a short antenna.

By using an approximate superposition method, Harrison [1] determined the current distribution along a doubly reactance-loaded antenna. He demonstrated that a doubly loaded linear antenna might be tuned in such a manner that its input impedance becomes purely real and its efficiency is increased relative to that of an unloaded, base tuned antenna. In this thesis an improved method is employed to solve for the current distribution on a doubly loaded short antenna, and a more comprehensive investigation is carried out. It is indicated that the antenna doubly loaded by appropriately chosen impedances has a nearly uniform current distribution between the loading points and that its input impedance has an increased resistive component (by a factor of two to four relative to that of an unloaded antenna) and a reactive component which vanishes. The power radiated by the short antenna is therefore increased significantly.

In the improved directivity case, La Paz and Miller [2] first attempted to determine the maximum directivity theoretically available from a linear source antenna by solving for the

and De

corres

might

curre

[4]

for

rese

dire

curi

tri

tec

dev

for

će: ex

lo

c,

i

÷

P

â

•

1

corresponding optimum antenna current distribution. Later, Boukamp and De Bruijin [3] pointed out that arbitrarily high directivities might be achieved from a linear antenna by properly adjusting its current distribution. A similar conclusion was reached by Riblet [4]. Although no methods were suggested by the above investigators for implementing the required optimum current distributions, their researches imply that various degrees of improvement in the antenna directivity may be achieved by careful adjustment of the antenna current distribution. In this thesis, the optimum current distribution is implemented by utilizing a double impedance loading technique, and an expression for the optimum loading impedance is developed.

By applying King's modified method[5][6] an approximate solution for the current distribution along the doubly loaded antenna is developed in Chapter 2 in terms of the antenna dimensions, its excitation frequency, and the impedance and position of the double loading. The input impedance of antenna is also established in this chapter. Based on these solutions for the current distribution and input impedance, the optimum loadings for enhanced radiation and improved directivity are investigated and the numerical results are presented in Chapters 3 and 4. An extensive study of a doubly loaded array is conducted in Chapter 5 to investigate the characteristics of doubly loaded, coupled short antennas as related to the enhanced radiation and improved directivity.

An experimental study of the doubly loaded antennas (both for isolated and coupled antennas) is also performed in this research.

It is theor

anten

shape

thes

It is observed that the experimental results closely verify the theoretical prediction. In addition to the doubly impedance loaded antennas, short linear antenna end-loaded with various sizes and shapes of loading are also experimentally studied carefully in this thesis.

is ,

CHAPTER 2

CURRENT DISTRIBUTION ON A DOUBLY LOADED SHORT ANTENNA

2.1 Geometry of the Doubly Loaded Short Antenna:

The terminology short antenna refers to a linear antenna which is not physically small, but rather one which is electrically small as measured in wave lengths. A criterion for such an antenna may be defined by the inequality

$$h/\lambda_{o} = 2\pi h/\beta_{o} \le 0.1 \tag{2.1}$$

where β_0 is the free-space wave number and h is the half-length of the antenna.

The geometry of the short, doubly loaded, linear antenna is as indicated in Fig. 2.1. The short cylindrical antenna is assumed to be constructed of a perfect conductor of radius a and half-length h. An ideal, harmonic voltage source of angular frequency $\boldsymbol{\omega}$ and potential \boldsymbol{V}_0 excites the cylinder at its center z=0 (the antenna is assumed to lie along the z-axis of cylindrical coordinates), and the two identical lumped impedances \boldsymbol{Z}_L are loaded symmetrically on the antenna surface at z=d and z=-d. The gaps in the cylinder at the locations of the source and the loading impedances are assumed to be of length 2δ . Since both the source and the loading impedances are considered to be idealized point elements, then δ is assumed to approach zero in the subsequent mathematical analysis.

It is taken that the half-length h of the cylindrical antenna is very much greater than its radius a. As a result of this thin-wire

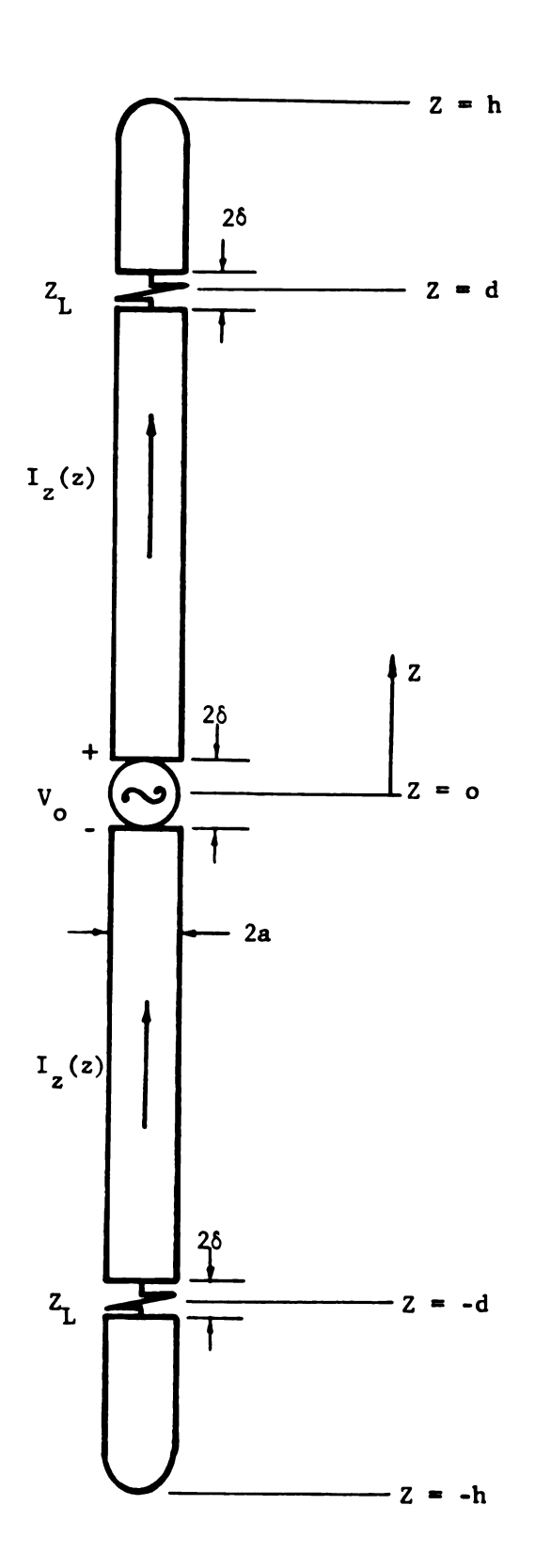


Fig. 2.1 The Doubly Loaded Short Antenna

assum

anter

(h > 2)

the tha

cen

2 .

ce

A

ê ;

assumption, and due to the rotational symmetry of the cylinder, the antenna current will flow primarily along the axial or z-direction.

The dimensional restrictions and axial current approximation of $\begin{cases} h >> a \\ \beta_0 << 1 & \text{(or } \frac{2\pi}{\lambda_0} \ a << 1) \\ \vec{I}(z) = \hat{z} I_z(z) & \dots & \text{axial antenna current} \end{cases}$

allow important simplification and lead to an approximate solution for the distribution of current along the antenna. It is well known [7] that subject to these restrictions $I_z(z)$ can be assumed to be concentrated along the axis of the cylinder when calculating the vector potential at its surface with negligible error.

2.2 Boundary Conditions for Calculating the Antenna Current:

The current excited on the cylinder is symmetric about its center (z=0) and must vanish at either of its extremities $(z=\pm h)$. A pair of boundary conditions on the antenna current may therefore be expressed as

$$\begin{cases} I_z(z) = I_z(-z) \\ I_z(+h) = 0 \end{cases}$$
 (2.2)

From the boundary condition that the tangential component of electric field should be continuous at the surface of the antenna, it follows

$$E_z^i(r = a^+) = E_z^a(r = a^-)$$
 (2.3)

where $E_z^i(r=a^+)$ is the induced electric field just outside of the surface of cylinder at $r=a^+$ which is maintained by the current and

charg side

2 3

a per

r = 6

wher elem

Эn

By t

I₂(.

As

âs

charge on the antenna, and $E_z^a(r=a^-)$ is the electric field just inside its surface at $r=a^-$.

2.3 Integral Equation for the Antenna Current:

Since the cylindrical antenna is assumed to be constructed of a perfect conductor, its internal impedance z^i per unit length is equal zero, and the electric field inside the conductor surface at $r = a^-$ is nonvanishing only at z = 0 and $z = \pm d$, i.e.

$$E_{\mathbf{z}}^{\mathbf{a}}(z) = \begin{cases} \frac{\mathbf{Z}_{\mathbf{L}}\mathbf{I}_{\mathbf{z}}(d)}{2\delta} & \text{for } -d-\delta < \mathbf{z} < -d+\delta \\ \frac{\mathbf{V}_{\mathbf{c}}}{2\delta} & \text{for } -\delta < \mathbf{z} < \delta \\ \frac{\mathbf{Z}_{\mathbf{L}}\mathbf{I}_{\mathbf{z}}(d)}{2\delta} & \text{for } d-\delta < \mathbf{z} < d+\delta \end{cases}$$
(2.4)

where $I_z(d)$ and $I_z(-d)$ are the antenna currents at the impedance elements at $z=\pm d$, and $E_z^a(z)$ is equal to zero for every other point on $-h \le z \le h$. The total voltage drop along the antenna is therefore

$$-\int_{-h}^{h} E_{z}^{a}(z) dz = V_{o} - I_{z}(d) Z_{L} - I_{z}(-d) Z_{L}.$$

By the symmetry condition of the antenna current, eq. (2.2), $I_z(-d) = I_z(d)$, and the last result may be expressed as

$$-\int_{-h}^{h} E_{z}^{a}(z) dz = V_{0} - 2I_{z}(d) Z_{L}.$$

As indicated earlier, the loading impedances and source are considered as point elements of length $2\delta \rightarrow 0$, such that

$$\lim_{2\delta \to 0} -\int_{-h}^{h} E_{z}^{a}(z) dz = V_{0} - I_{z}(d) Z_{L} - I_{z}(-d) Z_{L}$$
 (2.5)

By t

and

wher

give

For

acco

Wher

tain Pote:

antei

cyli

Sinc

one

By the properties of the Dirac delta function and by equations (2.4) and (2.5), then in the limit when $2\delta \rightarrow 0$

$$E_z^a(z) = -V_0 \delta(z) + I_z(d) Z_L [\delta(z-d) + \delta(z+d)]$$
 (2.6)

where $\delta(z)$ is the Dirac delta function.

The induced field just outside the surface of the antenna is given by

$$E_z^{i}(z) = (-\nabla \phi)_z - (\frac{\partial \vec{A}}{\partial t})_z.$$

For the case of a time-harmonic excitation where all quantities vary accordingly to the implied time-dependence factor $e^{j\omega t}$, then

$$E_{z}^{i}(z) = -(\nabla \phi)_{z} - j\omega A_{z}$$
 (2.7)

where ϕ is the scalar potential at the surface of the cylinder maintained by the charge on the antenna, and $\vec{A} = \hat{z} A_z(z)$ is the vector potential at the cylinder surface maintained by the current in the antenna (it is assumed that the current is concentrated along the cylinder axis).

The Lorentz condition may be applied to relate ϕ and \vec{A} as

$$\nabla \vec{A} + j \frac{\beta_0^2}{\omega} \phi = 0.$$

Since $\vec{I}(z) = \hat{z} I_z(z)$ axially directed, then $\vec{A} = \hat{z} A_z(z)$ has only one component $A_z(z)$ and the Lorentz condition becomes

$$\frac{\partial^{A}_{z}}{\partial z} + j \frac{\beta^{2}_{o}}{\omega} \phi = 0 . \qquad (2.8)$$

: P

C.

Substituting ϕ in terms of A_z , according to eq. (2.8), into eq. (2.7) results in

$$E_z^i(z) = -\frac{j\omega}{\beta_0^2} \left[\frac{\partial^2}{\partial z^2} + \beta_0^2 \right] A_z(z) . \qquad (2.9)$$

In order to satisfy boundary condition eq. (2.3)

$$E_z^i(r = a^+) = E_z^a(r = a^-)$$
 (2.3)

expressions eq. (2.6) and eq. (2.9) are equated to yield a secondorder inhomogeneous differential equation for the vector potential at the antenna surface as

$$\left[\frac{3^{2}}{3z^{2}} + \beta_{o}^{2}\right] A_{z}(z) = \frac{j\beta_{o}^{2}}{w} \left\{-V_{o}\delta(z) + Z_{L}I_{z}(d)\left[\delta(z-d) + \delta(z+d)\right]\right\}. \tag{2.10}$$

The complementary solution of eq. (2.10) is obtained easily as

$$A_z^c(z) = -\frac{j}{v_0} (C_1 \cos \beta_0 z + C_2 \sin \beta_0 z)$$
 (2.11)

where \mathbf{v}_{o} is the velocity of light and \mathbf{C}_{1} and \mathbf{C}_{2} are arbitrary constants.

Since the particular integral for an equation of the form

$$\frac{d^2y}{dx} + a^2y = f(x)$$

is given by $y^p(x) = \frac{1}{a} \int_0^x f(s) \sin a(x-s) ds$ then eq. (2.10) has a particular solution of the form

$$A_z^p(z) = C_4 \sin\beta_0 |z| + C_5 \sin\beta_0 |z-d| + C_6 \sin\beta_0 |z+d|.$$

Substituting this directly into eq. (2.10), the arbitrary constants C_4 , C_5 and C_6 are determined and $A_z^p(z)$ is obtained as

3)

t.

ŝ.

ā.

Зу

is

tia

$$A_z^p(z) = -\frac{j}{v_o} \left[\frac{v_o}{2} \operatorname{Sin\beta}_o |z| - \frac{z_L I_z(d)}{2} (\operatorname{Sin\beta}_o |z-d| + \operatorname{Sin\beta}_o |z+d|) \right].$$

The general solution to differential equation (2.10) is thus

$$A_{z}(z) = A_{z}^{c}(z) + A_{z}^{p}(z)$$

$$= -\frac{j}{v_{o}} \left[c_{1} \cos \beta_{o} z + c_{2} \sin \beta_{o} z + \frac{v_{o}}{2} \sin \beta_{o} |z| \right]$$

$$-\frac{z_{L}^{I} z^{(d)}}{2} \left(\sin \beta_{o} |z-d| + \sin \beta_{o} |z+d| \right) \right]. \qquad (2.12)$$

By the symmetry of the antenna current, $I_z(z) = I_z(-z)$, it can be shown that the vector potential is also symmetric about the center of the cylinder, i.e., $A_z(-z) = A_z(z)$. It is therefore obvious that arbitrary constant C_2 should be equal to zero, and eq. (2.12) becomes

$$A_{z}(z) = -\frac{1}{v_{o}} \left[C_{1} \cos \beta_{o} z + \frac{v_{o}}{2} \sin \beta_{o} |z| - \frac{z_{L} I_{z}(d)}{2} (\sin \beta_{o} |z-d| + \sin \beta_{o} |z+d|) \right]. \tag{2.13}$$

At z = h, result (2.13) becomes

$$A_{z}(h) = -\frac{i}{v_{o}} \{C_{1}Cos\beta_{o}h + \frac{v_{o}}{2}Sin\beta_{o}h - \frac{z_{L}I_{z}(d)}{2}[Sin\beta_{o}(h-d) + Sin\beta_{o}(h+d)]\}$$
(2.14)

By combining equations (2.13) and (2.14), the arbitrary constant C_1 is eliminated from eq. (2.13), and an expression for the vector potential difference at the surface of the antenna is obtained as

$$A_{z}(z) - A_{z}(h) = -\frac{1}{v_{o}} \operatorname{Sec\beta}_{o} h \{ j v_{o} A_{z}(h) (\operatorname{Cos\beta}_{o} z - \operatorname{Cos\beta}_{o} h)$$

$$-\frac{v_{o}}{2} \operatorname{Sin\beta}_{o}(h - |z|) + \frac{z_{L} I_{z}(d)}{2} [2\operatorname{Sin\beta}_{o} h \operatorname{Cos\beta}_{o} d \operatorname{Cos\beta}_{o} z$$

$$- \operatorname{Cos\beta}_{o} h (\operatorname{Sin\beta}_{o} |z - d| + \operatorname{Sin\beta}_{o} |z + d|)] \}. \qquad (2.15)$$

the

can

wit

Whe

Ιf

te

According to the dimensional assumptions $h \gg a$ and $\beta_o a \ll 1$, the Helmoltz integral for the vector potential at the antenna surface can be simplified as the line integral over an axial current distribution with negligible inaccuracy, i.e.

$$A_{z}(z) = \frac{\mu_{o}}{4\pi} \int_{-h}^{h} I_{z}(z') K_{a}(z,z') dz' \quad \text{for } -h \le z \le h$$

where μ_0 = the permeability of free space

$$K_a(z,z^{\dagger}) = \frac{e^{-j\beta_0 R}}{R}$$
 ... Green's function

$$R = \sqrt{(z-z')^2 + a^2}$$
 ... distance between an observation point on the surface of antenna at z and an element of current on its axis at z'.

If the left hand side of eq. (2.15) is replaced by the Helmholtz integral expression, an integral equation for $I_{z}(z)$ is obtained as

$$\int_{-h}^{h} I_{z}(z')K_{d}(z,z')dz'$$

$$= -\frac{j4\pi}{\zeta_{o}} \operatorname{Sec\beta_{o}h} \{ jv_{o}A_{z}(h) (\operatorname{Cos\beta_{o}}z - \operatorname{Cos\beta_{o}h}) - \frac{v_{o}}{2} \operatorname{Sin\beta_{o}}(h-|z|)$$

$$+ \frac{z_{L}I_{z}(d)}{2} \left[2\operatorname{Sin\beta_{o}h} \operatorname{Cos\beta_{o}d} \operatorname{Cos\beta_{o}z} - \operatorname{Cos\beta_{o}h}(\operatorname{Sin\beta_{o}}|z-d| + \operatorname{Sin\beta_{o}}|z+d|) \right] \}. \qquad (2.16)$$

where ζ_0 is the characteristic impedance of free space

$$= \sqrt{\frac{\mu_0}{\epsilon_0}} = 120\pi \text{ ohms}.$$

 $\mbox{Kd}(z,z')$ is the difference kernel of kernel $\mbox{Ka}(z,z')$ and $\mbox{Ka}(h,z')$, i.e.

Ξq.

t!.e

2 4

sho

mod th

20

Wo

ān,

A z

an eq

a;

$$K_{d}(z,z') = K_{a}(z,z') - K_{a}(h,z')$$

$$= \frac{e^{-j\beta_{0}R}}{R} - \frac{e^{-j\beta_{0}Rh}}{R_{h}}$$

$$R = \sqrt{(z-z')^{2} + a^{2}}, R_{h} = \sqrt{(h-z')^{2} + a^{2}}$$

Eq. (2.16) is a modified form of Hallen's integral equation [8] for the antenna current $I_z(z)$, and is valid for $-h \le z \le h$.

2.4 Approximate Solution of the Integral Equation:

It is found that the current distribution on the doubly loaded short antenna can be approximated quite accurately by obtaining an approximate solution to integral equation (2.16) according to King's modified method [5][6]. This method consists essentially of assuming the current excited on the antenna to be proportional to the vector potential difference (referred to the end of the antenna). In other words, it is assumed that the ratio of vector potential difference to antenna current is relatively constant along the cylinder. Since $A_z(z) - A_z(h)$ vanishes at $z = \pm h$, then $I_z(z = \pm h) = 0$ and the induced current satisfies the boundary condition at the end of the antenna. The application of this method to the solution of integral equation (2.16) is the subject of this section.

By a peaking property of the difference kernel $K_d(z,z')$

$$K_{d}(z,z') = K_{a}(z,z') - K_{a}(h,z')$$

 $\sim \delta(z-z') - \delta(h-z')$

and by applying the Helmholtz integral it is found that

S ŝ 5

$$A_{z}(z) - A_{z}(h) = \frac{\mu_{o}}{4\pi} \int_{-h}^{h} I_{z}(z') K_{d}(z,z') dz'$$

$$\sim \frac{\mu_{o}}{4\pi} \left[I_{z}(z) - I_{z}(h) \right]$$

$$I_{z}(z) - I_{z}(h) \sim \frac{4\pi}{\mu_{o}} \left[A_{z}(z) - A_{z}(h) \right].$$

or

Since $I_z(h) = 0$, then

$$I_z(z) \sim A_z(z) - A_z(h)$$

and the induced antenna current $\, \mathbf{I}_{\mathbf{z}}(\mathbf{z}) \,$ is therefore taken to be of the form

$$I_{z}(z) = C_{c}(\cos \beta_{o}z - \cos \beta_{o}h) + C_{s}\sin \beta_{o}(h - |z|)$$

$$+ C_{i}[2\sin \beta_{o}h \cos \beta_{o}d \cos \beta_{o}z - \cos \beta_{o}h(\sin \beta_{o}|z - d|$$

$$+ \sin \beta_{o}|z + d|)]. \qquad (2.17)$$

Note that in eq. (2.17)

$$I_z(z = +h) = 0$$

implying that the boundary condition at the antenna extremities is automatically satisfied, and the current is symmetric as it should be. The approximate solution (2.17) is further optimized by forcing it to satisfy integral equation (2.16) at z=0.

The complex constants C_s , C_c , and C_i are evaluated by substituting the approximate current distribution $I_z(z)$ of eq. (2.17) back into integral equation (2.16) as

$$\begin{split} &C_{c}\int_{-h}^{h}(\cos\beta_{o}z' - \cos\beta_{o}h)K_{d}(z,z')dz' + C_{s}\int_{-h}^{h}\sin\beta_{o}(h-|z'|)K_{d}(z,z')dz' \\ &+ C_{i}\int_{-h}^{h}[2\sin\beta_{o}h \cos\beta_{o}d \cos\beta_{o}z' - \cos\beta_{o}h(\sin\beta_{o}|z'-d| + \sin\beta_{o}|z'+d|]K_{d}(z,z')dz' \\ &= -j\frac{4\pi}{\zeta_{o}}\operatorname{Sec\beta_{o}h}\{jv_{o}A_{z}(h)(\cos\beta_{o}z - \cos\beta_{o}h) - \frac{v_{o}}{2}\operatorname{Sin\beta_{o}}(h-|z|) \\ &+ \frac{z_{L}I_{z}(d)}{2}[2\sin\beta_{o}h \cos\beta_{o}d \cos\beta_{o}z - \cos\beta_{o}h(\sin\beta_{o}|z-d| + \sin\beta_{o}|z+d|)]\}. \end{split}$$

The complex kernel $K_d(z,z')$ may be expressed in terms of its real and imaginary parts, i.e.

$$\begin{split} K_{d}(z,z') &= \frac{e}{R}^{-j\beta_{0}R} - \frac{e^{-j\beta_{0}R_{h}}}{R_{h}} \\ &= K_{dr}(z,z') + jK_{di}(z,z') \\ \end{split}$$
 where
$$K_{dr}(z,z') &= \frac{1}{R} \cos_{0}R - \frac{1}{R_{h}} \cos_{0}R_{h} \\ K_{di}(z,z') &= \frac{1}{R_{h}} \sin_{0}R_{h} - \frac{1}{R} \sin_{0}R_{h} \end{split}$$

Since $K_{dr}(z,z')$ becomes very large when z' is near z, it follows that the principle contribution to the part of the integral that has $K_{dr}(z,z')$ as kernel comes from elements of current near z'=z. On the other hand, K_{di} remains small when z=z'. This suggests that the principal contribution to the part of the integral that has $K_{di}(z,z')$ as kernel comes from all elements of current that are at some distance from z. Due to this peaking property of kernel $K_{dr}(z,z')$ and non-peaking property of kernel $K_{di}(z,z')$, the various integrals on the left hand side of equation (2.18) may be verified numerically to have the following approximate representation:

$$\int_{-h}^{h} (\cos \beta_{o} z' - \cos \beta_{o} h) K_{dr}(z, z') dz' \sim (\cos \beta_{o} z - \cos \beta_{o} h)$$
 (2.19a)

$$\int_{-h}^{h} (\cos \beta_{o} z' - \cos \beta_{o} h) K_{di}(z, z') dz' \sim (\cos \beta_{o} z - \cos \beta_{o} h)$$
(2.19b)

$$\int_{-h}^{h} \operatorname{Sin\beta}_{O}(h-|z'|) K_{dr}(z,z') dz' \sim \operatorname{Sin\beta}_{O}(h-|z|)$$
(2.19c)

$$\int_{-h}^{h} \sin \beta_{o}(h - |z'|) K_{di}(z, z') dz' \sim (\cos \beta_{o} z - \cos \beta_{o} h)$$
 (2.19d)

$$\int_{-h}^{h} \left[2 \sin \beta_{o} h \cos \beta_{o} d \cos \beta_{o} z' - \cos \beta_{o} h \left(\sin \beta_{o} | z' - d| + \sin \beta_{o} | z' + d| \right) \right] K_{dr}(z, z') dz'$$

$$\sim \left[2 \sin \beta_{0} h \cos \beta_{0} d \cos \beta_{0} z - \cos \beta_{0} h (\sin \beta_{0} | z - d| + \sin \beta_{0} | z + d|)\right] \qquad (2.19e)$$

$$\int_{-h}^{h} \left[2 \sin \beta_{o} h \cos \beta_{o} d \cos \beta_{o} z' - \cos \beta_{o} h \left(\sin \beta_{o} \right| z' - d \right| + \sin \beta_{o} \left| z' + d \right| \right) \right] K_{di}(z,z') dz'$$

$$\sim (\cos \beta_{0} z - \cos \beta_{0} h) \tag{2.19f}$$

where (2.19a), (2.19c) and (2.19e) are based on the characteristics of kernel $K_{\rm dr}(z,z')$, and the remainders, (2.19b), (2.19d) and (2.19f), are based on numerical considerations. It can be shown numerically that these remainders are roughly proportional to the shifted cosine function $(\cos\beta_0 z - \cos\beta_0 h)$.

These properties suggest that equation (2.18) can be split into three parts by equating corresponding terms on the right and left hand sides as follows:

$$C_{c}\int_{-h}^{h} (\cos\beta_{o}z' - \cos\beta_{o}h) K_{dr}(z,z') dz' + j C_{c}\int_{-h}^{h} (\cos\beta_{o}z' - \cos\beta_{o}h) K_{di}(z,z') dz'$$

-
$$\cos \theta_{o} h (\sin \theta_{o} | z' - d| + \sin \theta_{o} | z' + d|)] K_{di}(z, z') dz'$$

$$= \frac{4\pi}{\zeta_0} v_0 A_z(h) Sec\beta_0 h(Cos\beta_0 z - Cos\beta_0 h)$$
 (2.20a)

$$C_{s} \int_{-h}^{h} \sin \beta_{o}(h-|z'|) K_{dr}(z,z') dz' = j \frac{2\pi V_{o}}{\zeta_{o}} \operatorname{Sec} \beta_{o} h \operatorname{Sin} \beta_{o}(h-|z|)$$
 (2.20b)

٠.

С

the app

The

adv by

:::3

+ :

z

C_i

C

Equ the

=

Pos

I_z(

$$C_{i}\int_{-h}^{h} \left[2\sin\beta_{o}h \cos\beta_{o}d \cos\beta_{o}z'' - \cos\beta_{o}h(\sin\beta_{o}|z'-d| + \sin\beta_{o}|z'+d|)K_{r}(z,z')dz'' \right]$$

$$= -j \frac{4\pi}{\zeta_{o}} \operatorname{Sec\beta_{o}h} \left[2\sin\beta_{o}h \cos\beta_{o}d \cos\beta_{o}z - \cos\beta_{o}h(\sin\beta_{o}|z-d| + \sin\beta_{o}|z+d|) \right]$$

$$(2.20c)$$

The approximate current distribution $I_z(z)$ automatically satisfies the boundary condition $I_z(z=\pm h)=0$. In order to optimize the approximate solution, the unknown coefficients are evaluated by forcing the integral equation to be satisfied at z=0 (which has the advantage of providing accurate input impedances). This is implemented by equating z to zero in the last results as

$$C_{c} \int_{-h}^{h} (\cos \beta_{o} z' - \cos \beta_{o} h) K_{dr}(o, z') dz' + j C_{c} \int_{-h}^{h} [\cos \beta_{o} z' - \cos \beta_{o} h) K_{di}(o, z') dz' + j C_{s} \int_{-h}^{h} \sin \beta_{o} (h - |z'|) K_{di}(0, z') dz' + j C_{i} \int_{-h}^{h} [2 \sin \beta_{o} h) \cos \beta_{o} d \cos \beta_{o} z'$$

-
$$\cos \beta_0 h \left(\sin \beta_0 | z' - d | + \sin \beta_0 | z' + d | \right) \right] K_{di}(0, z') dz'$$

$$= \frac{4\pi}{\zeta_0} v_0 A_z(h) (Sec\beta_0 h-1)$$
 (2.21a)

$$C_{s}\int_{-h}^{h} \sin\beta_{o}(h-|z'|)K_{dr}(o,z')dz' = j\frac{2\pi V}{\zeta_{o}}Sec\beta_{o}hSin\beta_{o}h \qquad (2.21b)$$

 $C_{i} \int_{-h}^{h} \left[2 \sin \beta_{o} h \cos \beta_{o} d \cos \beta_{o} z' - \cos \beta_{o} h (\sin \beta_{o} | z' - d| + \sin \beta_{o} | z' + d|) \right] K_{dr}(o, z') dz'$

$$= -j \frac{4\pi}{\zeta_0} Z_L I_z(d) Sec\beta_0 h Sin\beta_0 (h-d). \qquad (2.21c)$$

Equations (2.21a \sim c) are solved for C_s , C_i , and C_c in terms of the antenna dimensions, the excitation frequency, the impedance and position of the double loading, and the undetermined constant terms $I_z(d)$ and vector potential $A_z(h)$ as

$$C_{s} = \frac{j2\pi V_{o}}{C_{o}T_{sdr}} \operatorname{Sec\beta}_{o} h \operatorname{Sin\beta}_{o} h$$
 (2.22a)

$$C_{i} = -j \frac{4\pi}{\zeta_{0} T_{idr}} Z_{L} I_{z}(d) Sec\beta_{0} h Sin\beta_{0}(h-d)$$
 (2.22b)

$$C_{c} = \frac{4\pi}{\zeta_{o}T_{cd}} \left[v_{o}A_{z}(h) \left(Sec\beta_{o}h - 1 \right) + \frac{v_{o}T_{sdi}}{2T_{sdr}} Sec\beta_{o}h Sin\beta_{o}h \right]$$

$$- \frac{T_{idi}}{T_{idr}} Z_{L}I_{z}(d) Sec\beta_{o}h Sin\beta_{o}(h-d) \right] \qquad (2.22c)$$

where

$$\begin{split} T_{sdr} &= \int_{-h}^{h} \sin \beta_{o} \left(h - \left| z' \right| \right) K_{dr} (o, z') dz' \\ T_{idr} &= \int_{-h}^{h} \left[2 \sin \beta_{o} h \cos \beta_{o} d \cos \beta_{o} z' - \cos \beta_{o} h (\sin \beta_{o} \left| z' - d \right| \right. \\ &+ \left. \sin \beta_{o} \right| z' + d \left| \right| \right] K_{dr} (o, z') dz' \\ T_{cd} &= \int_{-h}^{h} (\cos \beta_{o} z' - \cos \beta_{o} h) K_{d} (o, z') dz' \\ T_{zdi} &= \int_{-h}^{h} \sin \beta_{o} \left(h - \left| z' \right| \right) K_{di} (o, z') dz' \\ T_{idi} &= \int_{-h}^{h} \left[2 \sin \beta_{o} h \cos \beta_{o} d \cos \beta_{o} z' - \cos \beta_{o} h (\sin \beta_{o} \left| z' - d \right| \right. \\ &+ \left. \sin \beta_{o} \left| z' + d \right| \right) \right] K_{di} (o, z') dz' . \end{split}$$

The unknown constant quantities $I_z(d)$ and $A_z(h)$ may be evaluated by applying the conditions

$$\begin{cases} I_{z}(z=d) = I_{z}(d) \\ A_{z}(h) = \frac{\mu_{o}}{4\pi} \int_{-h}^{h} I_{z}(z') K_{a}(h,z') dz' \end{cases}$$

where

$$\begin{cases} K_{a}(h,z') = \frac{e^{-j\beta_{0}R_{h}}}{R_{h}} \\ R_{h} = \sqrt{(h-z'')^{2} + a^{2}} \end{cases}.$$

To evaluate $I_z(d)$, C_s , C_i and C_c are substituted into eq. (2.17) and, by using the condition $I_z(z=d) = I_z(d)$, the current $I_z(d)$ is obtained in terms of $A_z(h)$ as

$$I_{z}(d) = \frac{4\pi}{\zeta_{o}^{T} c d^{D}_{1}} \left[v_{o}^{A} z(h) \left(\operatorname{Sec\beta}_{o} h - 1 \right) + \frac{v_{o}^{T} T_{s} di}{T_{s} dr} \operatorname{Sec\beta}_{o} h \operatorname{Sin\beta}_{o} h \right] \left(\operatorname{Cos\beta}_{o}^{d} - \operatorname{Cos\beta}_{o} h \right) + j \frac{2\pi v_{o}^{T} T_{s} dr^{D}_{1}}{\zeta_{o}^{T} T_{s} dr^{D}_{1}} \operatorname{Sec\beta}_{o} h \operatorname{Sin\beta}_{o} h \operatorname{Sin\beta}_{o} (h - d) \quad (2.23)$$

where

$$D_{1} = 1 + \frac{4\pi}{\zeta_{o}^{T}_{cd}} \frac{T_{idi}}{T_{idr}} Z_{L} Sec\beta_{o}h Sin\beta_{o}(h-d) (Cos\beta_{o}d - Cos\beta_{o}h)$$

$$+ j \frac{8\pi}{\zeta_{o}^{T}_{idr}} Z_{L} Sec\beta_{o}h Cos\beta_{o}d Sin^{2}\beta_{o}(h-d).$$

Having evaluated $I_z(d)$ as in (2.23), it may be substituted back into eq. (2.22) and by using eq. (2.17), and the realtion

$$A_z(h) = \frac{\mu_0}{4\pi} \int_{-h}^{h} I_z(z') K_a(h,z') dz', A_z(h)$$
 is determined completely as

$$A_{z}(h) = \frac{\frac{\mu_{o} T_{ca} V_{o}}{2\zeta_{o} T_{cd} D_{2}}}{\frac{2}{\zeta_{o} T_{cd} D_{2}}} \left\{ \frac{\frac{T_{sdi}}{T_{sdr}} D_{5} - \frac{4\pi Z_{L} T_{idi} T_{sdi}}{\zeta_{o} T_{cd} D_{1} T_{idr} T_{sdr}} D_{3} - j \frac{4\pi T_{idi} Z_{L}}{T_{idr} D_{1} \zeta_{o} T_{sdr}} D_{4} \right\} + j \frac{\frac{\nu_{o} V_{o} T_{sa} D_{5}}{2\zeta_{o} T_{sdr} D_{2}}}{\frac{2}{\zeta_{o} T_{sdr}} D_{1} C_{o} T_{sdr}}$$

$$- j \frac{2\pi \mu_{o} Z_{L} T_{ia} V_{o}}{\zeta_{o} T_{idr} D_{1} D_{2} T_{sdr}} \left\{ \frac{T_{sdi}}{T_{cd}} D_{3} + j D_{4} \right\}$$

$$(2.24)$$

where

$$\begin{split} T_{ca} &= \int_{-h}^{h} (\cos\beta_{o}z' - \cos\beta_{o}h) K_{a}(h,z') dz' \\ T_{sa} &= \int_{-h}^{h} \sin\beta_{o}(h - |z'|) K_{a}(h,z') dz' \\ T_{ia} &= \int_{-h}^{h} [2\sin\beta_{o}h \cos\beta_{o}d \cos\beta_{o}z' - \cos\beta_{o}h(\sin\beta_{o}|z' - d| + \sin\beta_{o}|z' + d|)] K_{a}(h,z') dz' \end{split}$$

: : /

The

cie

Pre

ćis

Ja

W^L.

FC

$$\begin{split} D_2 &= 1 - \frac{T_{ca}}{T_{cd}} (\text{Sec}\beta_o h - 1) + \frac{4\pi T_{idi} T_{ca} Z_L}{T_{idr} (T_{cd})^2 \zeta_o D_1} (\text{Sec}\beta_o h - 1) (\text{Cos}\beta_o d - \text{Cos}\beta_o h) \text{Sec}\beta_o h + \text{Sin}\beta_o (h - d) \\ &\quad - \text{Cos}\beta_o h) \text{Sec}\beta_o h + \text{Sin}\beta_o (h - d) \\ &\quad + \text{Ji} \frac{4\pi Z_L T_{ia}}{T_{idr} T_{cd} D_1 \zeta_o} (\text{Sec}\beta_o h - 1) \text{Sec}\beta_o h + \text{Sin}\beta_o (h - d) (\text{Cos}\beta_o d - \text{Cos}\beta_o h) \\ D_3 &= \text{Sec}^2\beta_o h + \text{Sin}\beta_o h + \text{Cos}\beta_o d - \text{Cos}\beta_o h) \text{Sin}\beta_o (h - d) \\ D_4 &= \text{Sec}^2\beta_o h + \text{Sin}\beta_o h + \text{Sin}^2\beta_o (h - d) \\ D_5 &= \text{Sec}\beta_o h + \text{Sin}\beta_o h + \dots \end{split}$$

The values of $I_z(d)$ and $A_z(h)$ are completely determined by expression (2.23) and (2.24), and the evaluation of the complex coefficients C_s , C_c , and C_i is consequently completed.

By combining equations (2.17), (2.22), (2.23), and (2.24) the distribution of current excited on the short, doubly loaded antenna may finally be expressed in the form

$$I_{z}(z) = \frac{V_{o}}{60} \{ FC_{5}(\cos\beta_{o}z - \cos\beta_{o}h) + FC_{4}\sin\beta_{o}(h - |z|)$$

$$- j FC_{2}[2\sin\beta_{o}h \cos\beta_{o}d \cos\beta_{o}z - \cos\beta_{o}h(\sin\beta_{o}|z - d|$$

$$+ \sin\beta_{o}|z + d|)] \}$$

$$(2.25)$$

where

$$FC_{1} = FC_{1} - FC_{3}$$

$$FC_{1} = \frac{1}{T_{cd}T_{sdr}} \{ \left[\frac{T_{ca}}{T_{cd}D_{2}} (T_{sdi}D_{5} - \frac{Z_{L}T_{idi}T_{sdi}}{30D_{1}T_{cd}T_{idr}} D_{3} - j \frac{Z_{L}D_{4}T_{idi}}{30D_{1}T_{cd}} \right] + j \frac{D_{5}T_{sa}}{30D_{1}D_{2}T_{idr}} - j \frac{Z_{L}T_{ia}}{30D_{1}D_{2}T_{idr}} (\frac{T_{sdi}D_{3} + jD_{4}}{T_{cd}}) \right] (Sec_{5}^{h-1}) + T_{sdi}D_{5} \}$$

$$FC_{2} = \frac{z_{L}}{T_{idr}} Sec\beta_{o}h Sin\beta_{o}(h-d) \{\frac{1}{30D_{1}} FC_{1}(Cos\beta_{o}d - Cos\beta_{o}h)\}$$

$$+ j \frac{D_{5}}{30D_{1}T_{sdr}} Sin\beta_{o}(h-d) \}$$

$$FC_{3} = \frac{T_{idi}}{T_{cd}} FC_{2}$$

$$FC_{4} = j \frac{D_{5}}{T_{sdr}}$$

This result expresses the antenna current distribution in terms of the antenna dimension, its excitation frequency and the impedance and position of the double loading.

2.5 Input Impedance of Doubly Loaded Short Antenna:

The input impedance of the antenna is defined as

$$z_{in} = \frac{V_{o}}{I_{z}(z=o)} = R_{in} + j X_{in}$$
.

From eq. (2.25), this impedance can be expressed in the form

$$z_{in} = 60 \{FC_5(1 - Cos\beta_0 h) + FC_4 Sin\beta_0 h - j \ 2FC_2 Sin\beta_0 (h - d)\}^{-1}$$
 (2.26)

The input impedance of result (2.26) is expressed in terms of the antenna dimensions, the excitation frequency, and the parameter of the double loading. Expressions (2.25) and (2.26) for the antenna current distribution and input impedance of a doubly loaded short antenna are the main results of this chapter, and they will be utilized in the subsequent chapters for the study of short antennas with enhanced radiation and high directivity.

CHAPTER 3

SHORT ANTENNA WITH ENHANCED RADIATION

3.1 Introduction:

A conventional short, linear antenna has a very small input resistance and a large capacitive input reactance. For an antenna having $h \leq 0.1 \; \lambda_0$, the input resistance is extremely small compared with that of a longer antenna, i.e., one of near resonant length. The power radiated by the antenna is strongly dependent upon its input resistance, since this resistance determines the degree of matching between the transmission system and the antenna. The radiated power of the short antenna is therefore very small due to the mismatch between its small input resistance and the characteristic impedance of a typical transmission system which might be used to excite the antenna. It is the purpose of this research to enhance the power radiated by a short antenna by increasing the input resistance while simultaneously tuning its input reactance to zero.

In order to enhance its radiated power, the antenna should be operated at reasonance (since zero input reactance is required). This resonance condition can be implemented by inserting a low-loss series inductor at the input terminals or by loading low-loss lumped inductors on the cylindical wire antenna. In the latter case, a high Q capacitor may also be inserted at the input terminals for tuning purposes as will be indicated in Sec. 3.4. The conventional base tuning arrangement, however, cannot increase the input resistance to the antenna, and therefore it is ignored in this study except for comparison purposes.

The double impedance loading is implemented by lumped inductors in this study. It has been found that a purely non-dissipative optimum loading may be utilized at various positions along the surface of the cylindrical antenna. Of course, the terminology non-dissipative loading refers to an ideal lossless inductor which cannot be realized physically. A very low-loss or high O inductor is mounted on the antenna to implement an optimum loading in the experimental investigation. By tuning the inductor to its optimum value at a fixed position along the antenna surface, the input reactance X_{in} of the antenna is eliminated and its input resistance is increased by a factor of the order of two to four $(2 \sim 4)$ over its value for an unloaded antenna (maximum increase is by a factor of 4), and the radiated power of the short antenna is therefore enhanced significantly. It has also been found that for some proper choices of loading impedances and locations, the input impedance of a short antenna can be adjusted to have a large resistive component and an inductive reactive component. This case appears rather attractive since the antenna can now be tuned to reasonance at its terminals with a high-Q series capacitance which is more readily implemented than a high-Q inductor.

The details of all these configurations are discussed in the following sections.

3 2 Radiated Power and Radiation Resistance:

The power radiated by a short antenna can be obtained easily from the well known result [7].

$$\begin{cases} E_{\theta}^{r} = -j\omega A_{\theta}^{r}(R_{0}, \theta) \\ B_{\phi}^{r} = \frac{1}{v_{0}} E_{\theta}^{r}(R_{0}, \theta) \end{cases}$$
(3.1)

where R_0 is the distance from the observation point to the center of the antenna, and superscript r indicates the radiation field. E_θ^r , B_ϕ^r and A_θ^r are expressed in spherical coordinates. The total time-average power radiated by the antenna is thus given by

$$P_{rad.} = \frac{\pi R_0^2 \omega^2}{\zeta_0} \int_0^{\pi} |A_{\theta}^r| \sin\theta \ d\theta$$
 (3.2)

where A_{θ}^{r} can be expressed in terms of the antenna current $I_{z}(z)$ (given by eq. (2.24)) as

$$A_{\theta}^{r} \doteq -\frac{\mu_{0}}{4\pi} \sin\theta \int_{-h}^{h} I_{z}(z') \frac{e}{R} dz'$$

$$= -\frac{\mu_{0}}{4\pi} \frac{e}{R_{0}} \sin\theta \int_{-h}^{h} I_{z}(z') e^{j\theta_{0}z'\cos\theta} dz' \qquad (3.3)$$

subject to the usual approximations,

$$\begin{cases} R = R_0 - z' \cos \theta & \text{for phase factor} \\ R = R_0 & \text{for amplitude terms} \end{cases}$$

According to the definition of a short antenna, $\beta_0 z'$ is much smaller $+j\beta_0 z'\cos\theta$ than one, therefore e can be well approximated by the leading terms of a power series expansion as

$$e^{+j\beta_0 z'\cos\theta} = 1 + j\beta_0 z'\cos\theta - \frac{1}{2}\beta_0^2 z'^2\cos^2\theta$$
.

Since the antenna current is symmetric about its center z = 0, then $I_z(z) = I_z(-z)$ and the second term of the power series integrates to zero such that equation (3.3) becomes

$$A_{\theta}^{r} = -\frac{\mu_{0}}{4\pi} \frac{e^{-j\beta_{0}R_{0}}}{R_{0}} \sin\theta \int_{-h}^{h} I_{z}(z') (1 - \frac{1}{2}\beta_{0}^{2}z'^{2}\cos^{2}\theta) dz'$$
 (3.4)

Since $\beta_0 h \ll 1$ for a short antenna, then the second term in the integral of eq. (3.4) is normally very small compared with the first. Thus $\int_{-h}^{h} I_z(z')dz' >> \frac{1}{2} \int_{-h}^{h} \beta_0^2 z'^2 \cos^2\theta \ I_z(z')dz'$, provided only that the left side of the inequality is not forced to approach zero by reversing the phase of the current along the antenna. Eq. (3.4) can therefore be approximated by the expression

$$A_{\theta} = -\frac{\mu_{0}}{4\pi} \frac{e^{-j\beta_{0}R_{0}}}{R_{0}} \quad \sin\theta \int_{-h}^{h} I_{z}(z') dz'$$

$$= -\frac{\mu_{0}}{4\pi R_{0}} e^{-j\beta_{0}R_{0}} \sin\theta A_{c} \qquad (3.5)$$

where

$$A_{c} = \int_{-h}^{h} I_{z}(z')dz'$$
 the area under the current distribution

By substituting eq. (3.5) into eq. (3.2), the radiated power is obtained as

$$P_{\text{rad.}} = \frac{\zeta_0^{\pi}}{3\lambda_0^2} |A_c|^2 \sim |A_c|^2$$
 (3.6)

The radiation resistance of the antenna can be defined as

$$R_{\text{rad.}} = \frac{2 P_{\text{rad.}}}{I_z^2 (z=0)}$$

and therefore

$$R_{\text{rad.}} = \frac{2 \zeta_0^{\pi}}{3\lambda_0^2 I_z^2 (z=0)} |A_c|^2 \sim \frac{|A_c|^2}{I_z^2 (z=0)}.$$
 (3.7)

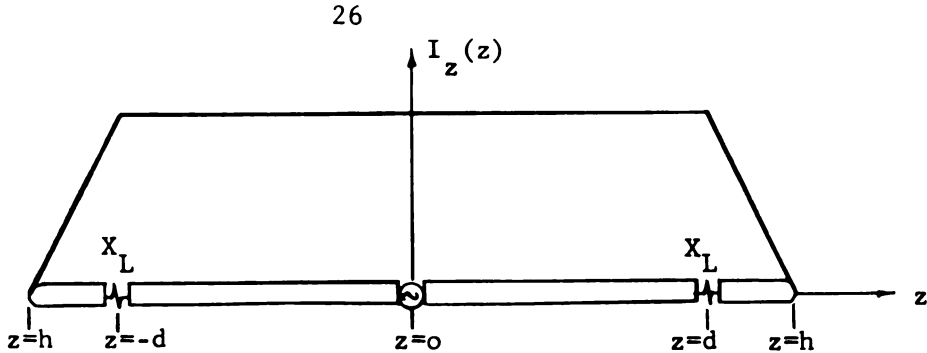
The results of eq. (3.6) and (3.7) are very useful relations in the following sections.

3.3 Doubly Loaded Short Antenna with Increased Input Resistance and Zero Input Reactance:

Since the input impedance of the doubly loaded antenna is a function of the impedance and position of the loading, the dimensions of the antenna, and its excitation frequency, it is difficult to formulate an expression for the optimum loading impedance required to make $X_{in} = 0$ and simultaneously maximize R_{in} based on the already complicated equation (2.24). Therefore the optimum impedance loading which will increase the input resistance and simultaneously provide zero input reactance will be determined by using a high speed computer to calculate and examine the antenna current and input impedance, for given antenna dimensions, with various impedances (low-loss inductors of various Q) loaded at different locations along the cylinder.

3.3.1 Typical Current Distribution

Suppose that the short antenna is loaded by an optimum non-dissipative impedance of reactance $[X_L]_{op}$ at a fixed position along its surface such that its input reactance X_{in} is tuned to zero. It is found from eq. (2.24) by numerical calculation that the current distribution on the antenna has the general form indicated in Fig. 3.1. The amplitude of the current is almost constant between the loading points along the antenna, and decreases to zero between the loading points and the extremities of the antenna. The phase of the current is minimum and nearly constant at all points along the antenna.



Typical current distribution along antenna with optimum reactance loading to make $X_{in} = 0$.

The current distributions along antennas with $h = 0.1\lambda_0$ and d = 0.5h, 0.7h and 0.9h for the case of an optimum reactance loading are plotted in Figures 3.2 to 3.4. It is found that the area under the current distribution becomes greater as the loading points are shifted toward the extremities of the cylinder. Since the radiated power is approximately proportional to the square of the area under the current distribution, this indicates that the radiated power may be enhanced more significantly if the loading is located near the end points of the antenna (provided that the optimum impedance is non-dissipative as discussed in Section 3.5).

3.3.2 Input Impedance, Radiation Resistance, and Optimum Loading Impedance

The input impedance of the doubly loaded antenna is expressed by eq. (2.26) of Chapter 2 as

$$z_{in} = 60\{FC_5(1 - Cos\beta_0h) + FC_4Sin\beta_0h - j2FC_2Sin\beta_0(h-d)\}^{-1}$$

From this equation, the input impedances are calculated and plotted in Fig. 3.5. The case of both zero and optimum non-dissipative impedance loadings at positions d = 0.5h, 0.7h and 0.9h along antennas of different length and constant diameter are considered at a frequency f = 200MHz. It is demonstrated by these numerical

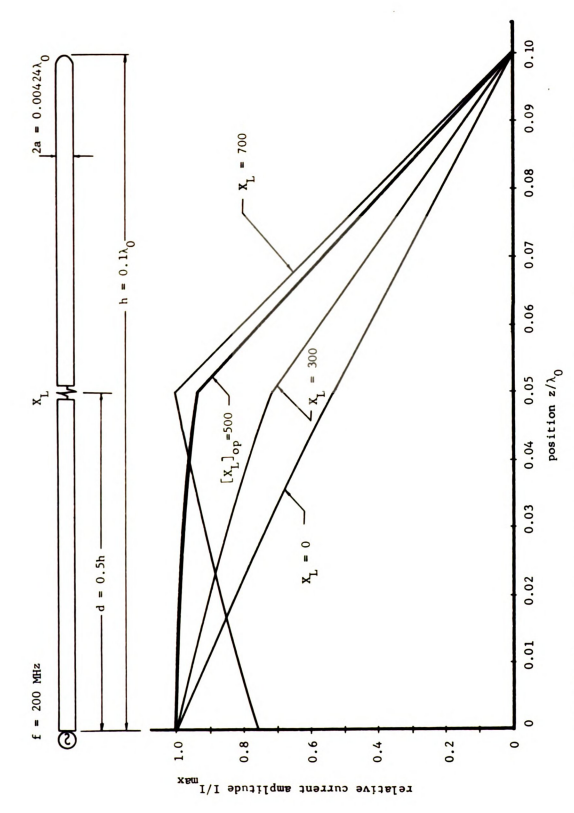
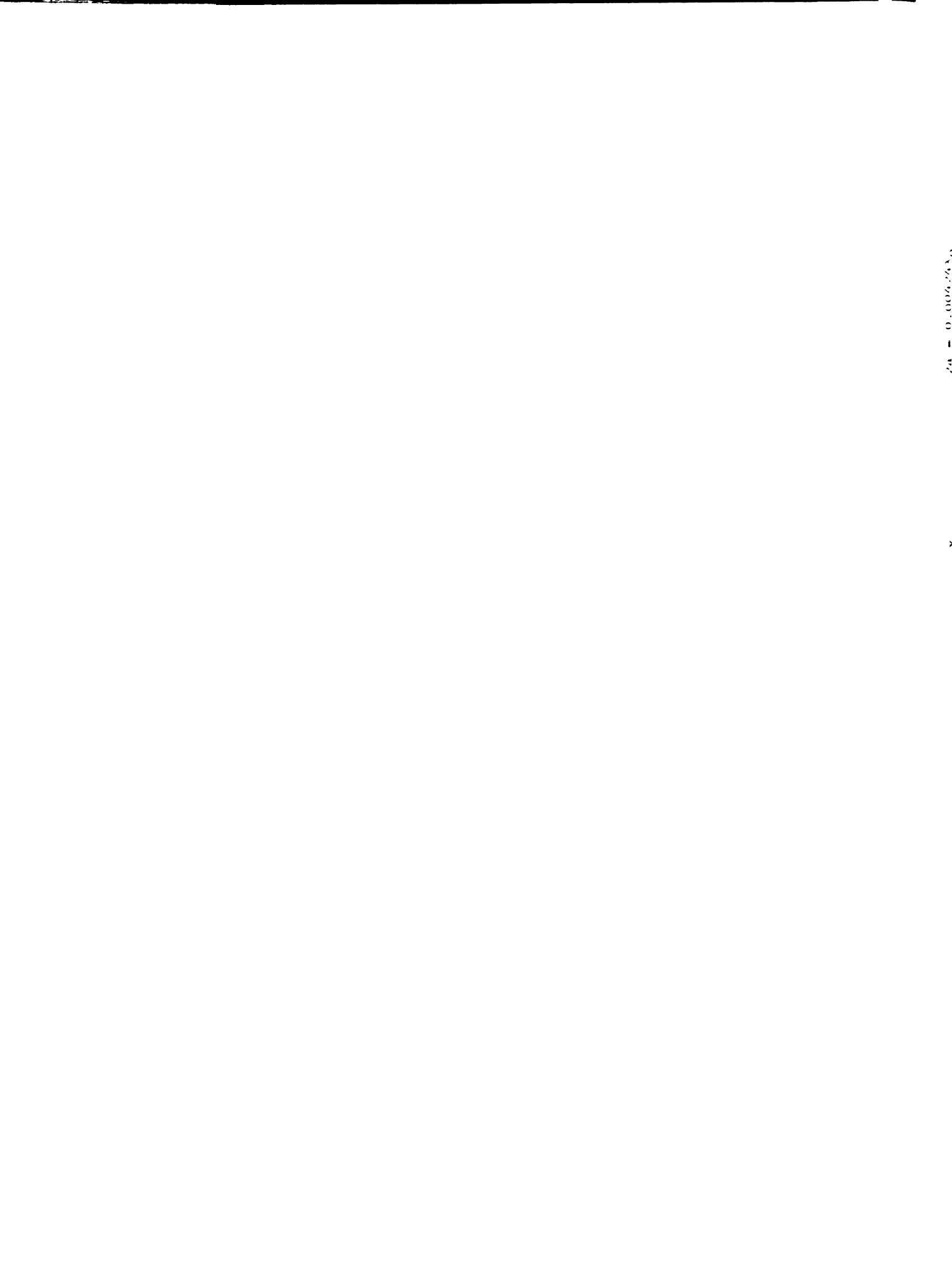


Fig. 3.2 Theoretical Antenna Current Distribution Corresponding to Enhanced Radiation Condition Compared with that of Other Loadings $(h=0.1)_Q,\ d=0.5h)$.



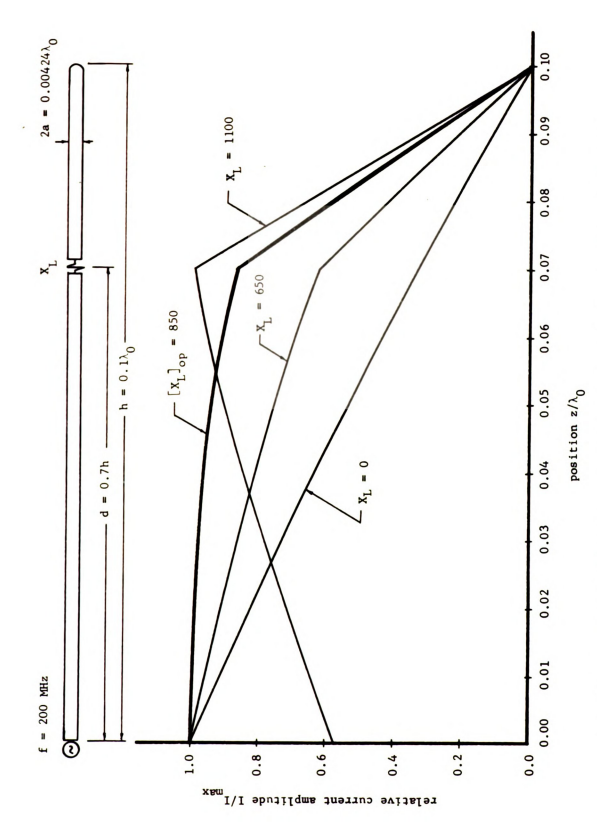


Fig. 3.3 Theoretical Antenna Current Distribution Corresponding to Enhanced Radiation Condition Compared with that of Other Loadings $(h=0.1)_Q,\ d=0.7h)$.

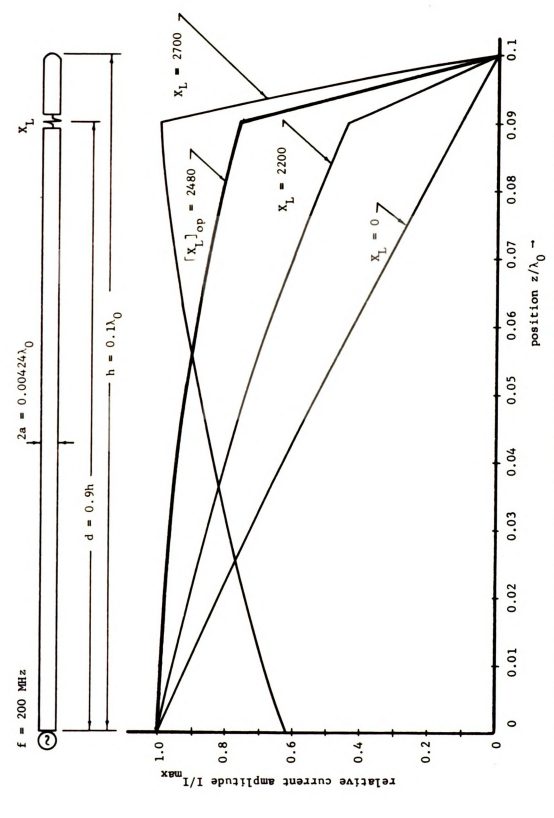
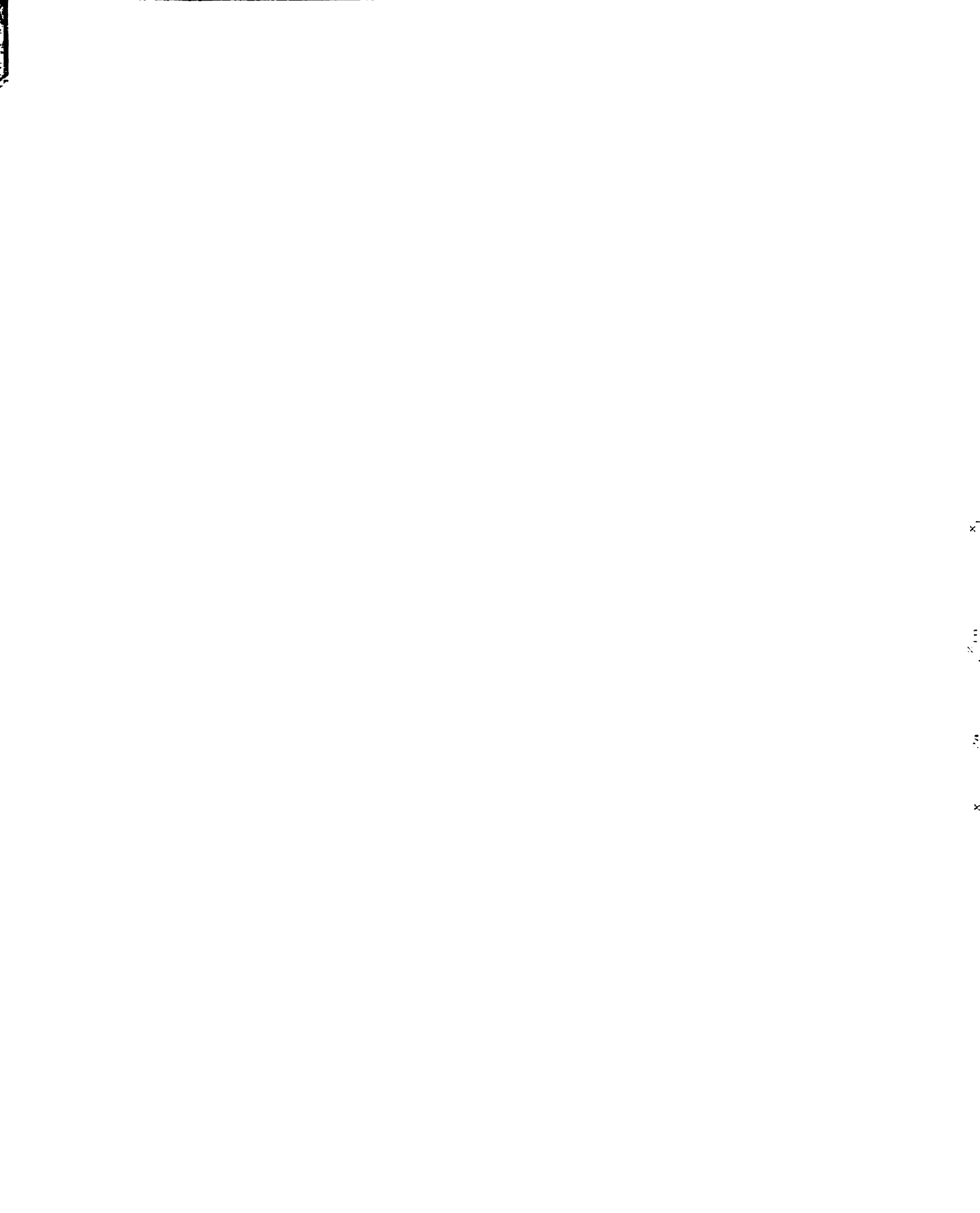


Fig. 3.4 Theoretical Antenna Current Distribution Corresponding to Enhanced Radiation Condition Compared with that of Other Loadings $\,(h=0.1\lambda_0,\,d=0.9h)\,.$



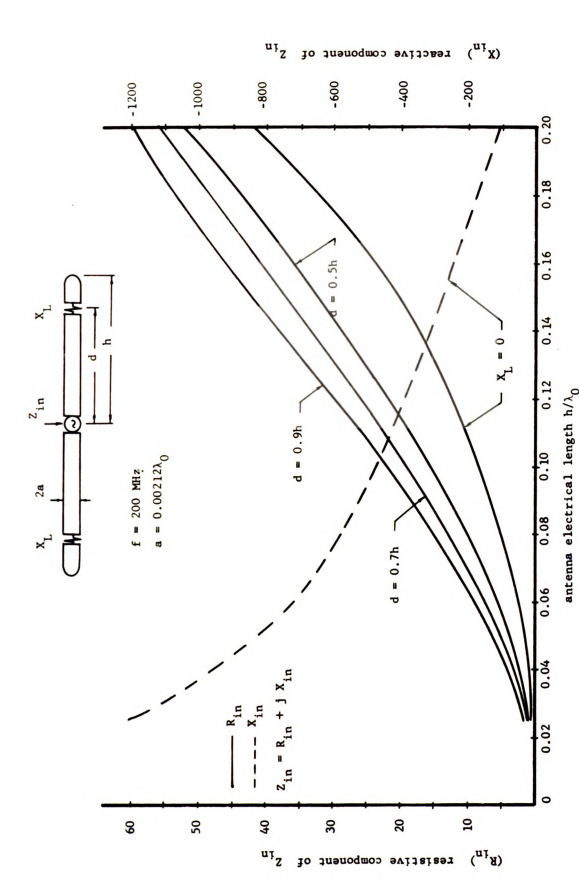


Fig. 3.5 Theoretical Antenna Input Impedances for Zero and Optimum (enhancement) Reactive Loadings at Fixed Positions as Functions of Antenna Length

t

n Po

of cl results that the input resistance is increased as the loading position is shifted toward the extremities of antenna. It is also indicated that the input resistance to a short antenna with optimum reactance loading is increased by a factor of two to three relative to that of an unloaded conventional antenna.

The radiation resistance and input impedance of a short antenna with a lossy optimum impedance loaded at d = 0.7h are listed in Tables 3.1, 3.2 and 3.3 for various value of loading Q. These numerical results indicate how the radiation resistance and input resistance are affected by the Q of the loading impedance.

The optimum loading reactances $[X_L]_{op}$ for antenna with different half-lengths h, constant radius a, and various loading positions d are presented in Fig. 3.6 and Fig. 3.7. It is indicated that the optimum loading reactance $[X_L]_{op}$ is a decreasing function of antenna length for a fixed loading position d/h, and $[X_L]_{op}$ increases for fixed h as the loading position is moved toward the extremities of antenna.

3.3.3 Radiated Power Compared with that of Unloaded Antenna

It has been demonstrated in eq. (3.6) of Sec. 3.2 that the radiated power is approximately proportional to the area beneath the current distribution along the antenna. By investigating the current distributions along antennas having both zero and optimum non-dissipative loadings, as in Fig. 3.2 to Fig. 3.4, the radiated power of the antenna with optimum loading can be enhanced by a factor of one to four relative to that of the unloaded antenna. This conclusion is reached by considering the matching between the antenna

Table 3.1 Input Impedance and Radiation Resistance of Short Antenna Doubly Loaded by Reactances \mathbf{X}_L of Various \mathbf{Q} .

 $v_0 = 1 \text{ volt}, f = 200 \text{ MHz}, a/\lambda_0 = 0.00212, d/h = 0.7, h/\lambda_0 = 0.05, X_L = 1450$

Q	Radiation	$Z_{in} = R_{in} + j X_{in}$	
`	Resistance		
100		Rin	Xin
100	3.79665	30.49565	-5.0386
200	4.45551	17.80993	-4.57154
300	4.67505	13.57864	-4.47566
400	4.78479	11.46267	-4.43894
500	4.85063	10.193	-4.42050
600	4.89452	9.34653	-4.40971
700	4.92587	8.74189	-4.40273
800	4.94938	8.28841	-4.39790
900	4.96766	7.9357	-4.39438
1000	4.98229	7.65352	-4.39171
1100	4.99425	7.42265	-4.38963
1200	5.00422	7.23026	-4.38796
1300	5.01266	7.06747	-4.38659
1400	5.01990	6.92793	-4.38546
1500	5.02616	6.807	-4.38451
1600	5.03165	6.70118	-4.38369
1700	5.03649	6.60781	-4.38298
1800	5.04079	6.5482	-4.38237
1900	5.04464	6.45056	-4.38183
2000	5.04810	6.38373	-4.38135
&	5.11391	5.11391	-4.37369

Table 3.2 Input Impedance and Radiation Resistance of Short Antenna Doubly Loaded by Reactances \mathbf{X}_L of Various Q.

 ${\rm v_0}$ = 1 volt, f = 200 MHz, a/ λ_0 = 0.00212, d/h = 0.7, h/ λ_0 = 0.075, ${\rm X_L}$ = 1080

Q	Radiation	Z = R + j X in	
	Resistance	R	Xin
100	10 43993	28.51376	-8.65307
200	10.78496	19.82499	-8.28564
300	10.89967	16.92681	-8.19977
400	10 95697	15.47745	-8.16371
500	10.99132	14.60777	-8.14427
600	11.01422	14.02795	-8.13223
700	11.03057	13.61379	-8.12408
800	11.04283	13.30315	-8.11821
900	11.05237	13.06155	-8.11379
1000	11.05999	12.86826	-8.11035
1100	11 06623	12.71012	-8.10759
1200	11.07143	12.57833	-8.10534
1300	11.07583	12.46681	-8.10346
1400	11.07960	12.37123	-8.10187
1500	11.08287	12.28839	-8.10051
1600	11.08573	12.2159	-8.09933
1700	11.08825	12.15195	-8.0983
1800	11.09049	12.10951	-8.09739
1900	11.09250	12.04423	-8.09658
2000	11.09430	11.99845	-8.09586
&	11 . 12860	11.1286	-8.08302

Table 3.3 Input Impedance and Radiation Resistance of Short Antenna Doubly Loaded by Reactances \mathbf{X}_{L} of Various Q.

 $v_0 = 1 \text{ volt}, f = 200 \text{ MHz}, a/\lambda_0 = 0.00212, d/h = 0.7, h/\lambda_0 = 0.1, X_L = 850$

	•		
Q	Radiation	$Z_{in} = R_{in} + j X_{in}$	
	Resistance	R _{in}	Xin
100	18.81215	31.92312	5.67854
200	19.00825	25.566	6.01933
300	19.07317	23.44536	6.10916
400	19.10554	22.38480	6.14916
500	19.12493	21.74840	6.17274
600	19.13785	21.32410	6.1817
700	19.14707	21.02101	6.19727
800	19.15398	20.79369	6.02473
900	19.15936	20.61688	6.21044
1000	19.16366	20.47574	6.21495
1100	19.16717	20.35970	6.2186
1200	19.17010	20.26326	6.22161
1300	19.17258	20.18165	6.22414
1400	19.17471	20.1117	6.2263
1500	19.17655	20.05107	6.22816
1600	19.17816	19.99803	6.22977
1700	19.17958	19.95122	6.23119
1800	19 . 18084	19.90962	6.23245
1900	19.18197	19.87239	6.22358
2000	19. 18299	19.83889	6.23458
80	19.20230	19.2023	6.25314

outh from the such Miles X,

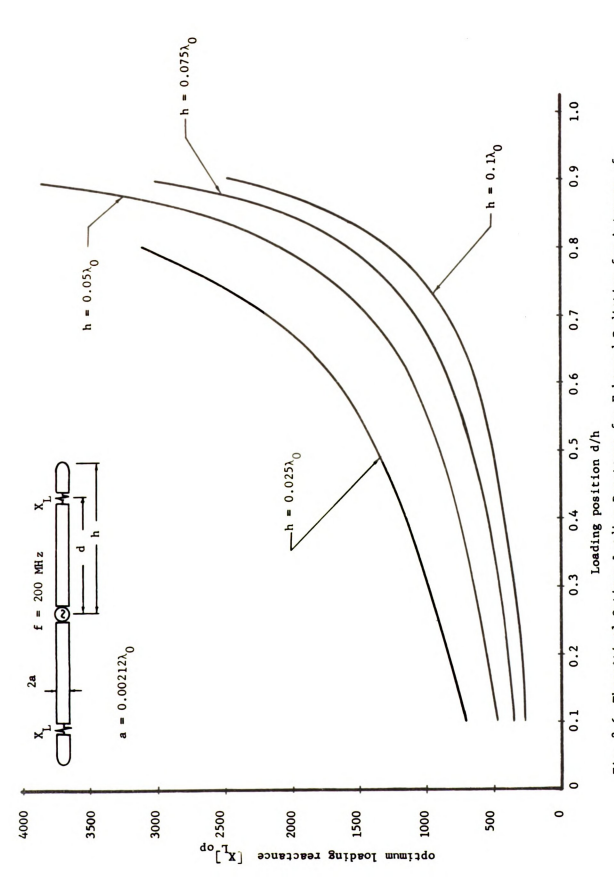


Fig. 3.6 Theoretical Optimum Loading Reactance for Enhanced Radiation for Antennas of Various Lengths as a Function of Loading Position (h = 0.025_o $\sim 0.1\lambda_o$)

X ZHW OOC # 1

x, , , a

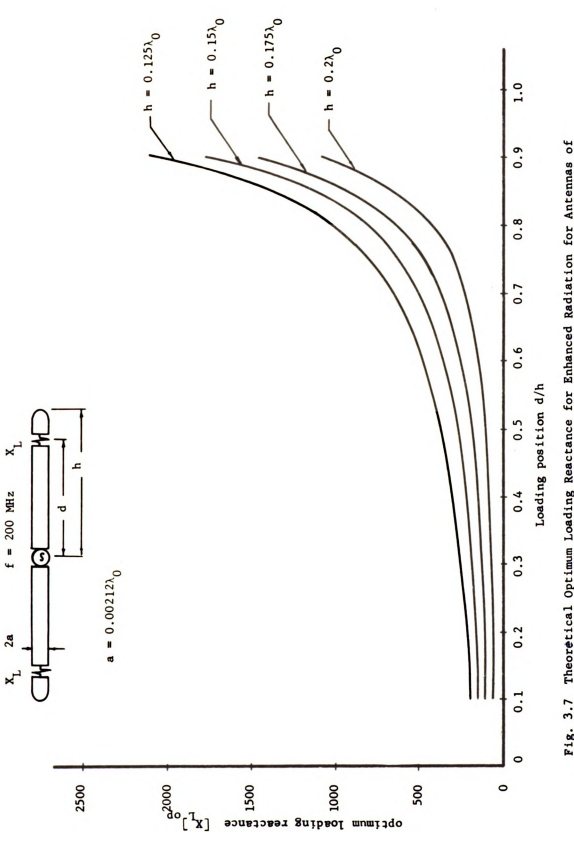


Fig. 3.7 Theoretical Optimum Loading Reactance for Enhanced Radiation for Antennas of Various Lengths as a Function of Loading Position (h = 0.125) $_0$ ~ 0.2 $_0$

input impedance and the transmission line which excites the antenna.

3.3.4 Radiation Pattern

The radiation fields of the short antenna with optimum impedance loading are obtained from eq. (3.1) and eq. (3.5) as

$$\begin{cases} E_{\theta}^{r} \doteq -j \frac{\varsigma_{0}}{2\lambda_{0}} \frac{e^{-j\beta_{0}R_{0}}}{R_{0}} & A_{c} \\ B_{\Phi}^{r} \doteq -j \frac{\mu_{0}}{2\lambda_{0}} \frac{e^{-j\beta_{0}R_{0}}}{R_{0}} & A_{c} \end{cases}$$

$$(3.8)$$

Since the current distribution $I_{\rm g}(z)$ of eq. (2.24) depends only upon the dimensions of antenna, its excitation frequency, and the impedance and position of the loading, eq. (3.8) can be expressed as

$$\begin{cases} E_{\theta}^{r} = E_{0}F(\theta) \\ B_{\Phi}^{r} = B_{0}F(\theta) \end{cases}$$

$$j\beta_{0}R_{0}$$

where

$$E_{0} = -j \frac{c_{0}}{2\lambda_{0}} \frac{e^{-j\beta_{0}R_{0}}}{R_{0}} A_{c}$$

$$B_{0} = -j \frac{\mu_{0}}{2\lambda_{0}} \frac{e^{-j\beta_{0}R_{0}}}{R_{0}} A_{c}$$

$$F(\theta) = Sin\theta$$

The radiation pattern of the short antenna with optimum reactance loading is consequently similar to that of an unloaded short antenna as indicated by Fig. 3.8. It is roughly independent of the impedance and position of the loading inductors.

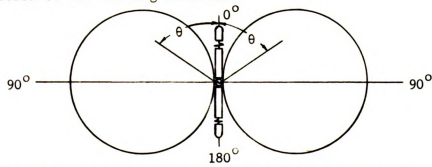


Fig. 3.8 Radiation Pattern of the Short Antenna with Optimum Reactance Loading.

3.4 Loaded Short Antenna with Increased Input Resistance and Inductive Input Reactance:

By investigating the current distribution of eq. (2.24) and input impedance of eq. (2.26), for different non-dissipative impedance loadings, it is found that the input resistance of the short antenna can be increased to a very large value, while the input reactance simultaneously changes from capacitive to inductive. This newly observed phenomenon occurs when the reactance of the non-dissipative loading (having fixed position) is further increased beyond its value $\begin{bmatrix} X_L \end{bmatrix}_{op}$ for which $X_{in} = 0$. In this case, the antenna can be tuned easily to resonance by a high Q series capacitor at its input terminals. Consequently, the matching between antenna and transmission system is improved, with the result that the power radiated by the short antenna is significantly enhanced relative to that of an unloaded short antenna.

3.4.1 Typical Current Distribution

If a short antenna is loaded by an appropriate non-dissipative impedance at a given position along its surface, such that its input resistance is increased and its input reactance becomes inductive, the current distribution of eq. (2.24) has a general form presented in Fig. 3.9.

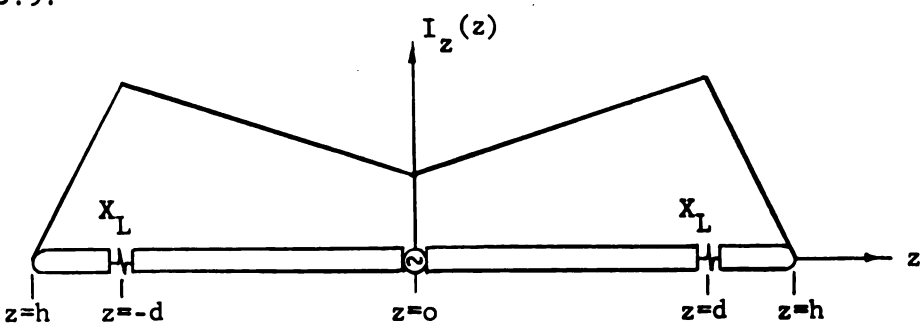


Fig. 3.9 Current Distribution along Antenna with Increased Input Resistance and Inductive Input Reactance.

The crea

and

phas

and acta

the

that

imat

this

tanc

syst

With obta

duct

impe

3 :

ca_{T.}

in

005 I e i

Pc :

The amplitude of the current is small at the input terminals, increases almost linearly to its maximum value at the loading points and then decreases to zero at the extremities of the antenna. The phase of the current is almost constant along the antenna.

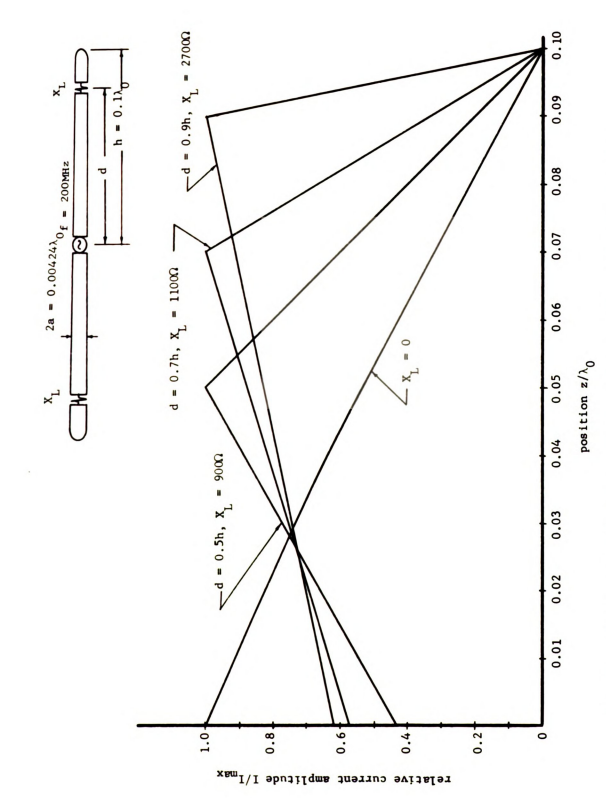
The current distributions along antennas with $h = 0.1\lambda_0$ and d = 0.5h, 0.7h and 0.9h for appropriately chosen loading reactances are plotted in Fig. 3.10. These optimum reactances (and the corresponding current distributions) are chosen in such a way that the input resistance to the antenna is increased to approximately six times that of an unloaded antenna, the criterion for this choice being in this case to match the antenna input resistance to the characteristic impedance of the exciting transmission system.

3.4.2 Input Impedance

By using eq. (2.26), the input impedance of a short antenna with increased input resistance and inductive input reactance are obtained numerically as in table 3.4. It is found that the inductive input reactance is a stronger function of the loading impedance than is the input resistance.

3.4.3 Radiated Power

Since the input resistance of the short antenna in this case can be increased by a much greater factor than for the case described in Sec. 3.3, the degree of matching with its transmission system is consequently improved significantly as the antenna is tuned to reasonance by a non-dissipative series capacitor at its driving point. Theoretically, therefore, more power is radiated by this



The Current Distributions on an Antenna with Increased Input Resistance and Input Inductive Reactance for Various Loading Reactances. Fig. 3.10

Table 3.4 Input Impedance of Short Antenna with Increased Input Resistance and Inductive Input Reactance.

1 0 075			
$h = 0.075\lambda_0, a = 0.00212\lambda_0$		$h = 0.1\lambda_0$, $a = 0.00212\lambda_0$	
Loading X _L Reactance	Z (for d = 0.5h)	Loading X Reactance	Z (for d = 0.5h)
0	4.3810 - j 608.58	0	8.116 - j 468.287
700	9.641 + j 72.322	600	19.36 + j 190.30
800	11.772 + j 291.736	700	25.43 + j 463.33
900	15.044 + j 592.851	800	36.397 + j 883.67
1000	20.53 + j 1031.74	900	60.135 + j 1614.56
1100	31.028 + j 1730.99	1000	132.122 + j 3201.50
Х _L	Z_{in} (for d = 0.7h)	Х _L	z_{in} (for $d = 0.7h$)
0	4.381 - j 608.58	0	8.116 - j 468.287
1100	11.59 + j 25.307	900	21.63 + j 89.38
1200	14.77 + j 236.85	1000	29.32 + j 325.86
1300	20.53 + j 569.52	1100	45.945 + j 747.74
1400	33.32 + j 1169.06	1200	98.03 + j 1713.40
X _L	$z_{in}(for d = 0.9h)$	X _L	z in(for d = 0.9h)
0	4.381 - j 608.58	0	8.116 - j 468.287
3 100	17.943 + j 206.2	2500	23.24 + j 20.865
3 200	27.95 + j 605.7	2600	31.177 + j 210.15
3 300	64.23 + j 1642.44	2700	50.567 + j 588.9
		2800	136.93 + j 1725.83

short antenna than by the antenna of Sec. 3.3. For the practical non-ideal case, this is not always true, since the powers dissipated in the loading inductors and tuning capacitor are larger than in Sec.

3.3, and therefore, the radiated power may sometimes be reduced more than the former case.

3.5. Conventional Top-Loaded (or End-Loaded) Antenna:

In Sec. 3.3, it is indicated that the current distribution along a short antenna with optimum double reactance loading is almost constant between the loading points, and it is further indicated in Sec. 3.2 that the power radiated by the antenna is approximately proportional to the square of the area beneath the antenna current distribution. Therefore, if the loading position is shifted to the end of the antenna, or if the antenna is end-loaded by an optimum reactance, the current will remain nearly constant along the entire length of the antenna, and the radiated power will be increased by four times relative to that of the unloaded antenna. Since the end loaded antenna represents an extremely difficult theoretical problem, only an experimental study will be conducted in Chapter 6. Various types of end and impedance loadings will be studied experimentally to investigate the characteristics of end-loaded antennas.

3.6 Comparison of Doubly Loaded Antenna with Unloaded Base-Tuned Antenna for Radiated Power and Efficiency:

In Sec. 3.1, it is indicated that the input power supplied through a transmission system to a double loaded antenna which is

tuned to resonance is always greater than that supplied to an unloaded antenna which is base tuned.

If the double loading or base tuning inductors are non-ideal (it is assumed that the capacitor for tuning the doubly loaded antenna to resonance is an ideal capacitor), and consequently dissipate a certain fraction of the input power, the efficiency of the antenna should be considered. The efficiency of an antenna is defined as

Efficiency =
$$\frac{(P_{in} - P_{dissip.})}{P_{in}} \times 100\%$$

Therefore, the effiencies of the optimum doubly loaded antenna (only the doubly loaded antenna with increased input resistance and zero input reactance will be discussed in this section, since the efficiency for case with increased input resistance and inductive input reactance is similar to the former one if the tuning capacitor is assumed to be ideal) and the base tuned, unloaded antenna designated as $(E_{\rm ff})_{\rm no}$, respectively, are calculated as

$$(E_{ff.})_{op} = [1 - 2 \frac{I_z^2(z=d)}{I_z^2(z=0)} \frac{(R_L)_{op}}{(R_{in})_{op}}] \times 100\%$$

$$(E_{ff})_{no} = \left[\frac{(R_{in})_{no}}{(R_{in})_{no} + R_{b}}\right] \times 100\%$$

where

$$(R_L)_{op} = \frac{(X_L)_{op}}{Q} = \text{resistance of optimum double loading inductors } [X_L]_{op} \text{ with given } Q.$$

$$R_b = \frac{X_b}{Q} = \text{resistance of base tuning inductor } X_b \text{ with given } Q$$
.

The efficiencies of antenna with fixed dimensions, for both the optimum doubly loaded and the base tuned cases, which result with different Q values for the inductors are indicated in Fig. 3.11. From these numberical results, it is evident that the antenna efficiencies are very nearly equal for both the doubly loaded and the unloaded (or base-tuned) antennas. The power radiated by the doubly loaded antenna is therefore greater than that of the base tuned antenna, since the input power for the former case is always greater than for the latter if the antennas are driven by matched generators. The same conclusion is indicated by the numerical results presented in Fig. 3.12, where the ratio $(P_{\rm rad.})_{\rm op}/(P_{\rm rad.})_{\rm no}$ is plotted for various value of Q for the optimum reactance $(X_{\rm L})_{\rm op}$ and the base tuning reactance $X_{\rm b}$ when the antennas are driven by matched generators. It is demonstrated that $(P_{\rm rad.})_{\rm op}$ is always greater than $(P_{\rm rad.})_{\rm no}$ under these conditions.

3.7 Bandwidth of Short Antenna with Enhanced Radiation:

The optimum loading reactance for enhanced radiation and the reactance of a fixed inductance loading are indicated as a function of frequency in Fig. 3.13 for an antenna of fixed dimensions. The fixed loading inductance is chosen such that its reactance \mathbf{X}_L is equal to the optimum reactance $\begin{bmatrix} \mathbf{X}_L \end{bmatrix}_{op}$ at a frequency of 200 MHz. It is observed that the optimum loading reactance is a decreasing function of frequency. The reactance of the fixed inductor, however, is directly proportional to frequency. As indicated in Fig. 3.13, the optimum reactance $\begin{bmatrix} \mathbf{X}_L \end{bmatrix}_{op}$ is 850 Ω at \mathbf{f} = 200 MHz for an

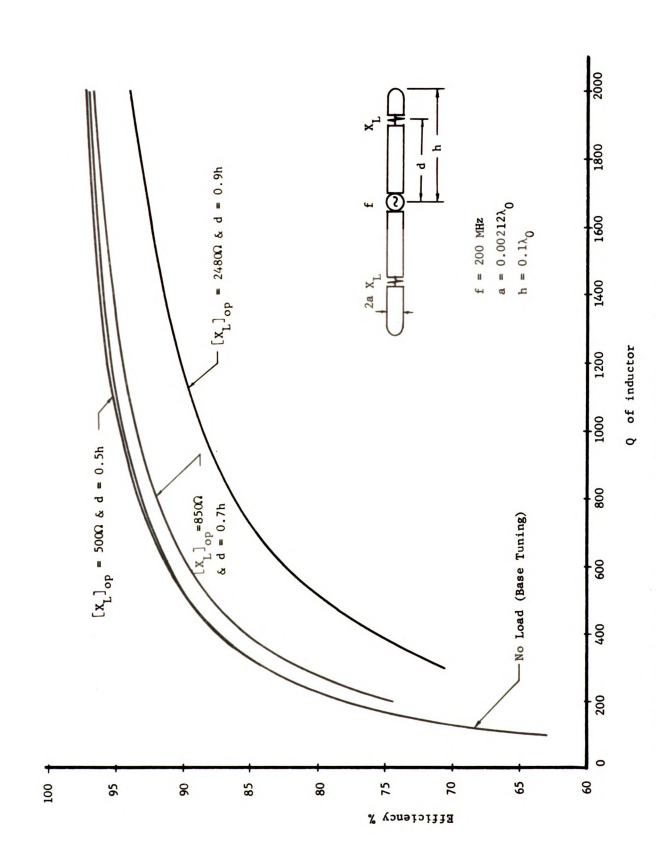


Fig. 3.11 Efficiencies of Optimum Reactively Loaded and Base-Tuned Antennas as Functions of Inductor Q.

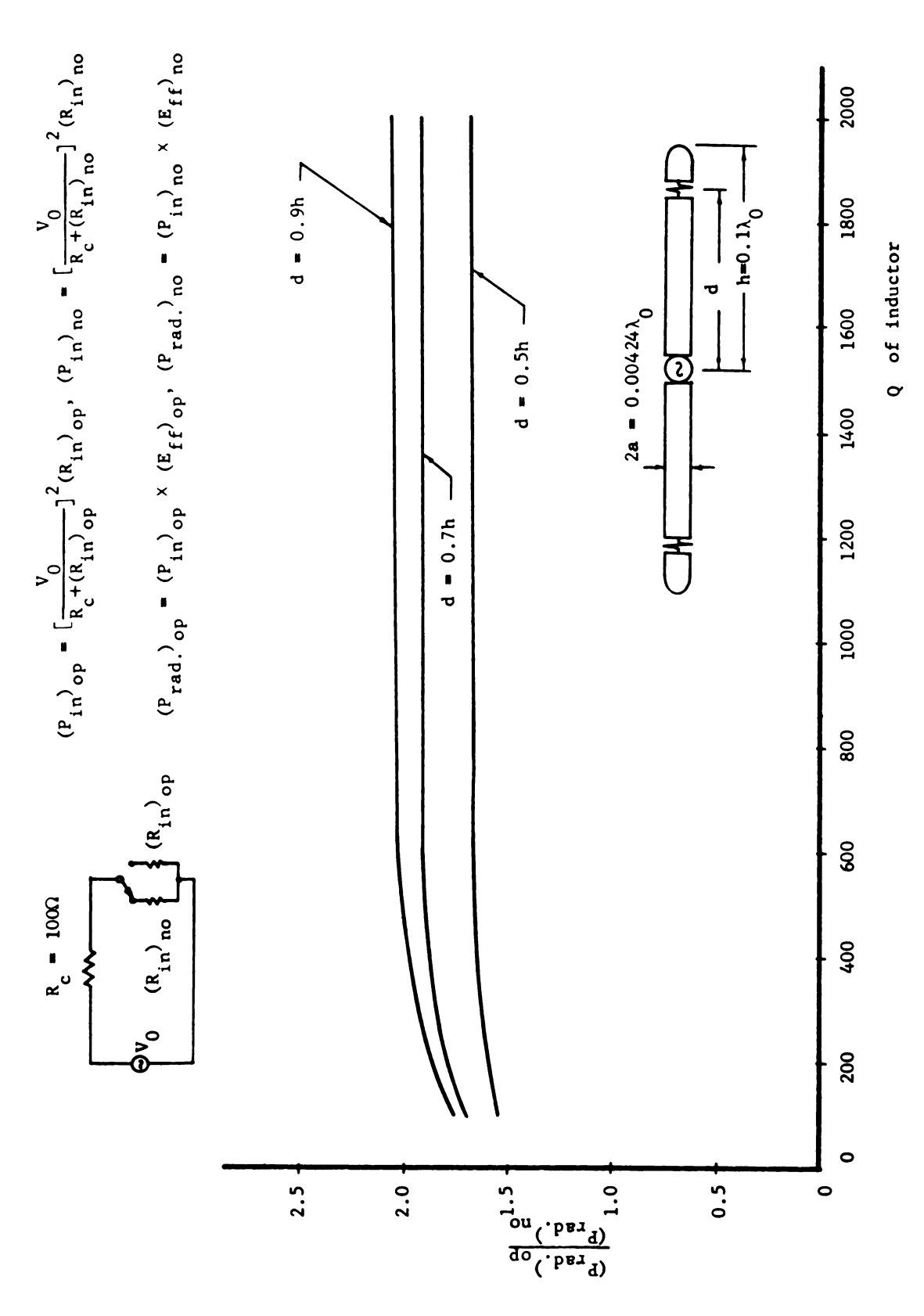
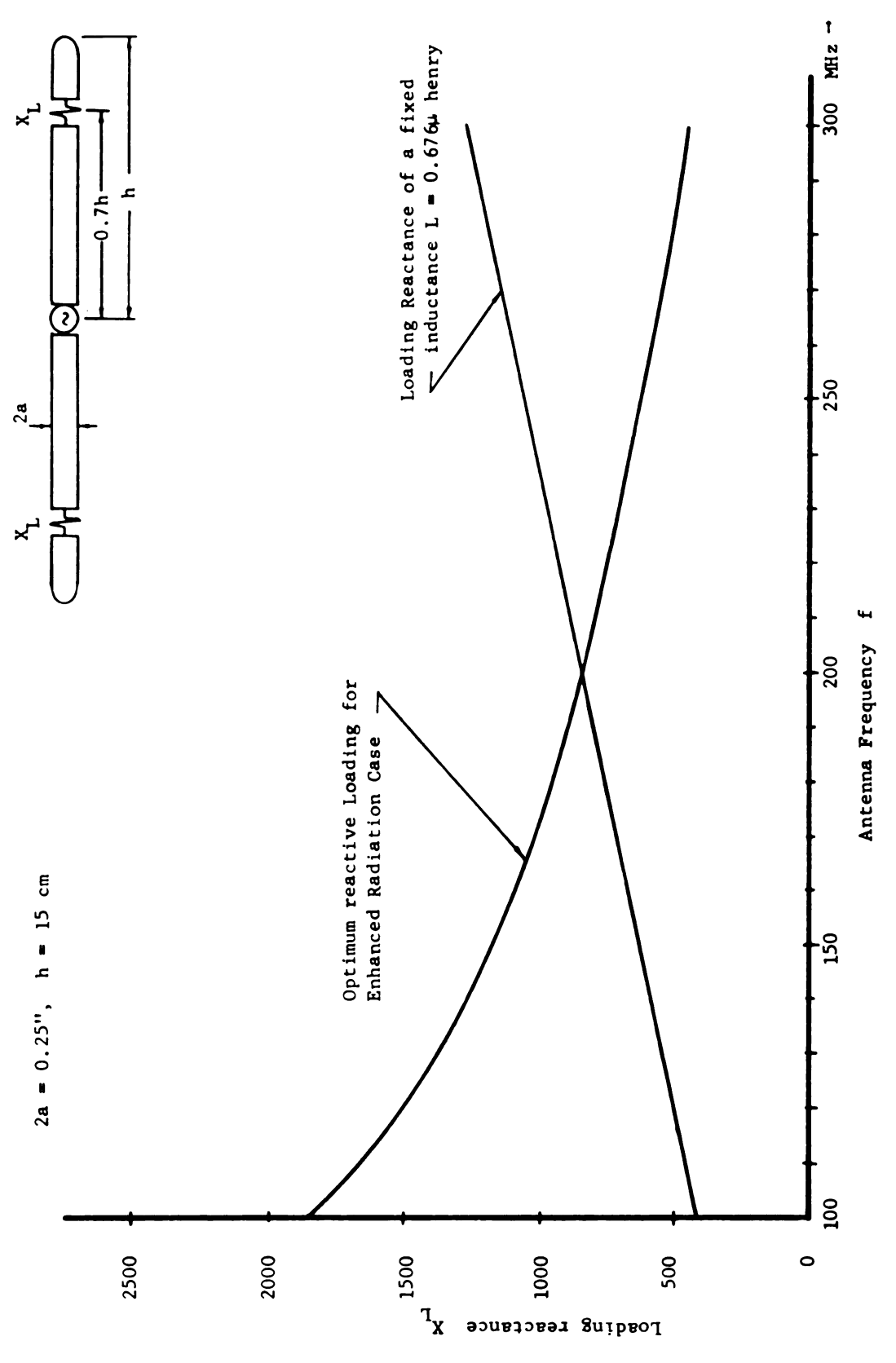


Fig. 3.12 The Ratio of Powers Radiated by Optimumly Loaded Antenna and Base-Tuned Antenna as a Function of Inductor Q.



Theoretical Optimum Loading Reactance for Enhanced Radiation Compared with the Loading Reactance of a Fixed Inductor $(L = 0.676\mu henry)$. Fig. 3.13

antenna with a=0.125 inch, h=15 cm. As the frequency is varied to 200 MHz \pm 10 MHz, the actual reactance of the fixed inductance (L = 0.676 μ Henry) varies to 850 Ω \pm 50 Ω , while the optimum reactance varies to 850 Ω \pm 50 Ω . This implies that the difference between the actual reactance of a fixed inductor and the optimum reactance for enhanced radiation is \pm 100 Ω for a frequency difference of \pm 10 MHz. For a 5% variation in frequency the reactance of a fixed inductor varies by 11.8% from the optimum reactance. This result appears to imply that the bandwidth associated with a lumped inductor implementation of the optimum loading reactance will be quite narrow.

The input impedance of an unloaded antenna and an antenna doubly loaded with a fixed inductance of $L=0.676\mu$ Henry are compared in Fig. 3 14. It is noted that the impedance of the doubly loaded antenna varies with frequency much more strongly than does that of the unloaded antenna. This implies again that the bandwidth of the doubly loaded antenna with enhanced radiation is relatively small.

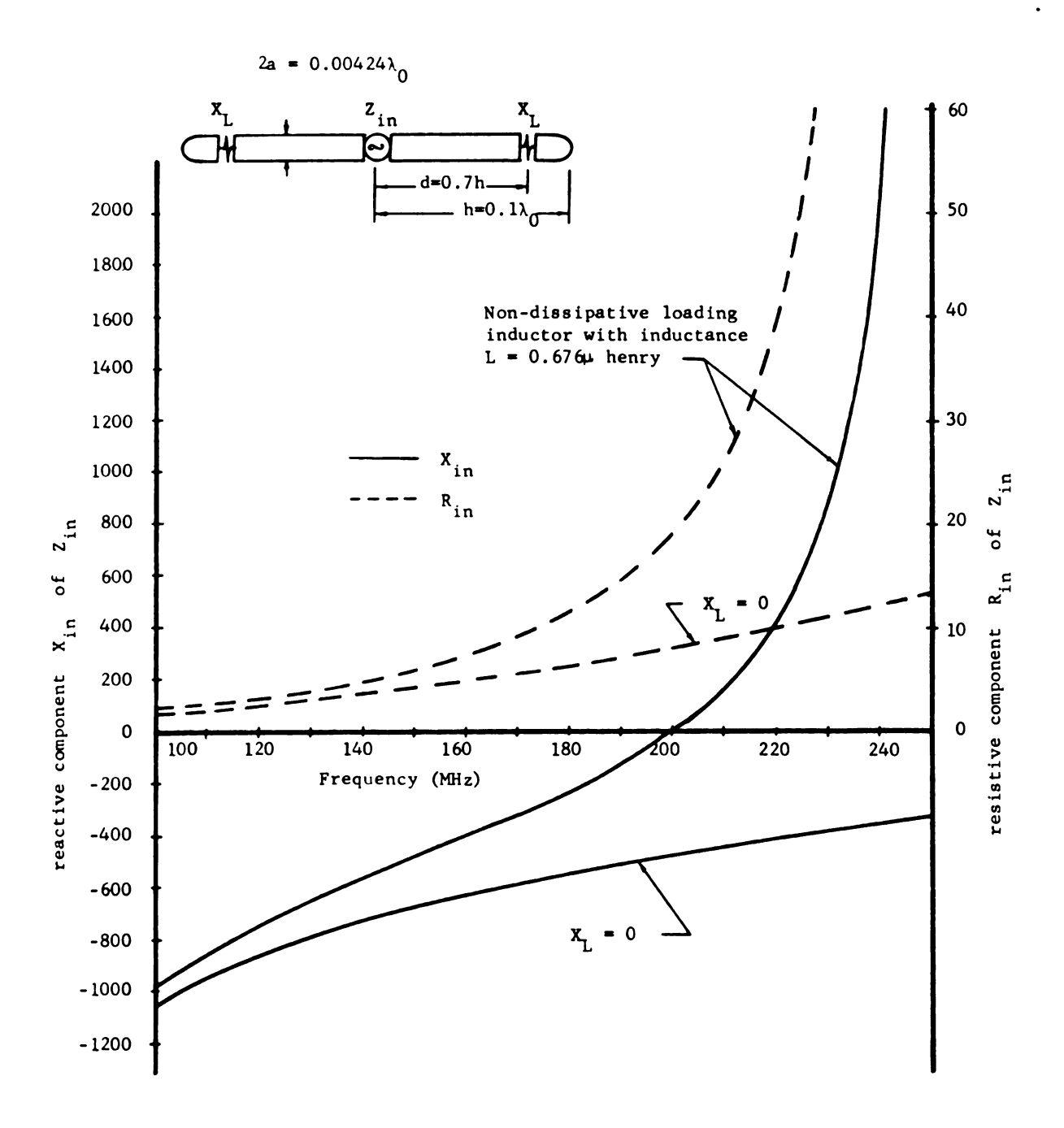


Fig. 3.14 Theoretical Input Impedances for Zero and Reactive Loading (L = 0.6764henry) as Functions of Frequency

CHAPTER 4

SHORT ANTENNAS WITH IMPROVED DIRECTIVITY

4.1 Introduction:

It is well known that a conventional short linear antenna has low directivity since its radiation pattern has a very large beamwidth. In this research, a double impedance loading technique is applied to appropriately modify the antenna current and thereby improve its directivity.

In 1943, La Paz and Miller [2] attempted to determine the maximum directivity theoretically available from a line source antenna by solving for the corresponding optimum antenna current distribution. Later, Bouwkamp and De Bruijin [3] pointed out that arbitrarily high directivities might be achieved from a linear antenna by properly adjusting its current distribution. Similar results for antennas of different geometries were also derived by Riblet [4] in 1948. In 1949, Chu [9] indicated that several problems inherently associated with highly directive antennas are an unusually high q, a narrow bandwidth, and a low efficiency.

Although no methods were suggested for realizing the required optimum current distributions, the research of the above investigators implies that various degrees of improvement in directivity, with associated degradation of the radiated power, may be achieved by careful adjustment of the antenna current distribution.

It is the object of this research to investigate the possibility of physically realizing the optimum current distribution to improve the directivity of a short linear antenna. This current distribution

is implemented by doubly loading the antenna by a pair of lumped impedances.

Through the use of an optimum impedance loading it is found that an optimum current distribution is realized when the phase of the current is reversed along the short antenna. The directivity corresponding to such a distribution of current is improved significantly. It is found that such a current distribution results in an antenna having poor efficiency and small radiated power, and that these characteristics are closely associated with the improved directivity.

A theory is developed to predict the optimum loading impedance for improving the directivity of a short antenna and to determine its input impedance, current distribution, efficiency, and radiated power in the following sections.

4.2 Radiation Field of a Short Antenna with Improved Directivity;

For calculating the radiation fields of a short antenna with increased directivity, a mathematical approach similar to that in Sec. 3.2 is applied. Eq. (3.4) can be used directly subject to the same assumptions and approximations, i.e.,

$$A_{\theta}^{r} = -\frac{\mu_{o}}{2\pi} \frac{e^{-j\beta_{o}R_{o}}}{R_{o}} \sin\theta \int_{o}^{h} I_{z}(z') (1 - \frac{1}{2}\beta_{o}^{2}z'^{2}\cos^{2}\theta) dz'$$
 (4.1)

where $I_z(z')$ is the current distribution of eq. (2.24). The well known \vec{E} and \vec{B} -fields in the radiation zone of the antenna

$$\begin{cases} E_{\theta}^{r} = -j & \omega & A_{\theta}^{r} \\ B_{\phi}^{r} = \frac{1}{v_{Q}} & E_{\theta}^{r} \end{cases}$$

are therefore obtained as

$$\begin{cases}
E_{\theta}^{r} \stackrel{:}{=} \frac{j \zeta_{o}}{\lambda_{o}} \frac{e^{-j\beta_{o}R_{o}}}{R_{o}} & \text{A } F(\beta_{o}h,\theta) \\
B_{\phi}^{r} \stackrel{:}{=} \frac{j \mu_{o}}{\lambda_{o}} \frac{e^{-j\beta_{o}R_{o}}}{R_{o}} & \text{A } F(\beta_{o}h,\theta)
\end{cases} (4.2)$$

where

$$A = \int_0^h I_z(z')dz'$$
 the area below the current distribution of eq. (2.24)

$$F(\beta_0 h, \theta) = \sin\theta (1 - \frac{B}{A} \cos^2 \theta)$$
 (4.3)

and

$$B = \frac{1}{2} \int_{0}^{h} \beta_{o}^{2} z'^{2} I_{z}(z') dz'.$$

By investigating eq. (4.3), it is observed that the radiation pattern is a strong function of the ratio B/A. From numerical results for the current distribution $I_z(z)$ expressed by equation (2.24), it is found that the antenna current has approximately a variable-amplitude and constant-phase distribution along the antenna. This implies that although the amplitude of the current varies from point to point along the antenna, its phase is almost constant except for the possibility of a rapid 180° phase reverse that may be accounted for by changing the sign of the amplitude. By using this constant-phase variable-amplitude approximation, the current distribution $I_z(z)$ of eq. (2.24) may be represented approximately by some real function $i\theta_0$ multiplied by a constant phase factor $e^{i\theta_0}$, i.e.,

$$I_z(z) = f(z)e^{i\theta}$$

where f(z) may take both negative and positive values. Therefore, the ratio B/A is approximately equal to a real number, i.e.,

$$K = \frac{B}{A} = \frac{\frac{1}{2} \int_{0}^{h} (\beta_{o}z')^{2} I_{z}(z') dz'}{\int_{0}^{h} I_{z}(z') dz'} = \text{real number}.$$
 (4.4)

The radiation pattern of the doubly loaded, short antenna is the graphical representation of

$$F(\beta_0 h, \theta) = Sin\theta(1 - K \cos^2 \theta)$$
 (4.5)

It should be recalled that the directivity of an antenna is the ratio of the maximum radiation intensity to the average radiation intensity. In other words, the directivity is the ratio between the radiated power P_{max} , when the antenna is assumed to radiate with its maximum power in every direction and the total radiated power P_{rad} , of the antenna, i.e.,

D(directivity) =
$$\frac{P_{\text{max.}}}{P_{\text{rad.}}} = \frac{\frac{dP}{d\Omega}|_{\text{max.}}}{\frac{1}{4\pi}P_{\text{rad.}}} = \frac{\text{Max. radiation intensity}}{\text{Average radiation intensity}}$$
 (4.6)

where

$$P_{\text{max}}$$
 = $4\pi \frac{dP}{d\Omega}|_{\text{max}}$.

$$\frac{dP}{d\Omega} = R_0^2 \hat{R}_0 \cdot \vec{S}^r \dots \text{ power radiated per unit solid angle}$$

and

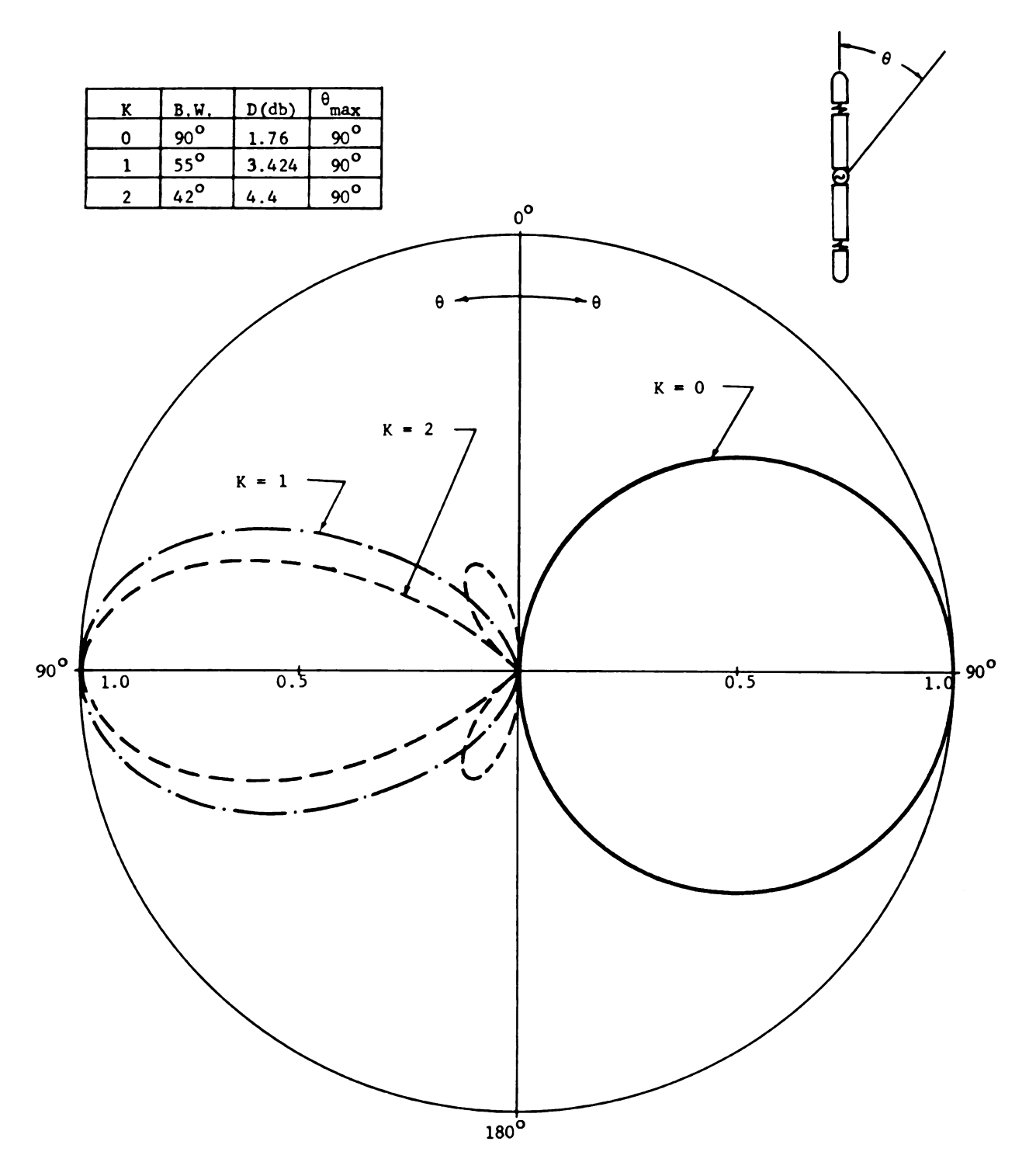


Fig. 4.1 Theoretical Radiation Patterns of Short Antennas with K = 0, 1, and 2.

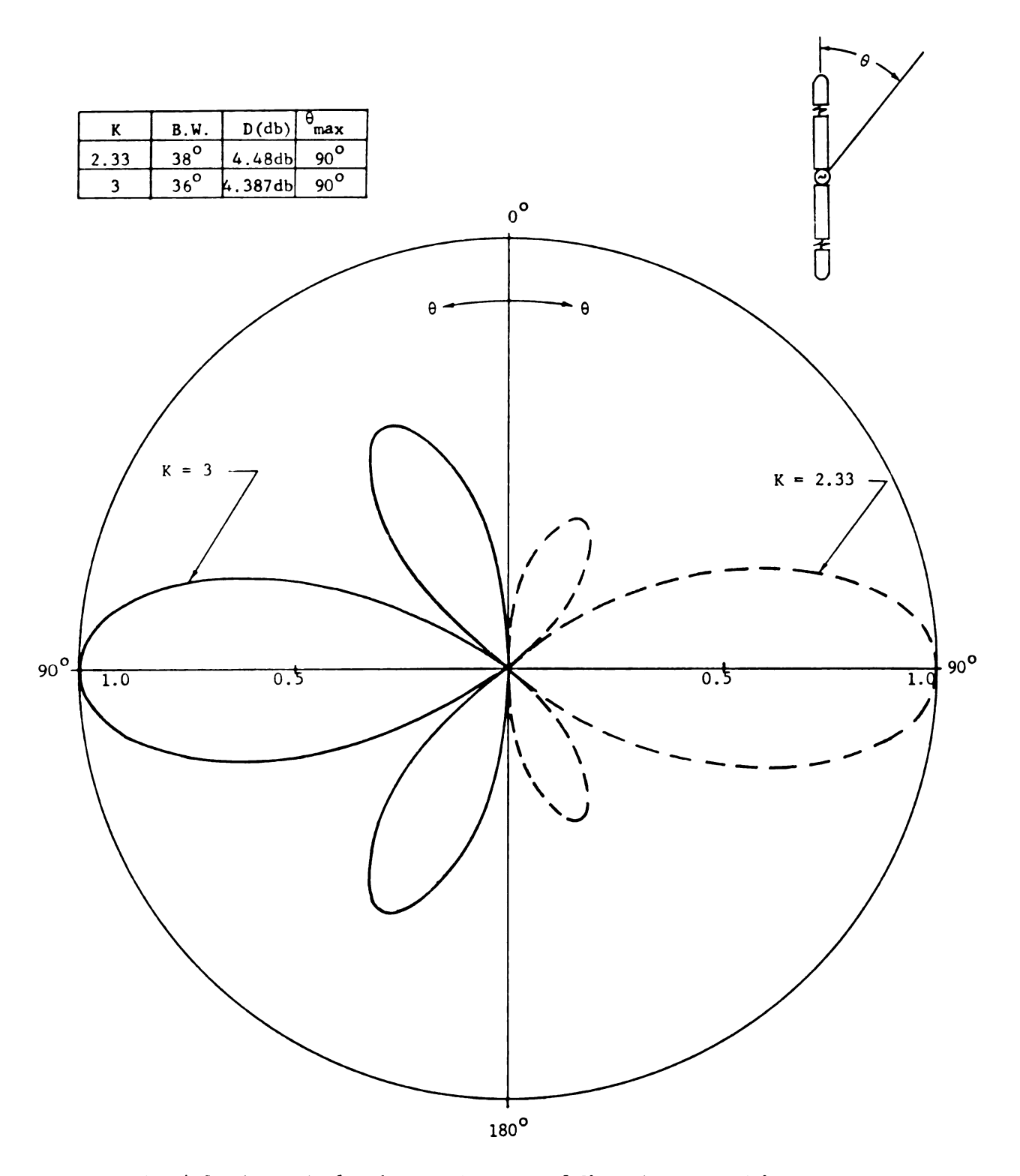


Fig. 4.2 Theoretical Radiation Patterns of Short Antennas with K=2.33 and 3.

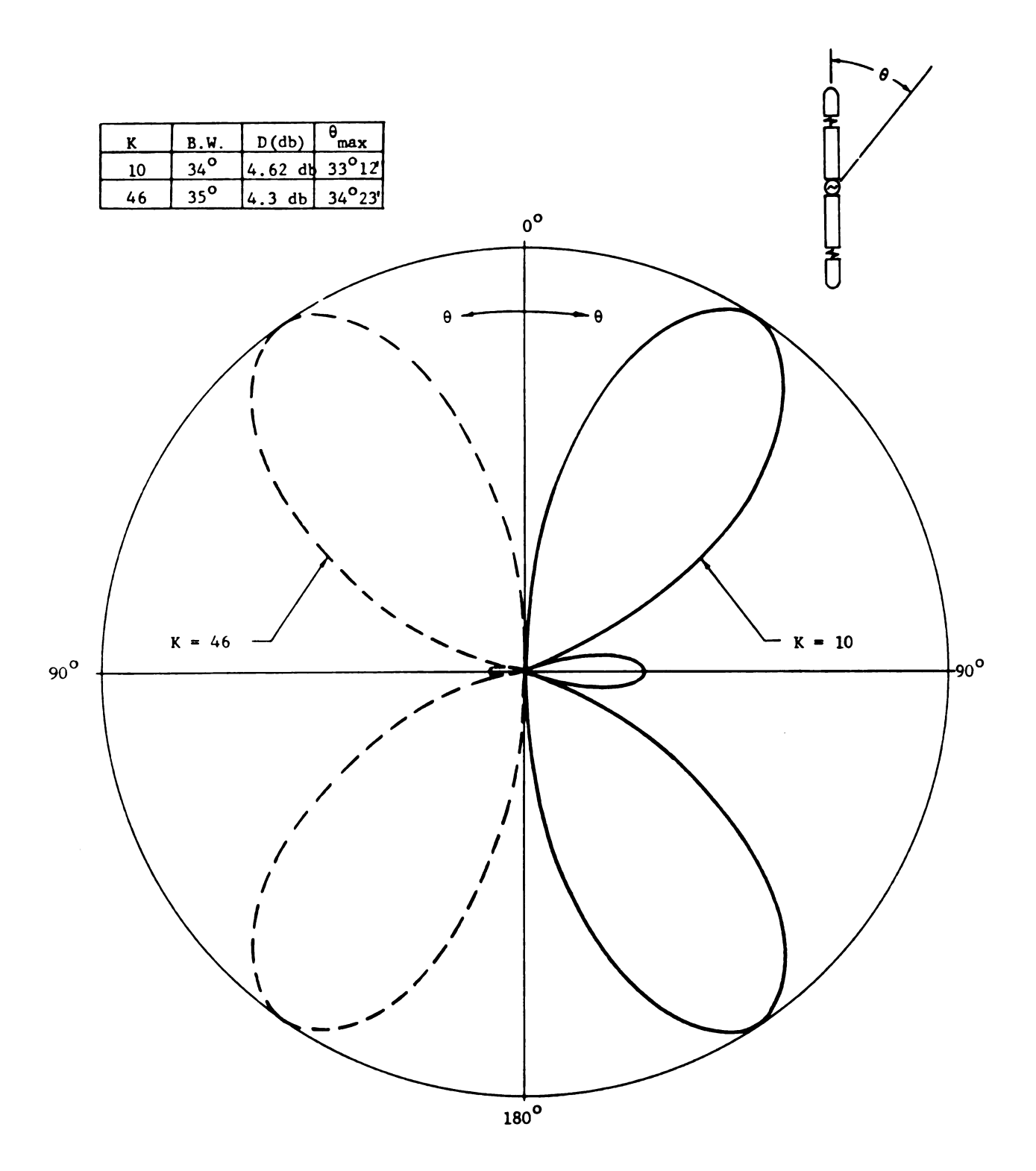


Fig. 4.3 Theoretical Radiation Patterns of Short Antennas with K = 10 and 46.

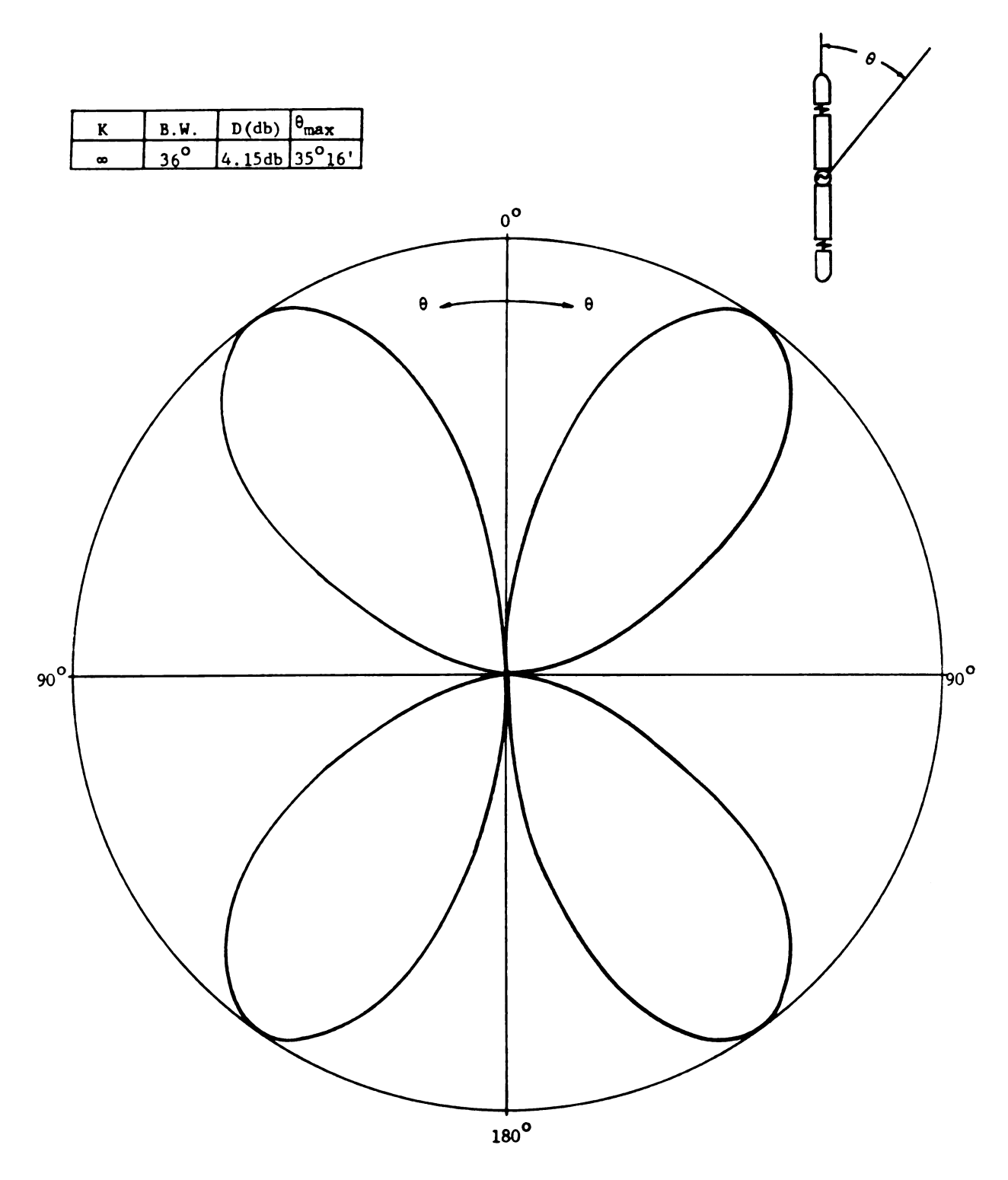


Fig. 4.4 Theoretical Radiation Pattern of Short Antennas with $K\,\rightarrow\,\infty$.

 $\vec{S}^r = \frac{1}{2}(\vec{E} \times \vec{H}^*)$ is the Poynting's vector in the radiation zone.

The directivity of an antenna in db is defined as

$$D_{db} = 10 \log_{10}(D) db.$$
 (4.7)

The beamwidth of an antenna radiation pattern is defined as the angle between the two half-power points of its major lobes.

From eq. (4.2), the total power radiated by an antenna for each specified K is obtained as

$$P_{\text{rad.}} = 2\pi R_o^2 \int_0^{\pi} \frac{1}{2} (\vec{E} \times \vec{H}^*) \cdot R_o \sin\theta \, d\theta$$

$$= \frac{\pi \zeta_o}{\lambda_o} A^2 \int_0^{\pi} \sin^3\theta (1 - K \cos^2\theta)^2 d\theta$$

$$= c_1 \left[\frac{4}{105} (3K^2 - 14K + 35) \right] \qquad (4.8)$$

$$c_1 = \frac{\zeta_o \pi A^2}{\lambda_o^2}$$

where

The average radiation intensity is then $\frac{1}{4\pi} P_{rad}$. By differentiating eq. (4.3) with respect to θ , the angle of maximum radiation, θ_{max} , is obtained as

$$\begin{cases} \theta_{\text{max}} = \frac{\pi}{2} & \text{for } 0 \le K \le 4 \\ \theta_{\text{max}} = \cos^{-1} \sqrt{\frac{2K+1}{3K}} & \text{for } K \ge 4 \end{cases}$$

This means that for K > 4, the major lobe is in off-broadside direction. The maximum power intensity is therefore determined as

$$\frac{dP}{d\Omega}\Big|_{\text{max.}} = R_{\text{o}}^{2}\hat{R} \cdot \vec{S}_{\text{max.}}^{\text{r}} = R_{\text{o}}^{2}\hat{R} \cdot \frac{1}{2}(\vec{E} \times \vec{H}^{\star})_{\text{max.}}$$

$$= \frac{1}{2} \frac{\zeta_{\text{o}}}{\lambda_{\text{o}}^{2}} A^{2} \left[\sin \theta_{\text{max.}} (1 - K \cos^{2} \theta_{\text{max.}})^{2} \right]$$

$$= \begin{cases} C_{1}/2\pi & \text{for o } \leq K \leq 4 \\ \frac{2C_{1}}{\pi} \frac{(K-1)^{3}}{27K} & \text{for } K \geq 4 \end{cases} \tag{4.9}$$

Therefore, the directivity for each specified K is obtained as

$$D(directivity) = \begin{cases} \frac{105}{2} & \frac{1}{(3K^2 - 14K + 35)} & \text{for } o \le K \le 4 \\ \frac{70}{9} & \frac{(K-1)^3}{(3K^2 - 14K + 35)K} & \text{for } K \ge 4 \end{cases}$$

The maximum directivity for the case of $\theta_{\text{max}} = 90^{\circ}$ (or $0 \le K \le 4$) is therefore determined from eq. (4.9) by letting $\frac{\partial D}{\partial K} = 0$. This leads to K = 2.33 as the optimum value. The case for $K \ge 4$ is not discussed further since its major lobe is in off-broadside direction.

The directivity in db is obtained by substituting eq. (4.9) into eq. (4.7) for $0 \le K \le 4$ and $K \ge 4$ respectively, as

$$D_{db} = \begin{cases} 10 & \log_{10} \left[\frac{105}{2} \frac{1}{(3K^2 - 14K + 35)} \right] & \text{for } 0 \le K \le 4 \\ 10 & \log_{10} \left[\frac{70}{9} \frac{(K-1)^3}{(3K^2 - 14K + 35)K} \right] & \text{for } K \ge 4 \end{cases}$$
(4.10)

The directivity and beamwidth of the short antenna, as determined by eq. (4.5), (4.9) and (4.10) are tabulated in Fig. 4.1 through Fig. 4.4 for the various values of K. For K = 0, the

radiation pattern is just that of a conventional short antenna (B.W. = 90°), and the directivity is D = 1.7db (θ_{max} = 90°). For K = 1, the major lobe becomes sharper (B.W. = 55°), and the directivity is improved from the original 1.76db to 3.424db $(\theta_{max} = 90^{\circ})$. When K = 2, although side-lobes appear, it is found that the beamwidth becomes relatively narrow (B.W. = 42°) and the directivity is increased to $D = 4.4 \text{db} \left(\theta_{\text{max}} = 90^{\circ}\right)$. For K = 2.33, the beamwidth is equal to 38° and the antenna has the highest directivity D = 4.48db in the broadside direction $(\theta_{\text{max}} = 90^{\circ})$. For K = 3, the side lobes grow larger and the directivity is decreased to 4.387db ($\theta_{\text{max}} = 90^{\circ}$). For K = 10, the lobe in the broadside direction becomes a minor lobe, and the minor lobe in the off-broadside direction becomes a major lobe with the maximum radiation in $\theta_{\text{max}} = 33^{\circ}12'$, and with a directivity equal to 4.64db (B.W. = 34°). For K = 46, the broadside field is decreased even more than the case of K = 10, and with D = 4.3db, $\theta_{\text{max}} = 34^{\circ}23'$ and B.W. = 35° . As $K \rightarrow \infty$, the broadside field vanishes completely and the radiation pattern has four symmetrical lobes (shown as in Fig. 4.4), each having B.W. = 36° , and the directivity is equal to 4.15db ($\theta_{max} = 35^{\circ}16'$). Since the most interesting radiation field is the broadside field $(\theta_{max} = 90^{\circ})$, therefore, it is found that the most desirable radiation pattern is achieved for the optimum value of K = 2.33. But for mathematical simplicity, the value of K = 2 will be used in the numerical examples in the following sections.

It is now evident that to have an improved directivity the value of K should closely approximate 2.33. From eq. (4.4), this

condition requires $\int_0^h I_z(z')dz'$ to be very small, thus implying phase-reversal of the current along the antenna.

4.3 Optimum Loading Impedance for Improved Directivity:

From the results of the previous section, it is evident that by properly choosing the real constant K, or by properly adjusting the current distribution $I_z(z)$, given by eq. (2.24), the directivity of a short linear antenna can be significantly improved relative to that of a conventional short antenna. Since the current distribution $I_z(z)$ of eq. (2.24) is a function of the antenna dimensions, the excitation frequency, and the impedance and position of the loading, the optimum loading impedance for improved directivity can be determined from eq. (4.4) and eq. (2.24) if K is specified and the antenna dimensions and its excitation frequency are given.

An expression for the optimum loading impedance $\begin{bmatrix} z_L \end{bmatrix}_{op}$ is obtained as follows:

Eq. (4.4) can be rewritten as

$$\frac{1}{2} \beta_{0}^{2} \int_{0}^{h} z'^{2} I_{z}(z') dz' = K \int_{0}^{h} I_{z}(z') dz'$$
 (4.11)

It is recalled that the current distribution $I_z(z)$ on the doubly loaded short antenna was given in eq. (2.24) as

$$I_{z}(z) = FC_{5}(\cos\beta_{o}z - \cos\beta_{o}h) + FC_{4}\sin\beta_{o}(h - |z|)$$

$$-j FC_{2}-2\sin\beta_{o}h \cos\beta_{o}d \cos\beta_{o}z - \cos\beta_{o}h(\sin\beta_{o}|z-d|$$

$$+ \sin\beta_{o}|z+d|)].$$

By substituting this expression into eq. (4.11) for a given value of K and carrying out the integration, a simple equation is obtained, after some rearrangement, as

$$FC_5D_6 + FC_4D_7 - j FC_2D_8 = 0$$
 (4.12)

where

$$\begin{split} D_6 &= \beta_o h (2 - \frac{1}{3} \beta_o^2 h^2) \cos \beta_o h + (\beta_o^2 h^2 - 2) \sin \beta_o h - 2K (\sin \beta_o h) \\ &- \beta_o h \cos \beta_o h) \\ D_7 &= \beta_o^2 h^2 + 2 (\cos \beta_o h - 1) - 2K (1 - \cos \beta_o h) \\ D_8 &= 2 (\beta_o^2 h^2 - 2) \cos \beta_o d + 2 (2 - \beta_o^2 d^2) \cos \beta_o h \\ &- 4K \sin^2 \beta_o h \cos \beta_o d + 4K (1 - \cos \beta_o h \cos \beta_o d) \cos \beta_o h. \end{split}$$

Since FC₂, FC₄ and FC₅ are all functions of the loading impedance Z_L , eq. (4.12) can be rearranged, after a great deal of algebraic manipulation, into a quadratic equation for Z_L , the solution to which gives the optimum loading impedance $\left[Z_L\right]_{OD}$, i.e.,

$$B_1 Z_L^2 + B_2 Z_L + B_3 = 0 (4.13)$$

where

$$D_{9} = \frac{T_{idi}}{30 T_{cd}T_{idr}} \operatorname{Sec} \beta_{o} h \operatorname{Sin} \beta_{o} (h-d) (\operatorname{Cos} \beta_{o} d - \operatorname{Cos} \beta_{o} h)$$

$$+ \frac{1}{15 T_{idr}} \operatorname{Sec} \beta_{o} h \operatorname{Cos} \beta_{o} d \operatorname{Sin}^{2} \beta_{o} (h-d)$$

$$D_{10} = 1 - \frac{T_{ca}}{T_{cd}} (\operatorname{Sec} \beta_{o} h - 1)$$

$$D_{11} = (\frac{T_{idi} T_{ca}}{T_{cd}} + j T_{ia}) \frac{(\operatorname{Sec} \beta_{o} h - 1)}{30 T_{idr} T_{cd}} \operatorname{Sec} \beta_{o} h \operatorname{Sin} \beta_{o} (h-d) (\operatorname{Cos} \beta_{o} d - \operatorname{Cos} \beta_{o} h)$$

$$D_{12} = \frac{(\operatorname{Sec} \beta_{o} h - 1)}{T_{cd} T_{sdr}} (\frac{T_{ca}}{T_{cd}} T_{sdi} D_{5} + j D_{5} T_{sa})$$

$$D_{13} = \frac{(\operatorname{Sec} \beta_{o} h - 1)}{30 T_{cd} T_{sdr}} [\frac{T_{ca} T_{idi} T_{sdi} D_{3}}{T_{cd}^{2} T_{idr}} + j D_{4} \frac{T_{ca} T_{idi}}{T_{cd}} T_{idr}$$

$$+ j \frac{T_{ia}}{T_{idr}} (\frac{T_{sdi}}{T_{cd}} D_{3} + j D_{4})]$$

$$D_{14} = \frac{T_{sdi} D_{5}}{T_{cd} T_{sdr}}$$

$$D_{15} = \frac{\operatorname{Sec} \beta_{o} h \operatorname{Sin} \beta_{o} (h - d)}{30 T_{idr}}$$

$$D_{16} = \operatorname{Cos} \beta_{o} d - \operatorname{Cos} \beta_{o} h$$

$$D_{17} = j \frac{D_{5}}{T_{sdr}} \operatorname{Sin} \beta_{o} (h - d) + D_{16} D_{14}$$

The quantities T_{idi}, T_{idr}, T_{cd}, T_{sdr}, T_{sdi}, T_{ca}, T_{ia} and FC₄ are all defined in Chapter 2.

 $D_{18} = \frac{T_{idi}}{T_{-d}}.$

By solving eq. (4.13), the optimum loading impedance is obtained as

$$[z_L]_{op} = \frac{-(B_2/B_1) + \sqrt{(B_2/B_1)^2 - 4(B_3/B_1)}}{2}$$
 (4.14)

By investigating the numerical results obtained from equation (4.14), it is found that only one value of optimum loading impedance $\begin{bmatrix} z_L \end{bmatrix}_{\text{OD}} \quad \text{is of interest, i.e.,}$

$$[z_L]_{OD} = \frac{-(B_2/B_1) - \sqrt{(B_2/B_1)^2 - 4(B_3/B_1)}}{2}$$
(4.15)

The other root to equation (4.14) is extraneous since it does not result in a phase reversal in the antenna current and therefore cannot result in any important in its directivity.

The optimum loading impedances for different antenna lengths and various loading positions d are plotted in Fig. 4.5 and 4.6 for the case of K=2.0. Since the resistive component of the optimum loading impedance is very small (always smaller than 1/10000 of the reactive component), only the reactive component is shown in these Figures, and the optimum loading impedance can be treated approximately as a pure reactance. From these Figures, it is observed that the optimum impedance has its smallest value when the loading position is approximately d=0.7h, and increases rapidly as the loading position is moved toward either the driving point or the extremity of the antenna.

4.4 Typical Current Distribution on Antenna with Optimum Loading:

When a short antenna is loaded by an optimum non-dissipative impedance (inductor), as determined from eq. (4.12) for K=2.0, at fixed position along its surface, the antenna current $I_z(z)$ of

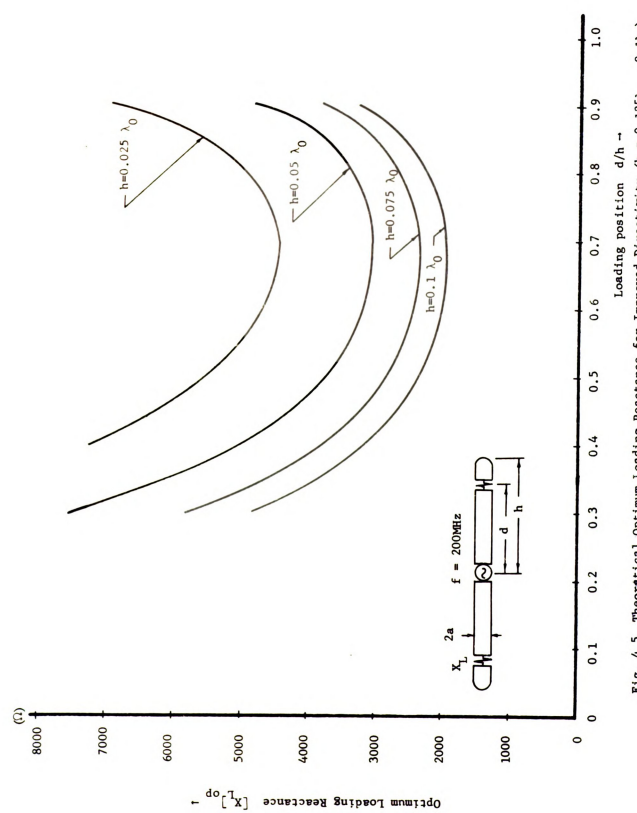


Fig. 4.5 Theoretical Optimum Loading Reactance for Improved Directivity (h = 0.125) $_{o}$ 0.13)

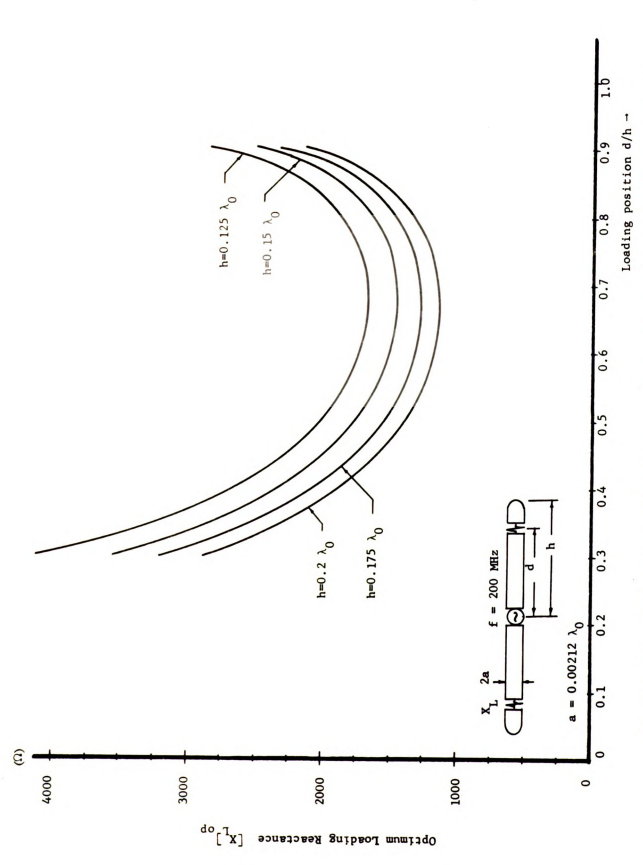


Fig. 4.6 Theoretical Optimum Loading Reactance for Improved Directivity (h = $0.125\lambda_o \sim 0.2\lambda_0$)

eq. (2.24) has the general form indicated in Fig. 4.7.

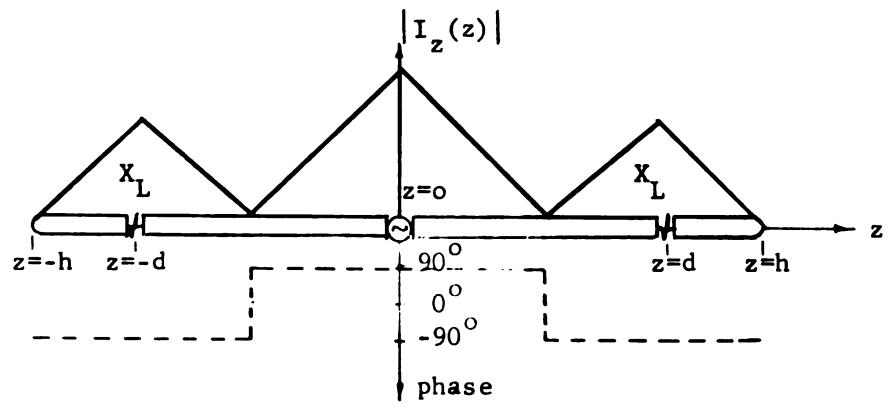


Fig. 4.7. Current Distribution on an Antenna with Optimum Loading for Improved Directivity.

The antenna current has zero amplitudes at points $(z = \pm z_0)$ between the driving point (z = 0) and the loading points $(z = \pm d)$, at which points the phase of the current is reversed by 180° . The total area under the current distribution along the antenna is therefore almost equal to zero, i.e., A = 0, resulting in a very small input resistance and significantly reduced radiation power.

The current distribution of eq. (2.24) for antennas of various lengths with optimum loading impedances $\begin{bmatrix} Z_L \end{bmatrix}_{op}$ at several different positions, are plotted in Fig. 4.8, 4.9 and 4.10.

4.5. Input Impedance of Short Antenna with Increased Directivity:

By using eq. (2.26), the input impedances of short antennas having both optimum and zero loadings are evaluated numerically as indicated in Fig. 4.11 and 4.12. By investigating these Figures, it is found that the input impedance of the antenna with optimum loading has a very large reactive component and a very small resistive component compared with those of the unloaded antenna. The large input reactance is mainly contributed by energy storage in the

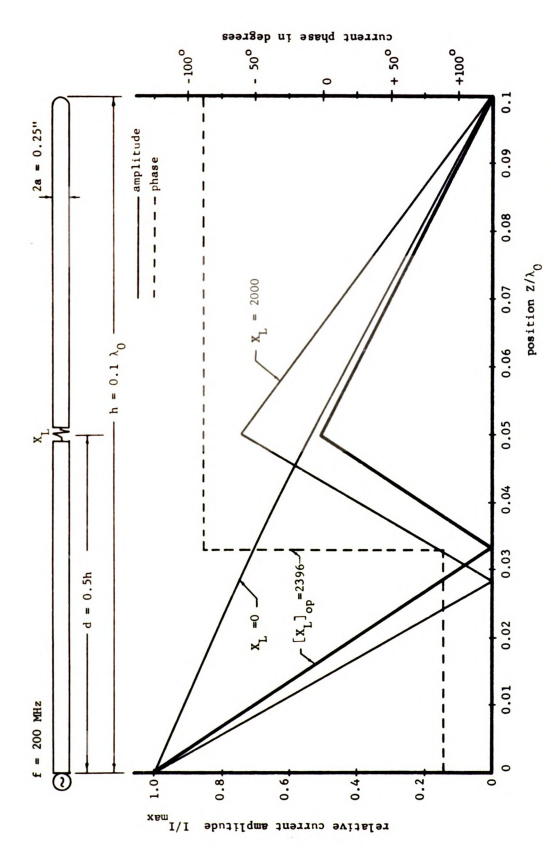


Fig. 4.8 Theoretical Antenna Current Distribution Corresponding to Improved Directivity Condition Compared with that of Other Loadings. (h = 0.1 λ_0 , d = 0.5h)

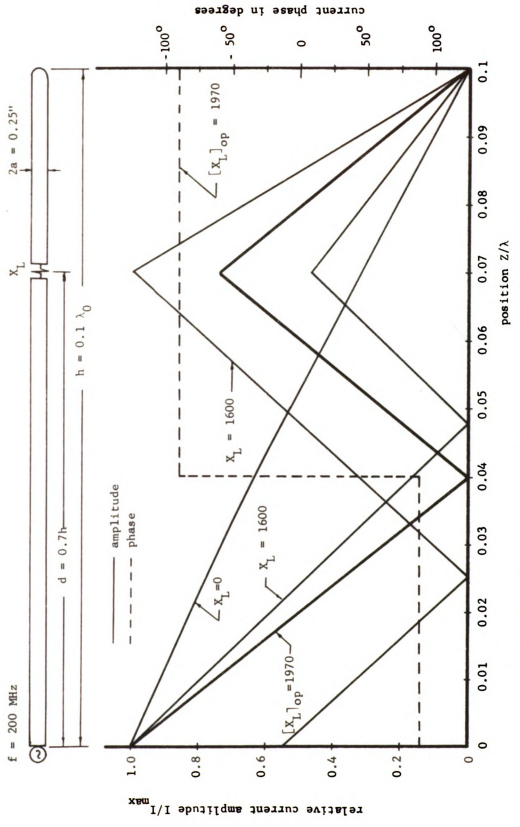


Fig. 4.9 Theoretical Antanna Current Distribution Corresponding to Improved Directivity Condition Compared with that of Other Loadings. (h = 0.1 λ_0 , d = 0.7h)

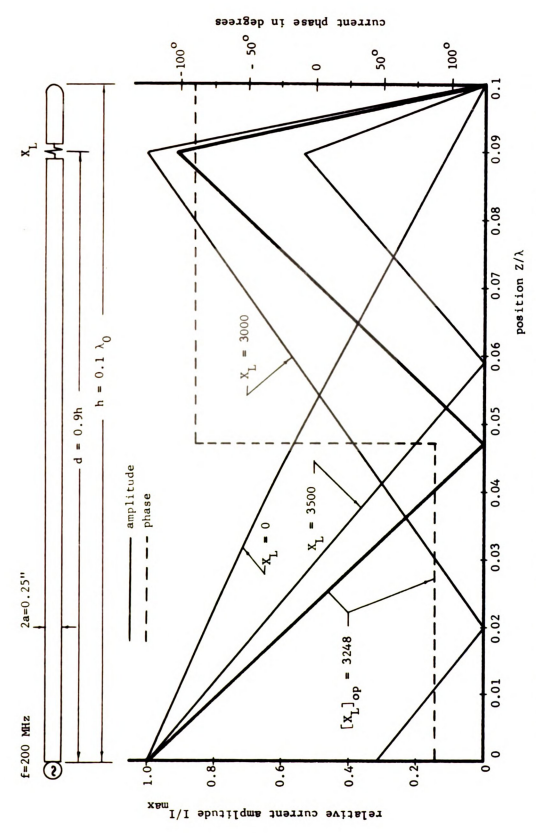


Fig. 4.10 Theoretical Antenna Current Distribution Corresponding to Improved Directivity Condition Compared with that of Other Loadings. (h = 0.1 λ_0 , d = 0.9h)

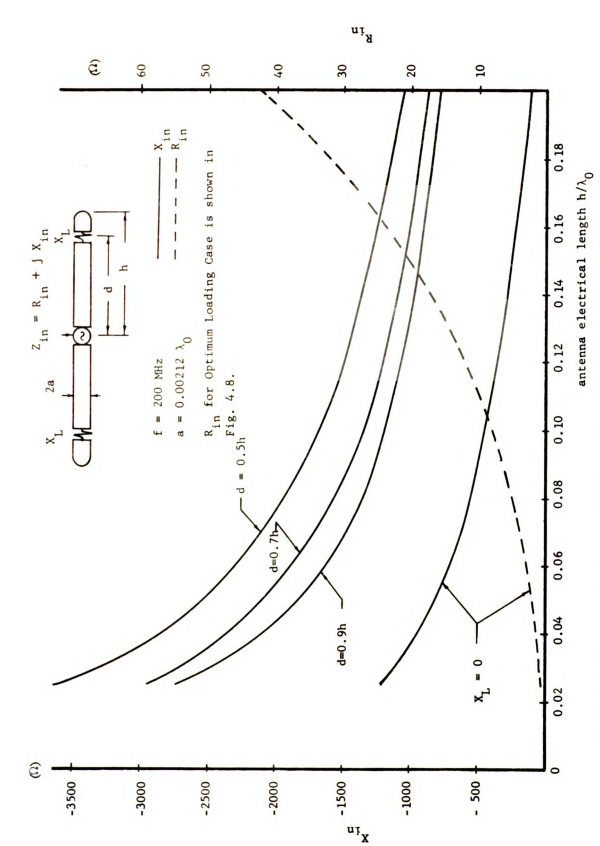


Fig. 4.11 Theoretical Input Impedance for Zero and Optimum (Improved Directivity) Reactive Loadings with Various Loading Positions.

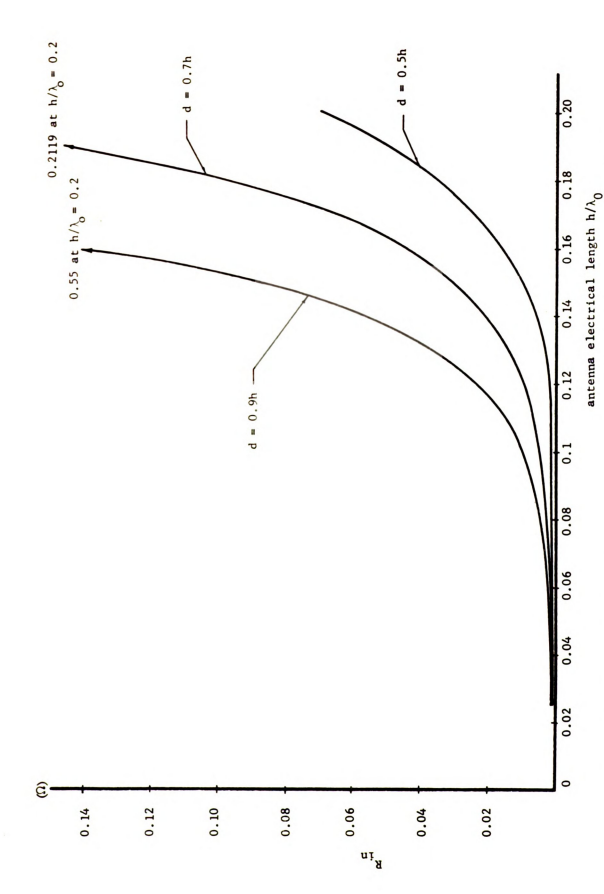


Fig. 4.12 Theoretical Input Resistance for Optimum Reactively Loaded Antennas with Various Loading Positions.

optimum (inductive) reactance loading, and the small input resistance is due to the current phase-reversal which occurs along the antenna with optimum loading.

4.6. Radiated Power and Efficiency of Antenna with Optimum Loading:

By applying equation (4.8) directly, the power radiated by the antenna with optimum loading is obtained as

$$P_{\text{rad.}} = \frac{\zeta_o |A|^2}{\lambda_o^2} \int_0^{\pi} (1 - K \cos^2 \theta)^2 \sin^3 \theta \ d\theta$$
 (4.16)

Therefore, the radiated power is approximately proportional to $|A|^2$, i.e.,

$$P_{rad} \sim |A|^2 = |\int_0^h I_z(z')dz'| \dots \text{ area}^2 \text{ below } I_z(z).$$

Since the current distribution associated with high directivity requires a phase reversal along the antenna, then consequently the integral $A = \int_0^h I_z(z')dz'$ nearly vanishes and the power radiated by the short antenna with optimum loading is very small.

The efficiency of the antenna with optimum loading is also relatively poor. This can be observed as follows. The efficiency of the doubly loaded antenna is determined in Sec. 3.6 as

Efficiency =
$$(1 - 2 \frac{I_z^2(z-d)}{I_z^2(z=o)} \frac{(R_L)_{op}}{R_{in}}) \times 100\%$$

where $(R_L)_{op} = \frac{(X_L)_{op}}{Q}$.

Since $(X_L)_{op}$ has values between 2000 and 7000 ohms for antenna with half-lengths between $h=0.025\lambda_o$ and $h=0.2\lambda_o$ and $a=0.00212\lambda_o$, and R_{in} has values between 0 and 0.5 ohms while $I_z(z=d)$ and $I_z(z=0)$ are comparable, then unless Q is very high most of the input

power to the antenna will be dissipated in the loading inductors.

The efficiency is therefore relatively poor.

CHAPTER 5

DOUBLY LOADED COUPLED SHORT ANTENNAS

The study of coupled, doubly loaded, short antennas involves an investigation of a closely spaced parasitic array of short cylindrical dipoles. It is the objective of this research to enhance the radiation or improve the directivity and radiation pattern of the short antenna array. Two identical parallel antennas doubly loaded by lumped impedances are investigated in this chapter. The theory developed in this chapter is based on the modified method of King and Wu [6], and the investigation of King and Sandler [10].

5.1 Geometry of the Doubly Loaded Short Array:

The geometry of two identical, doubly loaded, short antennas is as indicated in Fig. 5.1. Antenna 1 and antenna 2 are assumed to be constructed of two perfect conductors of the same radius a and length 2h (h is the half-length of antenna), and the distance between these two antennas is b. Two ideal, harmonic voltage sources of equal angular frequency w and potentials v_{10} and v_{20} excite the cylinder 1 and 2, respectively, at their centers z=0 (the antennas are assumed to be oriented parallel to the z-axis). In antenna 1, the two identical lumped impedances v_{10} are loaded symmetrically on the antenna surface at v_{10} are loaded on the surface of antenna 2 as indicated in the figure. The gaps in the cylinders at the location of the sources and the loading impedances

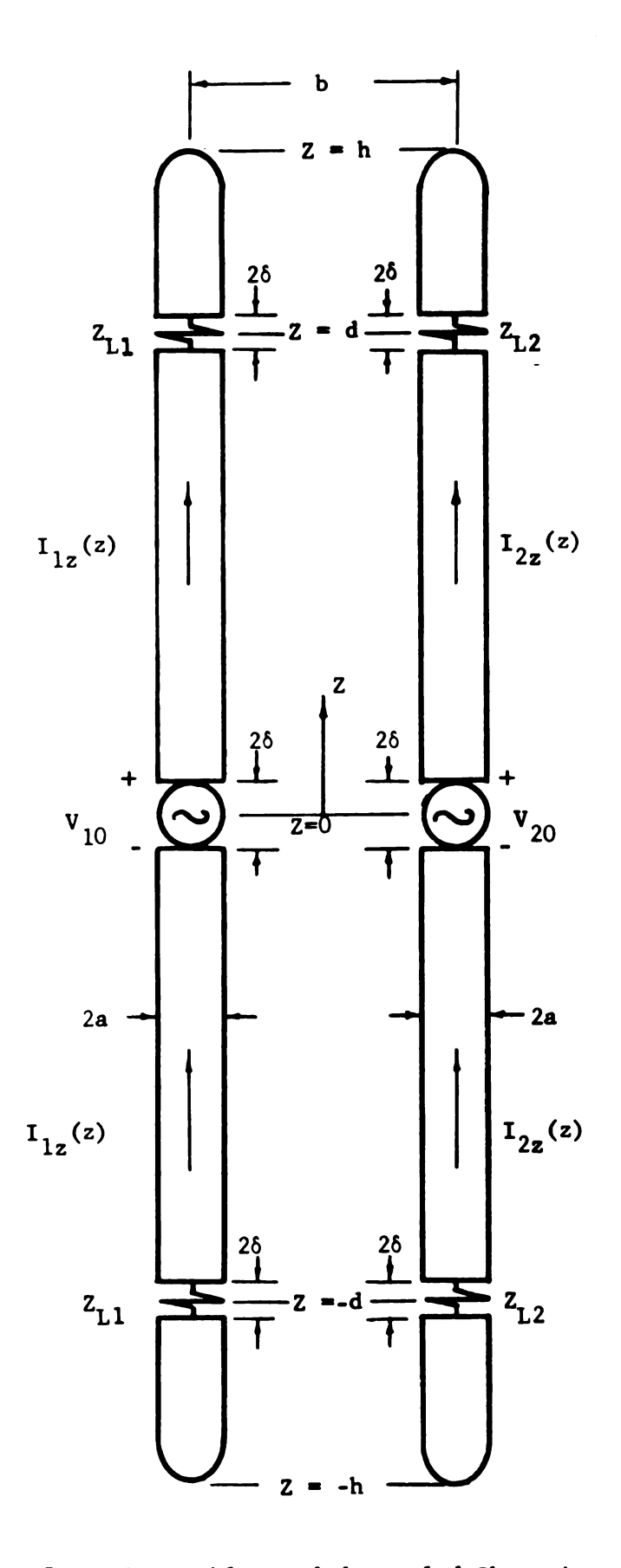


Fig. 5.1 The Doubly Loaded Coupled Short Antennas

are assumed to be of length 2δ . Since both the sources and the lumped loading impedances are considered to be idealized point elements, then δ is assumed to approach zero in the subsequent mathematical analysis.

The dimensions of interest for both antenna 1 and 2 are the same as those for the isolated linear antenna in Chapter 1, i.e.

$$\begin{cases} h/\lambda_o = \frac{\beta_o h}{2\pi} \le 0.1 \\ h >> a \end{cases}$$

$$\beta_o a << 1$$

$$b > a \& b < h \dots closely spaced array$$

where λ_{0} is the free-space wavelength and β_{0} is the corresponding wave number.

As a result of the above thin-wire assumption, and due to the symmetry of the cylinders, the currents on both antennas will flow primarily along the axial or z-direction, i.e.

$$\begin{cases} \vec{I}_1(z) = \hat{z} & I_{1z}(z) & \dots & \text{axial antenna current in element 1.} \\ \vec{I}_2(z) = \hat{z} & I_{2z}(z) & \dots & \text{axial antenna current in element 2.} \end{cases}$$

These dimensional restrictions and axial current approximations lead to a well known result [7] that $I_{1z}(z)$ and $I_{2z}(z)$ can be assumed to be concentrated along the axis of cylinders 1 and 2, respectively, when calculating the vector potential at their surfaces with negligible error.

5.2 Boundary Conditions for Calculating the Antenna Current Distributions:

The currents $I_{1z}(z)$ and $I_{2z}(z)$ on cylinders 1 and 2, respectively, are symmetric about the cylinder centers (z=0) and must vanish at either of their extremities $(z=\pm h)$. A pair of boundary conditions for each antenna current may therefore be expressed as

$$\begin{cases} I_{mz}(z) = I_{mz}(-z) \\ & \text{for } m = 1, 2. \end{cases}$$

$$I_{mz}(+h) = 0$$
(5.1)

Since the tangential component of electric field should be continuous at the antenna surfaces as

$$E_{mz}^{i}(r = a^{+}) = E_{mz}^{a}(r = a^{-})$$
 for $m = 1, 2$ (5.2)

where $E_{mz}^{i}(r=a^{+})$ is the induced electric field just outside the surface of cylinder m at $r=a^{+}$ which is maintained by the currents and charges on both antennas, and $E_{mz}^{a}(r=a^{-})$ is the applied electric field just inside their surfaces at $r=a^{-}$.

5.3 Integral Equations for Antenna Current Distributions:

The arguments and mathematical procedures for obtaining the 2nd-order inhomogeneous differential equations for the vector potential at the surfaces of antennas 1 and 2 are same as Sec. 2.3. The equation (2.10) can be applied directly here for two vector potentials $A_{1z}(z)$ and $A_{2z}(z)$: they are

$$\frac{\partial^{2} A_{1z}}{\partial z^{2}} + \beta_{0}^{2} A_{1z} = \frac{j\beta_{0}^{2}}{\omega} \left\{ -v_{10} \delta(z) + I_{1z}(d) Z_{L1} [\delta(z-d) + \delta(z+d)] \right\}$$
 (5.3)

$$\frac{\partial^{2} A_{2z}}{\delta z^{2}} + \beta_{0}^{2} A_{2z} = \frac{j\beta_{0}^{2}}{\omega} \left\{ -v_{20} \delta(z) + I_{2z}(d) Z_{L2} [\delta(z-d) + \delta(z+d)] \right\}$$
 (5.4)

where A_{1z} is the vector potential at the surface of antenna 1 due to currents on antennas 1 and 2, and A_{2z} is the vector potential at the surface of antenna 2, due to the currents on both antennas. $I_{1z} \stackrel{\text{(+d)}}{=} \text{ and } I_{2z} \stackrel{\text{(+d)}}{=} \text{ are the load currents at the impedance}$ elements Z_{L1} and Z_{L2} at $Z_{L2} = \frac{1}{2}$, and Z_{L3} is the Dirac delta function.

The complementary solutions of eq. (5.3) and (5.4) are obtained easily as

$$A_{1z}^{c}(z) = -\frac{j}{v_{o}} (C_{11}Cos\beta_{o}z + C_{12}Sin\beta_{o}z)$$

$$A_{2z}^{c}(z) = -\frac{j}{v_{o}} (C_{22}Cos\beta_{o}z + C_{21}Sin\beta_{o}z) .$$

where v_0 is the velocity of light in free-space, and c_{11} , c_{22} , c_{12} and c_{21} are arbitrary constants. The particular solution of equations (5.3) and (5.4) are found as

$$A_{1z}^{p}(z) = -\frac{1}{v_{o}} \left[\frac{v_{10}}{2} \sin \beta_{o} |z| - \frac{z_{L1}I_{1z}(d)}{2} (\sin \beta_{o} |z-d| + \sin \beta_{o} |z+d|) \right]$$

$$A_{2z}^{p}(z) = -\frac{1}{v_{o}} \left[\frac{v_{20}}{2} \sin \beta_{o} |z| - \frac{z_{L2}I_{1z}(d)}{2} (\sin \beta_{o} |z-d| + \sin \beta_{o} |z+d|) \right].$$

The general solutions to differential equations (5.3) and (5.4) are thus

$$A_{1z}(z) = A_{1z}^{c}(z) + A_{1z}^{p}(z)$$

$$= -\frac{i}{v_{o}} \left[C_{11} \cos \beta_{o} z + C_{12} \sin \beta_{o} z + \frac{v_{10}}{2} \sin \beta_{o} |z| \right]$$

$$-\frac{Z_{L1} I_{1z}(d)}{2} (\sin \beta_{o} |z-d| + \sin \beta_{o} |z+d|)$$
(5.5)

$$A_{2z}(z) = A_{2z}^{c}(z) + A_{2z}^{\rho}(z)$$

$$= -\frac{i}{v_{o}} \left[C_{22} Cos \beta_{o} z + C_{21} Sin \beta_{oz} + \frac{v_{20}}{2} Sin \beta_{o} |z| \right]$$

$$-\frac{z_{12} I_{2z}(d)}{2} (Sin \beta_{o} |z-d| + Sin \beta_{o} |z+d|) \right]. \qquad (5.6)$$

By the symmetry of the antenna currents $I_{mz}(z) = I_{mz}(-z)$ for m = 1, 2, and it can be shown that the vector potential is also symmetric about the center of either cylinder, i.e. $A_{mz}(z) = A_{mz}(-z)$. It is therefore obvious that arbitrary constants C_{12} and C_{21} should be equal to zero in order to satisfy this symmetry condition; equations (5.5) and (5.6) therefore become

$$A_{1z}(z) = -\frac{1}{v_o} [c_{11} \cos \beta_o z + \frac{v_{10}}{2} \sin \beta_o | z| - \frac{z_{L1} I_{1z}(d)}{2} (\sin \beta_o | z - d| + \sin \beta_o | z + d|)]$$

$$+ \sin \beta_o | z + d|)]$$

$$A_{2z}(z) = -\frac{1}{v_o} [c_{22} \cos \beta_o z + \frac{v_{20}}{2} \sin \beta_o | z| - \frac{z_{L2} I_{2z}(d)}{2} (\sin \beta_o | z - d| + \sin \beta_o | z + d|)]$$
(5.8)

at z = h, results (5.7) and (5.8) become

$$A_{1z}(h) = -\frac{1}{v_0} \{ C_{11} Cos \beta_0 h + \frac{v_{10}}{2} Sin \beta_0 h - \frac{z_{L1} I_{1z}(d)}{2} [Sin \beta_0 (h-d) + Sin \beta_0 (h+d)] \}$$
(5.9)

$$A_{2z}(h) = -\frac{j}{v_o} \{ C_{22} Cos \beta_o h + \frac{v_{20}}{2} Sin \beta_o h - \frac{z_{L2} I_{2z}(d)}{2} [Sin \beta_o (h-d) + Sin \beta_o (h+d)] \}.$$
 (5.10)

By combining equations (5.7) and (5.9), the arbitrary constants is eliminated from eq. (5.7), and an expression for the vector potential difference at the surface of antenna 1 is obtained as

$$A_{1z}(z) - A_{1z}(h) = \frac{1}{v_o} Sec\beta_o h \{ \frac{v_{10}}{2} M_{oz} + \frac{z_{L1}I_{1z}(d)}{2} Cos\beta_o h S_{oz} + \left[\frac{z_{L1}I_{1z}(d)}{2} P - U_1 \right] F_{oz} \}$$
 (5.11)

where

$$M_{OZ} = \sin\beta_{O}(h - |z|)$$

$$S_{OZ} = \sin\beta_{O}|z-d| + \sin\beta_{O}|z+d| - \sin\beta_{O}(h - d) - \sin\beta_{O}(h + d)$$

$$F_{OZ} = \cos\beta_{O}z - \cos\beta_{O}h$$

$$P = \sin\beta_{O}(h - d) + \sin\beta_{O}(h + d)$$

$$U_{1} = -j v_{O} A_{1z}(h)$$

Similary,

$$A_{2z}(z) - A_{2z}(h) = \frac{1}{v_o} \operatorname{Sec\beta}_o h \{ \frac{v_{20}}{2} M_{oz} + \frac{z_{L2} I_{2z}(d)}{2} \operatorname{Cos\beta}_o h S_{oz} - \left[\frac{z_{L2} I_{2z}(d)}{2} P - U_2 \right] F_{oz} \}$$
 (5.12)

where $U_2 = -j v_0 A_{2z}(h)$.

According to the dimensional assumptions $h \gg a$ and $\beta_0 a \ll 1$, the Helmoltz integral for the vector potential at the antenna surface can be simplified as the line integral over an axial current distribution with negligible inaccuracy, i.e.

$$A_{1z}(z) = \frac{\mu_{0}}{4\pi} \left[\int_{-h}^{h} I_{1z}(z') K_{11}(z,z') dz' + \int_{-h}^{h} I_{2z}(z') K_{12}(z,z') dz' \right]$$
 (5.13)

$$A_{2z}(z) = \frac{\mu_{0}}{4\pi} \left[\int_{-h}^{h} I_{1z}(z') K_{21}(z,z') dz' + \int_{-h}^{h} I_{2z}(z') K_{22}(z,z') dz' \right]$$
 (5.14)

where

 μ_{0} = the permeability of free space and

$$K_{11}(z,z') = \frac{e^{-j\beta} o^R 11}{R_{11}}$$

$$K_{12}(z,z') = \frac{e^{-j\beta} o^R 12}{R_{12}}$$

$$K_{12}(z,z') = \frac{e^{-j\beta} o^R 12}{R_{12}}$$
... Green's functions

$$K_{21}(z,z') = K_{12}(z,z')$$

$$K_{22}(z,z') = K_{11}(z,z')$$

$$Antennas$$
... for two identical linear antennas

$$R_{11} = R_{22} = \sqrt{(z-z^*)^2+a^2}$$
 ... the self-distance between an observation point on the surface of antenna at z and an element of current of same antenna on its axis at z^* .

$$R_{12} = R_{21} = \sqrt{(z-z')^2 + b^2}$$
 ... the mutual distance between an observation point on the surface of one antenna at z and an element of current of another antenna on its axis at z'.

If the left hand side of eq. (5.11) is replaced by the Helmholtz integral expression (5.13), an integral equation in terms of $I_{1z}(z)$ and $I_{2z}(z)$ is obtained as

$$\frac{\mu_{o}}{4\pi} \left[\int_{-h}^{h} I_{1z}(z') K_{d11}(z,z') dz' + \int_{-h}^{h} I_{2z}(z') K_{d12}(z,z') dz' \right]
= \frac{1}{v_{o}} \operatorname{Sec\beta}_{o} h \left\{ \frac{v_{10}}{2} M_{oz} + \frac{z_{L1} I_{1z}(z)}{2} \operatorname{S}_{oz} \operatorname{Cos\beta}_{o} h - \left[\frac{z_{L1} I_{1z}(d)}{2} P - U_{1} \right] F_{oz} \right\}
(5.15)$$

where

$$K_{d11}(z,z') = K_{11}(z,z') - K_{11}(h,z')$$

$$= \frac{e^{-j\beta} \circ^{R} 11}{R_{11}} - \frac{e^{-j\beta} \circ^{R} 11h}{R_{11h}}$$

$$K_{d12}(z,z') = K_{12}(z,z') - K_{12}(h,z')$$

$$= \frac{e^{-j\beta} \circ^{R} 12}{R_{12}} - \frac{e^{-j\beta} \circ^{R} 12h}{R_{12h}}$$

$$R_{11h} = \sqrt{(h-z')^{2} + a^{2}}$$

$$R_{12h} = \sqrt{(h-z')^{2} + b^{2}}.$$

 U_1 can be also replaced by the Helmholtz integral as

$$U_{1} = -j v_{0}^{A} I_{z}^{(h)}$$

$$= -j \frac{\zeta_{0}}{4\pi} \left[\int_{-h}^{h} I_{1z}(z') K_{11}(h,z') dz' + \int_{-h}^{h} I_{2z}(z') K_{12}(h,z') dz' \right] \qquad (5.16a)$$

Similary, equation (5.12) becomes

$$\frac{\frac{\mu}{4\pi} \int_{-h}^{h} I_{1z}(z') K_{d21}(z,z') dz' + \int_{-h}^{h} I_{2z}(z') K_{d22}(z,z') dz']$$

$$= \frac{j}{v_{o}} \operatorname{Sec\beta}_{o} h \left\{ \frac{v_{20}}{2} M_{oz} + \frac{z_{L2} I_{2z}(d)}{2} \operatorname{S}_{oz} \operatorname{Cos\beta}_{o} h - \left[\frac{z_{L2} I_{2z}(d)}{2} P - U_{2} \right] F_{oz} \right\}$$
(5.17)

where $K_{d22} = K_{d11}$, $K_{d21} = K_{d12}$, and

$$U_{2} = -j v_{o}^{A}_{2z}(h)$$

$$= -j \frac{\zeta_{o}}{4\pi} \left[\int_{-h}^{h} I_{1z}(z') K_{21}(h,z') dz' + \int_{-h}^{h} I_{2z}(z') K_{22}(h,z') dz' \right] \qquad (5.16b)$$

Equations (5.15) and (5.17) are a pair of coupled integral equations for the currents $I_{1z}(z)$ and $I_{2z}(z)$ on antennas 1 and 2, respectively, and are valid for $-h \le z \le h$.

5 4 Approximate Solution for the Antenna Currents:

The application of King and Sandler's method to the solution of integral equations (5.15) and (5.17) is the subject of this section. This method is mainly based on the King's modified method which consists essentially of assuming the current excited on the antenna to be proportional to the vector potential difference (referred to the end of the antenna).

By a peaking property of the difference kernels $K_{\rm d11}(z,z')$ and $K_{\rm d22}(z,z')$

$$K_{d11}(z,z') = K_{11}(z,z') - K_{11}(h,z')$$

$$\sim \delta(z-z') - \delta(h-z')$$

$$K_{d22}(z,z') = K_{22}(z,z') - K_{22}(h,z')$$

$$\sim \delta(z-z') - \delta(h-z')$$

it is found from the left hand sides of equations (5.15) and (5.17) for both large and small β_0 b that the currents $I_{1z}(z)$ and $I_{2z}(z)$ may be taken as the form

$$\begin{cases} I_{1z}(z) = G_1 F_{oz} + B_1 M_{oz} + C_1 S_{oz} \\ I_{2z}(z) = G_2 F_{oz} + B_2 M_{oz} + C_2 S_{oz} \end{cases}$$
 (5.18)

where G_1 , G_2 , B_1 , B_2 , C_1 and C_2 are arbitrary complex constants.

Note that in results (5.18) and (5.19)

$$I_{1z}(z = +h) = 0$$

$$I_{2z}(z = +h) = 0$$

matically satisfied, and the currents are symmetric as they should be. By substituting equations (5.18) and (5.19) into the integrals at the left hand side of eq. (5.15) and eq. (5.17) and by separating the Green's function into real and imaginary parts, the integrals in the left hand sides of (5.15) and (5.17) can be expressed in a general form as

$$\frac{\mu_{o}}{4\pi} \int_{-h}^{h} [G_{m}F_{oz}] + B_{m}M_{oz}] + C_{m}S_{oz}] K_{d11}(z,z')dz'
+ \frac{\mu_{o}}{4\pi} \int_{-h}^{h} [G_{n}F_{oz}] + B_{n}M_{oz}] + C_{n}S_{oz}] K_{d12}(z,z')dz'
= \frac{\mu_{o}}{4\pi} \int_{-h}^{h} [G_{m}F_{oz}] + B_{m}M_{oz}] + C_{m}S_{oz}] K_{d11r}(z,z')dz'
-j \frac{\mu_{o}}{4\pi} \int_{-h}^{h} [G_{m}F_{oz}] + B_{m}M_{oz}] + C_{m}S_{oz}] K_{d11i}(z,z')dz'
+ \frac{\mu_{o}}{4\pi} \int_{-h}^{h} [G_{n}F_{cz}] + B_{n}M_{oz}] + C_{n}S_{oz}] K_{d12r}(z,z')dz'
-j \frac{\mu_{o}}{4\pi} \int_{-h}^{h} [G_{n}F_{cz}] + B_{n}M_{oz}] + C_{n}S_{oz}] K_{d12i}(z,z')dz'$$
(5.20)

for m = 1,2 and n = 1,2 but $m \neq n$, and where F_{OZ} , M_{OZ} and S_{OZ} , are same as F_{OZ} , M_{OZ} and M_{OZ} except Z is replaced by Z', and

$$K_{dllr}(z,z') = K_{llr}(z,z') - K_{llr}(h,z')$$
$$= \frac{\cos \beta_{o} R_{1l}}{R_{1l}} - \frac{\cos \beta_{o} R_{1lh}}{R_{1lh}}$$

$$\begin{split} K_{\text{d12r}}(z,z') &= K_{12r}(z,z') - K_{12r}(h,z') \\ &= \frac{\cos\beta_{0}R_{12}}{R_{12}} - \frac{\cos\beta_{0}R_{12h}}{R_{12h}} \\ K_{\text{d11i}}(z,z') &= -[K_{11i}(z,z') - K_{11i}(h,z')] \\ &= \frac{\sin\beta_{0}R_{11h}}{R_{11h}} - \frac{\sin\beta_{0}R_{11}}{R_{11}} \\ K_{\text{d12i}}(z,z') &= -[K_{12i}(z,z') - K_{12i}(h,z')] \\ &= \frac{\sin\beta_{0}R_{12h}}{R_{12h}} - \frac{\sin\beta_{0}R_{12}}{R_{12}} \; . \end{split}$$

Since $K_{dl1r}(z,z')$ becomes very large when z' is near z, it follows that the main contribution to the part of the integral that has $K_{dl1r}(z,z')$ as kernel comes from elements of current near z'=z. On the other hand, $K_{dl2r}(z,z')$, $K_{dl1i}(z,z')$, and $K_{dl2i}(z,z')$ remain relatively small when z=z'. This suggests that the principle contribution to the part of the integral that has $K_{dl1i}(z,z')$, $K_{dl2r}(z,z')$ and $K_{dl2i}(z,z')$ as kernel come from all the elements of current that are some distance from z. Due to this peaking property of kernel $K_{dl1i}(z,z')$ and nonpeaking property of kernels $K_{dl1i}(z,z')$, $K_{dl2r}(z,z')$ and $K_{dl2i}(z,z')$, the various integrals on the right hand side of equation (5.20) may be verified numerically to have the following approximate representation:

$$\int_{-h}^{h} F_{oz}' K_{d11}(z,z')dz' = \int_{-h}^{h} F_{oz}' [K_{d11r}(z,z') + K_{d11i}(z,z')]dz'$$

$$= \Psi_{du}(z)F_{oz}$$

$$= \Psi_{du}(o)F_{oz}$$

$$= \Psi_{du}(o)F_{oz}$$
(5.21)

$$\int_{-h}^{h} F_{oz} K_{d12}(z,z') dz' = \Psi_{de}(z) F_{oz} = \Psi_{de}(o) F_{oz} = \Psi_{de}F_{oz}$$
 (5.22)

$$\int_{-h}^{h} M_{oz}, K_{dllr}(z,z')dz' = \Psi_{dvr}(z)M_{oz}$$

$$\stackrel{:}{=} \begin{cases} \Psi_{\text{dvr}}(o) M_{\text{oz}} & \text{for } \beta_{\text{o}} h \leq \frac{\pi}{2} \\ \Psi_{\text{dvr}}(h - \frac{\lambda_{\text{o}}}{4}) M_{\text{oz}} & \text{for } \beta_{\text{o}} h > \frac{\pi}{2} \end{cases}$$

$$= \Psi_{\text{dvr}} M_{\text{oz}} \qquad (5.23)$$

$$\int_{-h}^{h} M_{oz} K_{dlli}(z,z') dz' = \Psi_{dvi}(z) F_{oz} = \Psi_{dvi}(o) F_{oz} = \Psi_{dvi} F_{oz}$$
 (5.24)

$$\int_{-h}^{h} M_{oz}, K_{d12}(z,z')dz' = \Psi_{df}(z)F_{oz} = \Psi_{df}(o)F_{oz} = \Psi_{df}F_{oz}$$
 (5.25)

$$\int_{-h}^{h} S_{oz}' K_{d11r}(z,z') dz' = \Psi_{dwr}(z) S_{oz} = \Psi_{dwr}(o) S_{oz} = \Psi_{dwr} S_{oz}$$
 (5.26)

$$\int_{-h}^{h} S_{oz}' K_{dlli}(z,z') dz' = \Psi_{dwi}(z) F_{oz} = \Psi_{dwi}(0) F_{oz} = \Psi_{dwi} F_{oz}$$
 (5.27)

$$\int_{-h}^{h} S_{oz} K_{d12}(z,z') dz' = \Psi_{dg}(z) F_{oz} = \Psi_{dg}(o) F_{oz} = \Psi_{dg} F_{oz}$$
 (5.28)

where $\Psi_{du}(z)$, $\Psi_{de}(z)$, $\Psi_{dvr}(z)$, $\Psi_{dvi}(z)$, $\Psi_{df}(z)$, $\Psi_{dwr}(z)$, and $\Psi_{dg}(z)$ are very nearly constant parameters which may be evaluated as

$$\Psi_{du}(z) = (\cos \beta_{0} z - \cos \beta_{0} h)^{-1} \{C_{a}(z,h) - C_{a}(h,h) - \cos \beta_{0} h[E_{a}(z,h) - E_{a}(h,h)]\}$$

$$\begin{split} \Psi_{de}(z) &= (\text{Cos}\beta_{o}z - \text{Cos}\beta_{o}h)^{-1} \{ [\text{C}_{b}(z,h) - \text{C}_{b}(h,h)] \} \\ &- \text{Cos}\beta_{o}h [\text{E}_{b}(z,h) - \text{E}_{b}(h,h)] \} \\ \Psi_{dvr}(z) &= [\text{Sin}\beta_{o}(h-|z|)]^{-1} \text{Re} \{ \text{Sin}\beta_{o}h [\text{C}_{a}(z,h) - \text{C}_{a}(h,h)] \} \\ &- \text{Cos}\beta_{o}h [\text{S}_{a}(z,h) - \text{S}_{a}(h,h)] \} \\ \Psi_{dvi}(z) &= (\text{Cos}\beta_{o}z - \text{Cos}\beta_{o}h)^{-1} \text{Me} \{ \text{Sin}\beta_{o}h [\text{C}_{a}(z,h) - \text{C}_{a}(h,h)] \} \\ &- \text{Cos}\beta_{o}h [\text{S}_{a}(z,h) - \text{S}_{a}(h,h)] \} \\ \Psi_{df}(z) &= (\text{Cos}\beta_{o}z - \text{Cos}\beta_{o}h)^{-1} \{ \text{Sin}\beta_{o}h [\text{C}_{b}(z,h) - \text{C}_{b}(h,h)] \} \\ &- \text{Cos}\beta_{o}h [\text{S}_{b}(z,h) - \text{S}_{b}(h,h)] \} \\ \Psi_{dwr}(z) &= [\text{Sin}\beta_{o}|z-d| + \text{Sin}\beta_{o}|z+d| - \text{Sin}\beta_{o}(h-d) - \text{Sin}\beta_{o}(h+d)]^{-1} \\ &\times \text{Re}\{D_{a}(z,h) - D_{a}(h,h) - [\text{Sin}\beta_{o}(h-d) + \text{Sin}\beta_{o}(h+d)] [\text{E}_{a}(z,h) - \text{E}_{a}(h,h)] \} \\ \Psi_{dwi}(z) &= (\text{Cos}\beta_{o}z - \text{Cos}\beta_{o}h)^{-1} \text{Me}\{D_{a}(z,h) - D_{a}(h,h) - [\text{Sin}\beta_{o}(h-d) + \text{Sin}\beta_{o}(h+d)] [\text{E}_{a}(z,h) - \text{E}_{a}(h,h)] + \text{F}_{a}(z,h) - \text{F}_{a}(h,h) \} \\ \Psi_{dg}(z) &= (\text{Cos}\beta_{o}z - \text{Cos}\beta_{o}h)^{-1} \{ D_{b}(z,h) - D_{b}(h,h) - [\text{Sin}\beta_{o}(h-d) + \text{Sin}\beta_{o}(h+d)] [\text{E}_{b}(z,h) - \text{E}_{b}(h,h)] + \text{F}_{b}(z,h) - \text{F}_{b}(h,h) \} \end{split}$$

and where

$$C_{a}(z,h) = \int_{-h}^{h} \cos \beta_{o} z' \frac{e^{-j\beta_{o}R_{11}}}{R_{11}} dz'$$

$$C_{b}(z,h) = \int_{-h}^{h} \cos \beta_{o} z' \frac{e^{-j\beta_{o}R_{12}}}{R_{12}} dz'$$

$$S_{a}(z,h) = \int_{-h}^{h} \sin \beta_{o} |z'| \frac{e^{-j\beta_{o}R_{11}}}{R_{11}} dz'$$

$$\begin{split} &S_{b}(z,h) = \int_{-h}^{h} \sin\beta_{o} |z'| \frac{e^{-j\beta_{o}R_{12}}}{R_{12}} dz' \\ &E_{a}(z,h) = \int_{-h}^{h} \frac{e^{-j\beta_{o}R_{11}}}{R_{11}} dz' \\ &E_{b}(z,h) = \int_{-h}^{h} \frac{e^{-j\beta_{o}R_{12}}}{R_{12}} dz' \\ &D_{a}(z,h) = \int_{-h}^{h} \sin\beta_{o} |z'-d| \frac{e^{-j\beta_{o}R_{11}}}{R_{11}} dz' \\ &D_{b}(z,h) = \int_{-h}^{h} \sin\beta_{o} |z'-d| \frac{e^{-j\beta_{o}R_{11}}}{R_{12}} dz' \\ &F_{a}(z,h) = \int_{-h}^{h} \sin\beta_{o} |z'+d| \frac{e^{-j\beta_{o}R_{12}}}{R_{11}} dz' \\ &F_{b}(z,h) = \int_{-h}^{h} \sin\beta_{o} |z'+d| \frac{e^{-j\beta_{o}R_{12}}}{R_{12}} dz' . \end{split}$$

For $C_a(h,h)$, $S_a(h,h)$, $E_a(h,h)$, $D_a(h,h)$ and $F_a(h,h)$, the R_{11} is replaced by R_{11h} , and for $C_b(h,h)$, $S_b(h,h)$, $E_b(h,h)$, $D_b(h,h)$ and $F_b(h,h)$, the R_{12} is replaced by R_{12h} . Equations (5.23), (5.26) and the real part of equation (5.21) are based on the characteristics of kernel $K_{dllr}(z,z')$, i.e.

$$\int_{-h}^{h} F_{oz}'^{K}_{dllr}(z,z')dz' \sim F_{oz}$$

$$\int_{-h}^{h} M_{oz}'^{K}_{dllr}(z,z')dz' \sim M_{oz}$$

$$\int_{-h}^{h} S_{oz}'^{K}_{dllr}(z,z')dz' \sim S_{oz}$$

and equations (5.24), (5.25), (5.27), (5.28) and the imaginary part of equation (5.21) are based on numerical considerations. It is found numerically that these equations are approximately proportional to the shifted cosine function \mathbf{F}_{OZ} . The essentially constant

parameters $\Psi_{\mathrm{du}}(z)$, $\Psi_{\mathrm{de}}(z)$, $\Psi_{\mathrm{dvr}}(z)$, $\Psi_{\mathrm{dvi}}(z)$, $\Psi_{\mathrm{dwr}}(z)$, $\Psi_{\mathrm{df}}(z)$, $\Psi_{\mathrm{dwi}}(z)$ and $\Psi_{\mathrm{dg}}(z)$ can be replaced approximately by their values at z=0, while $\Psi_{\mathrm{dvr}}(z) \doteq \Psi_{\mathrm{dvr}}(0)$ for $\beta_0 h \leq \frac{\pi}{2}$ and $\Psi_{\mathrm{dvr}}(z) \doteq \Psi_{\mathrm{dvr}}(h-\frac{\lambda_0}{4})$ for $\beta_0 h > \frac{\pi}{2}$.

Substituting equations (5.21) through (5.28) into equation (5.20), the vector potential difference is therefore obtained as

$$\frac{4\pi}{\mu_{o}} [A_{mz}(z) - A_{mz}(h)] = (G_{m}^{\Psi} du + G_{n}^{\Psi} de + j B_{m}^{\Psi} dvi + B_{n}^{\Psi} df + j C_{m}^{\Psi} dwi + C_{n}^{\Psi} dg) F_{oz} + \Psi_{dur}^{B} B_{m}^{M} dz + \Psi_{dwr}^{C} C_{m}^{S} dwi + C_{n}^{\Psi} dg) F_{oz} + \Psi_{dur}^{B} B_{m}^{M} dz + \Psi_{dwr}^{C} C_{m}^{S} dwi + C_{n}^{W} dwi + C_{n}^{W} dyi + C_{n}^{W} dwi + C_{n}^{W} dyi + C_{n}^{W} dwi + C_{n}^{$$

Equations (5.16a) and (5.16b) also can be expressed as

$$\frac{4\pi}{\mu_{o}} A_{m}(h) = \int_{-h}^{h} I_{mz}(z') K_{11}(h,z') dz' + \int_{-h}^{h} I_{nz}(z) K_{12}(h,z') dz'$$

$$= G_{m} \Psi_{u} + B_{m} \Psi_{v} + C_{m} \Psi_{w} + A_{n} \Psi_{e} + B_{n} \Psi_{f} + C_{n} \Psi_{g}$$

$$for m = 1,2, n = 1,2, m \neq n. \qquad (5.30)$$
where
$$\Psi_{u} = C_{a}(h,h) - E_{a}(h,h) Cos \beta_{o} h$$

$$\Psi_{v} = C_{a}(h,h) Sin \beta_{o} h - S_{a}(h,h) Cos \beta_{o} h$$

$$\Psi_{w} = D_{a}(h,h) - E_{a}(h,h) Sin \beta_{o}(h-d) + F_{a}(h,h)$$

$$- E_{a}(h,h) Sin \beta_{o}(h+d)$$

$$\Psi_{e} = C_{b}(h,h) - E_{b}(h,h) Cos \beta_{o} h$$

$$\Psi_{f} = C_{b}(h,h) Sin \beta_{o} h - S_{b}(h,h) Cos \beta_{o} h$$

$$\Psi_{g} = D_{b}(h,h) - E_{b}(h,h) Sin \beta_{o}(h-d) + F_{b}(h,h)$$

- $E_h(h,h) \sin\beta_0(h+d)$.

Instead of substituting equation (5.29) into equations (5.15) and (5.17) as in Chapter 2, it is expedient to substitute (5.29) directly into differential equations (5.3) and (5.4). This procedure results in the following general result:

$$\frac{\mu_{o}}{4\pi} \left(\frac{d^{2}}{dz^{2}} + \beta_{o}^{2}\right) \left[A_{mz}(z) - A_{mz}(h)\right]$$

$$= \left(\frac{d^{2}}{dz^{2}} + \beta_{o}^{2}\right) \left\{ \left(G_{m}^{\Psi}_{du} + G_{n}^{\Psi}_{de} + j B_{m}^{\Psi}_{dvi} + B_{n}^{\Psi}_{df} + j C_{m}^{\Psi}_{dwi} + C_{n}^{\Psi}_{dg}\right) F_{oz} + \Psi_{dvr}^{B}_{moz} + \Psi_{dwr}^{C}_{moz} \right\}$$

$$= \frac{-j^{4\pi\beta_{o}}}{\zeta_{o}} \left\{ V_{mo}^{\delta}(z) - Z_{Lm}^{I}_{mz}(d) \left[\delta(z-d) + \delta(z+d)\right] \right\}$$

$$- \frac{4\pi}{\mu_{o}} \beta_{o}^{2} A_{mz}(h) \quad \dots \text{ for } m = 1, 2, n = 1, 2 \text{ but } m \neq n. \tag{5.31}$$

By differentiating the F_{OZ} , M_{OZ} , and S_{OZ} , the various delta function terms are obtained as

$$\frac{d^{2}}{dz^{2}} F_{cz} = -\beta_{o}^{2} Cos\beta_{o} z$$

$$\frac{d^{2}}{dz^{2}} M_{oz} = -2\beta_{o} Cos\beta_{o} h \delta(z) - \beta_{o}^{2} M_{oz}$$

$$\frac{d^{2}}{dz^{2}} S_{oz} = -\beta_{o}^{2} (Sin\beta_{o}|z-d| + Sin\beta_{o}|z+d|) + 2\beta_{o} [\delta(z-d) + \delta(z+d)].$$

Substituting the above results into eq. (5.31) and equating the coefficients of the corresponding delta function terms, three independent equations are obtained as

$$\left(\begin{array}{c} B_{\text{m}} V_{\text{dvr}} \cos \beta_{\text{o}} h = \frac{j}{\zeta_{\text{o}}} V_{\text{mo}} \end{array}\right)$$
 (5.32)

$$C_{m}^{\Psi}_{dwr} = j \frac{2\pi}{\zeta_{o}} Z_{Lm}^{I}_{mz}(d)$$
 (5.33)

$$\begin{pmatrix}
B_{m} \Psi_{dvr} \cos \beta_{o} h = \frac{j}{\zeta_{o}} V_{mo} \\
C_{m} \Psi_{dwr} = j \frac{2\pi}{\zeta_{o}} Z_{Lm} I_{mz} (d) \\
\cos \beta_{o} h [\Psi_{du} G_{m} + \Psi_{de} G_{n} + j \Psi_{dvi} B_{m} + \Psi_{df} B_{n} + \Psi_{dwi} C_{m} + \Psi_{dg} C_{n}] \\
+ \Psi_{dwr} C_{m} [\sin \beta_{o} (h+d) + \sin \beta_{o} (h-d)] = \frac{4\pi}{\mu_{o}} A_{mz} (h)$$
(5.32)

where m = 1,2 and n = 1,2 but $m \neq n$.

From eq. (5 32), the arbitrary constants B_1 and B_2 are completely determined by setting m = 1 and 2, i.e.

$$\begin{cases} B_1 = \frac{j2\pi}{\zeta_0} \frac{v_{10}}{v_{dvr} \cos \beta_0 h} = v_{10} D_0 \\ B_2 = v_{20} D_0 \end{cases}$$
 (5.35)

where

$$D_{o} = \frac{j 2\pi}{\zeta_{o} \Psi_{dvr} \cos \beta_{o} h}.$$

Constants C_1 and C_2 can be expressed in terms of $I_{1z}(d)$ and $I_{22}(d)$, respectively, by setting m = 1 and 2, i.e.

$$c_{1} = \frac{j2\pi}{\zeta_{0}} \frac{z_{L1}}{v_{dwr}} I_{1z}(d)$$
 (5.37)

$$c_2 = j \frac{2\pi}{\zeta_0} \frac{z_{L2}}{y_{dwr}} I_{2z}(d)$$
 (5.38)

Since

$$I_{1z}(d) = G_{1}(\cos\beta_{0}d - \cos\beta_{0}h) + B_{1}\sin\beta_{0}(h-d) + C_{1}(\sin2\beta_{0}d - 2\sin\beta_{0}h\cos\beta_{0}d)$$
 (5.39)

$$I_{2z}(d) = G_2(\cos\beta_0 d - \cos\beta_0 h) + B_2 \sin\beta_0 (h-d)$$

$$+ C_2(\sin2\beta_0 d - 2\sin\beta_0 h \cos\beta_0 d)$$
(5.40)

then C_1 and C_2 can be expressed in terms of G_1 and G_2 , respectively, i.e.

$$\begin{cases} c_1 = G_1 D_1 + D_2 V_{10} \\ c_2 = G_2 D_3 + D_4 V_{20} \end{cases}$$
 (5.41)

where

$$\begin{split} & D_1 = \frac{j \, 2\pi Z_{L1}}{\zeta_o \, T_{c1}} \, \left(\text{Cos} \beta_o d - \text{Cos} \beta_o h \right) \\ & D_2 = \frac{j \, 2\pi Z_{L1}}{\zeta_o \, T_{c1}} \, D_o \, \text{Sin} \beta_o \, (h-d) \\ & T_{c1} = \Psi_{dwr} - \left(\text{Sin} 2\beta_o d - 2 \text{Sin} \beta_o h \text{Cos} \beta_o d \right) \frac{j \, 2\pi}{\zeta_o} \, Z_{L1} \\ & D_3 = \frac{j \, 2\pi Z_{L2}}{\zeta_o \, T_{c2}} \, \left(\text{Cos} \beta_o d - \text{Cos} \beta_o h \right) \\ & D_4 = \frac{j \, 2\pi Z_{L2}}{\zeta_o \, T_{c2}} \, D_o \, \, \text{Sin} \beta_o \, (h-d) \\ & T_{c2} = \Psi_{dwr} - \left(\text{Sin} 2\beta_o d - 2 \text{Sin} \beta_o h \text{Cos} \beta_o d \right) \frac{j \, 2\pi}{\zeta_o} \, Z_{L2} \, . \end{split}$$

Equation (5.34) can produce two independent equations for the cases of m = 1 and n = 2, and m = 2 and n = 1; they are

$$\cos \beta_{o}^{h} \left[\Psi_{du}^{G}_{1} + \Psi_{de}^{G}_{2} + j \Psi_{dvi}^{B}_{1} + \Psi_{df}^{B}_{2} + j \Psi_{dwi}^{C}_{1} + \Psi_{dg}^{C}_{2} \right]
+ \Psi_{dwr}^{G}_{1} \left[\sin \beta_{o}^{(h+d)} + \sin \beta_{o}^{(h-d)} \right] = \frac{4\pi}{\mu_{o}} A_{1z}^{(h)}$$
(5.43)

$$\cos^{2} \theta_{0}^{h} \left[\Psi_{du}^{G} G_{2} + \Psi_{de}^{G} G_{1} + j \Psi_{dvi}^{B} G_{2} + \Psi_{df}^{B} G_{1} + j \Psi_{dwi}^{G} G_{2} + \Psi_{dg}^{G} G_{1} \right] \\
+ \Psi_{dwr}^{G} G_{2} \left[\sin^{2} \theta_{0}^{G} (h+d) + \sin^{2} \theta_{0}^{G} (h-d) \right] = \frac{4\pi}{\mu_{0}} A_{2z}(h). \tag{5.44}$$

Substituting equations (5.30), (5.35), (5.36), (5.41) and (5.42) into (5.43) and (5.44), two equations of G_1 and G_2 are obtained as

$$\begin{cases} G_1^T_{s1} + G_2^T_{s2} = w_1^V_{10} + w_2^V_{20} \\ G_1^T_{s3} + G_2^T_{s4} = w_3^V_{10} + w_4^V_{20} \end{cases}$$
(5.45)

$$\int_{G_1 T_{s3}} + G_2 T_{s4} = W_3 V_{10} + W_4 V_{20}$$
 (5.46)

where

$$T_{s1} = Cos\beta_o h(\Psi_{du} + j \Psi_{dwi}D_1) + 2D_1 \Psi_{dwr} Sin\beta_o hCos\beta_o d - (\Psi_u + D_1 \Psi_w)$$

$$T_{s2} = Cos\beta_o h(\Psi_{de} + \Psi_{dg}D_3) - (\Psi_e + D_3\Psi_g)$$

$$T_{s3} = Cos\beta_oh(\Psi_{de} + \Psi_{dg}D_1) - (\Psi_e + D_1\Psi_g)$$

$$T_{s4} = Cos\beta_oh(\Psi_{du} + j \Psi_{dwi}D_3) + 2D_3\Psi_{dwr}Sin\beta_ohSin\beta_od - (\Psi_u + D_3\Psi_w)$$

$$W_{1} = D_{o}^{\Psi} + D_{2}^{\Psi} - j(D_{o}^{\Psi}_{dvi} + \Psi_{dwi}D_{2})Cos\beta_{o}h - 2\Psi_{dwr}D_{2}Sin\beta_{o}hCos\beta_{o}d$$

$$W_2 = D_0 Y_f + D_4 Y_g - (D_0 Y_{df} + Y_{dg} D_4) \cos \beta_0 h$$

$$W_3 = D_0 \Psi_f + D_2 \Psi_g - (D_0 \Psi_f + \Psi_d D_2) \cos \beta h$$

$$W_4 = D_0 \Psi + D_4 \Psi - j(D_0 \Psi_{dvi} + \Psi_{dwi} D_4) \cos \beta_0 h - 2\Psi_{dwr} D_4 \sin \beta_0 h \cos \beta_0 d.$$

From equations (5.45) and (5.46), G_1 and G_2 are determined as

$$\int_{0}^{G} G_{1} = W_{5}V_{10} + W_{6}V_{20}$$
 (5.47)

$$\begin{cases}
G_1 = W_5 V_{10} + W_6 V_{20} \\
G_2 = W_7 V_{10} + W_8 V_{20}
\end{cases} (5.47)$$

where

$$W_{5} = \frac{W_{3}^{T}_{s2} - W_{1}^{T}_{s4}}{T_{s2}^{T}_{s3} - T_{s4}^{T}_{s1}}$$

$$W_{6} = \frac{W_{4}^{T}_{s2} - W_{2}^{T}_{s4}}{T_{s2}^{T}_{s3} - T_{s4}^{T}_{s1}}$$

$$W_{7} = \frac{W_{1}^{T}_{s3} - W_{3}^{T}_{s1}}{T_{s2}^{T}_{s3} - T_{s4}^{T}_{s1}}$$

$$W_{8} = \frac{W_{2}^{T}_{s3} - W_{4}^{T}_{s1}}{T_{s2}^{T}_{s3} - T_{s4}^{T}_{s1}}$$

Constants C_1 and C_2 are therefore also determined as

$$\begin{cases} c_1 = (w_5 D_1 + D_2) V_{10} + W_6 D_1 V_{20} \\ c_2 = W_7 D_3 V_{10} + (W_8 D_3 + D_4) V_{20} \end{cases}$$

Finally, the approximate solutions for $I_{1z}(z)$ and $I_{2z}(z)$ are completely determined as

$$I_{1z}(z) = G_{1}F_{0z} + B_{1}M_{0z} + C_{1}S_{0z}$$

$$= [W_{5}F_{0z} + D_{0}M_{0z} + (W_{5}D_{1} + D_{2})S_{0z}]V_{10} + (F_{0z} + D_{1}S_{0z})W_{6}V_{20}$$
(5.51)

$$I_{2z}(z) = G_{2}F_{oz} + B_{2}M_{oz} + C_{2}S_{oz}$$

$$= (F_{oz} + D_{3}S_{oz})W_{7}V_{10} + [W_{8}F_{oz} + D_{o}M_{oz} + (W_{8}D_{3} + D_{4})S_{oz}]V_{20}.$$
(5.52)

Equations (5.51) and (5.52) express the antenna current distributions in terms of the antenna dimensions, their excitation frequency, and the impedance and position of the double loadings.

5.5 Input Impedance of the Antenna Coupled with a Doubly Loaded Parasitic Element:

The input impedance of antenna 1 is defined as

$$z_{in} = \frac{v_{10}}{I_{1z}(z=0)} = R_{in} + j X_{in}.$$

If antenna 2 is a doubly loaded parasitic element with zero driving potential or $V_{20} = 0$, the input impedance of driven element 1 is obtained directly from eq. (5.51) as

$$(z_{in})_{v_{20}=0} = [w_5 F_{oz}(0) + D_o M_{oz}(0) + (w_5 D_1 + D_2) S_{oz}(0)]^{-1}.$$
 (5.53)

When antenna 2 is doubly loaded parasitic element center loaded by an impedance Z_0 , $V_{20} = -I_{2z}(0)Z_0$ and the impedance Z_{in} of the driven element is obtained from eq. (5.51) and eq. (5.52) as

$$(z_{in})_{V_{20}=-I_{20}(o)Z_{o}} = \{1 + [w_{8}F_{oz}(o) + D_{o}M_{oz}(o) + (w_{8}D_{3}+D_{4})S_{oz}(o)]z_{o}\}$$

$$\times [w_{5}F_{oz}(o) + D_{o}M_{oz}(o) + (w_{5}D_{1}+D_{2})S_{oz}(o)]^{-1}$$

$$\{1 + [w_{8}F_{oz}(o) + D_{o}M_{oz}(o) + (w_{8}D_{3} + D_{4})S_{oz}(o)]z_{o}$$

$$+ [F_{oz}(o) + D_{1}S_{oz}(o)][F_{oz}(o) + D_{3}S_{oz}(o)]z_{o}\}^{-1}.$$

$$(5.54)$$

5.6 Radiation From Coupled Short Antennas:

The well known radiation fields in the far zone of a linear antenna system are given by

$$\begin{cases} E_{\theta}^{r} = -j \omega A_{\theta}^{r} \\ B_{\phi}^{r} = \frac{1}{v_{\theta}} E_{\theta}^{r} \end{cases}$$

in terms of spherical coordinates.

The vector potential $A_{\theta}^{r}(z)$ at point $P(R_{10}, \theta, \phi)$ in the far zone due to the antenna currents $I_{1z}(z)$ of eq. (5.51) and $I_{2z}(z)$ of eq. (5.52) can be expressed as

$$A_{\theta}^{r}(R_{10},\theta,\phi) = -\frac{\frac{\mu_{o}}{4\pi}}{\sin\theta} \left[\int_{-h}^{h} I_{1z}(z') \frac{e^{-jR_{1}}}{R_{1}} dz' + \int_{-h}^{h} I_{2z}(z') \frac{e^{-jR_{2}}}{R_{2}} dz' \right]$$
(5.56)

where \mathbf{R}_1 and \mathbf{R}_2 are distances between an observation point in far zone and the source points on antenna 1 and antenna 2, respectively, and \mathbf{R}_{10} and \mathbf{R}_{20} are the distances between the center points of the antennas and the point \mathbf{P} as indicated in Fig. 5.2.

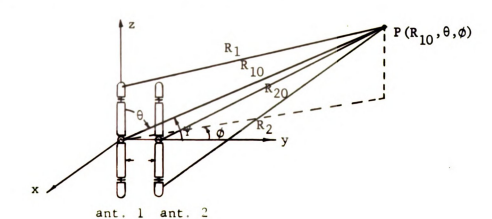


Fig. 5.2. Geometry for Calculation of Radiation Field

Since $\beta_0^{~b} \ll 1$, the distance $\rm R_{20}^{~}$ can be approximately expressed in terms of $\rm R_{10}^{~}$ as

$$\begin{cases} R_{20} \stackrel{:}{=} R_{10} \text{ - b CosY} & \dots & \text{for phase factor} \\ \\ R_{20} \stackrel{:}{=} R_{10} & \dots & \text{for amplitude terms} \end{cases}$$

where $Cos \Psi = Sin \theta Cos \phi$.

By using the same procedures of Sec. 3.2 and taking the three leading terms of the power series of the Green's functions in eq. (5.56), the odd terms of the series integrate to zero due to the symmetry of the antenna currents. Equation (3.4) can therefore be applied directly to eq. (5.56) to yield

$$A_{\theta}^{r}(R_{10},\theta,\phi) = -\frac{\mu_{o}}{2\pi} \sin\theta \left\{ \frac{e^{-j\beta_{o}R_{10}}}{R_{10}} \int_{o}^{h} I_{1z}(z') \left(1 - \frac{1}{2} \beta_{o}^{2} z'^{2} \cos^{2}\theta\right) dz' + \frac{e^{-j\beta_{o}R_{10}}}{R_{10}} e^{j\beta_{o}bCos\Psi} \int_{o}^{h} I_{2z}(z') \left(1 - \frac{1}{2} \beta_{o}^{2} z'^{2} \cos^{2}\theta\right) dz' \right\}.$$
(5.57)

The radiation fields E_{θ}^{r} and B_{ϕ}^{r} are then obtained as

$$\begin{cases} E_{\theta}^{r} = \frac{j \zeta_{o}}{\lambda_{o}} \frac{e^{-j\beta_{o}R_{10}}}{R_{10}} & B F(\beta_{o}h, \theta, \phi) \\ B_{\phi}^{r} = \frac{j \mu_{o}}{\lambda_{o}} \frac{e^{-j\beta_{o}R_{10}}}{R_{10}} & B F(\beta_{o}h, \theta, \phi) \end{cases}$$
(5.58)

where

$$F(\beta_{o}h,\theta,\phi) = \sin\theta\{1 - \frac{A}{B}\cos^{2}\theta + \frac{C}{B}e^{j\beta_{o}h\cos^{\phi}S\sin\theta} (1 - \frac{D}{C}\cos^{2}\theta\}$$
 (5.60)

$$A = \frac{1}{2} \int_{0}^{h} \beta_{o}^{2} z'^{2} I_{1z}(z') dz'$$

$$B = \int_{0}^{h} I_{1z}(z') dz'$$

$$C = \int_{0}^{h} I_{2z}(z') dz'$$

$$D = \frac{1}{2} \int_{0}^{h} \beta_{o}^{2} z'^{2} I_{2z}(z') dz'.$$

Since the phases of the currents on both elements are essentially constant, it is possible to write

$$\frac{A}{B}$$
 = real constant K_1 [same argument as in eq. (4.4)]

$$\frac{D}{C} = \text{real constant } K_2 \text{ [same argument as in eq. (4.4)]}$$

$$\frac{C}{B} = K_3 e^{j\alpha}$$

where α is the phase difference between $I_{1z}(z)$ and $I_{2z}(z)$, and K_3 is a real number.

Equation (5.60), therefore, becomes

$$F(\beta_0 h, \theta, \phi) = Sin\theta \{1 - K_1 \cos^2 \theta + K_3 e^{j\alpha} e^{j\beta_0 b \cos \phi Sin\theta} (1 - K_2 \cos^2 \theta) \}.$$

$$(5.61)$$

Equation (5.61) will be used in the discussion of Section 5.8.

5.7 Enhancement of Radiated Power:

The average power flow at $P(R_{10}, \theta, \phi)$ is obtained as

$$\vec{S}_{av.} = \frac{1}{2} \operatorname{Re} \left(\hat{\theta} \ E_{\theta}^{r} \times \hat{\phi} \ H_{\phi}^{r*} \right) = \frac{1}{2} \frac{\left| \vec{E}_{\theta}^{r} \right|^{2}}{\zeta_{o}} \hat{r} . \tag{5.62}$$

From equations (5.58) and (5.61) E_{θ}^{r} is obtained as

$$E_{\theta}^{r} \doteq \frac{j \zeta_{o}}{\lambda_{o}} \frac{e^{-j\beta_{o}R_{10}}}{R_{10}} \quad \text{B Sin}\theta \{1 - K_{1}^{\cos^{2}\theta} + K_{3}^{e^{j\alpha}} e^{j\beta_{o}^{\cos\phi}Sin\theta} (1 - K_{2}^{\cos^{2}\theta})\}$$

and since it is assumed that $\beta_0 b << 1$, then e = 1 and

$$E_{\theta}^{r} \doteq \frac{j \zeta_{o}}{\lambda_{o}} \frac{e^{-j\beta_{o}R_{10}}}{R_{10}} \quad B \sin\theta\{1 - K_{1}\cos^{2}\theta + K_{3}e^{j\alpha}(1 - K_{2}\cos^{2}\theta)\}. \quad (5.63)$$

Since $\beta_0\,h <<$ 1, unless the phase of the antenna current is reversed

$$\int_{0}^{h} I_{1z}(z') dz' \gg \int_{0}^{h} \beta_{0}^{2} z'^{2} I_{1z}(z') dz'$$

$$\int_{0}^{h} I_{2z}(z') dz' >> \int_{0}^{h} \beta_{0}^{2} z'^{2} I_{2z}(z') dz'$$

this means that $K_1 \ll 1$, $K_2 \ll 1$ and eq. (5.63) can be approximated as

$$E_{\theta}^{r} \doteq \frac{j \zeta_{o}}{\lambda_{o}} \frac{e^{-j\beta_{o}R_{10}}}{R_{10}} (B + C) \sin\theta. \tag{5.64}$$

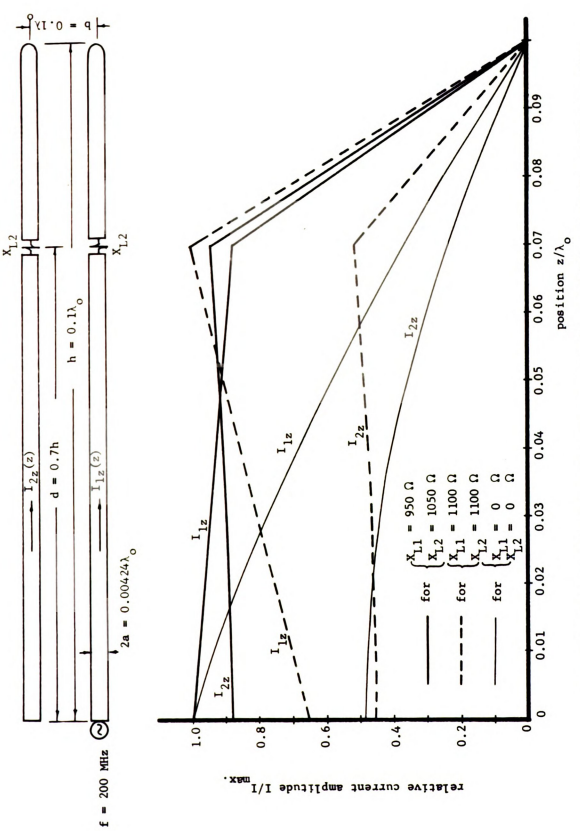
The total time-average power radiated by the antenna is thus given by

$$P_{rad} = 2\pi R_{10}^{2} \int_{0}^{\pi} \frac{1}{2} \frac{\left|\vec{E}_{\theta}^{r}\right|^{2}}{\zeta_{o}} \hat{r} \cdot \hat{r} \sin\theta \, d\theta$$

$$= \frac{4\pi}{3\lambda_{o}^{2}} \left| B + C \right|^{2} . \qquad (5.65)$$

Equation (5.65) shows that the power radiated by the coupled antenna is roughly proportional to $|B+C|^2$. Since B and C are simply the areas under the current distributions along the antennas 1 and 2, respectively, the radiated power P_{rad} may be enhanced by maximizing the area under the currents $I_{1z}(z)$ and $I_{2z}(z)$ while at the same time adjusting them to have a minimum phase difference. This can be accomplished by appropriately choosing the loading impedances X_{L1} and X_{L2} located at the fixed positions d_1 and d_2 along the surfaces of antennas 1 and 2.

The current distributions $I_{1z}(z)$ and $I_{2z}(z)$ for antennas which are optimumly loaded with optimum reactances $[X_{L1}]_{op}$ and $[X_{L2}]_{op}$ to have maximum areas and minimum phase difference, are plotted in Fig. 5.3 through Fig. 5.6 for various antenna spacings. From these figures, it is observed that the typical forms of the current distributions on the coupled antennas loaded with the optimum reactances exhibit nearly uniform amplitude distributions between



Theoretical Current Distribution on Doubly Loaded Coupled Antennas Corresponding to Enhanced Radiation Condition Compared with that of Other Loadings (b = $0.01\lambda_0$). Fig. 5.3

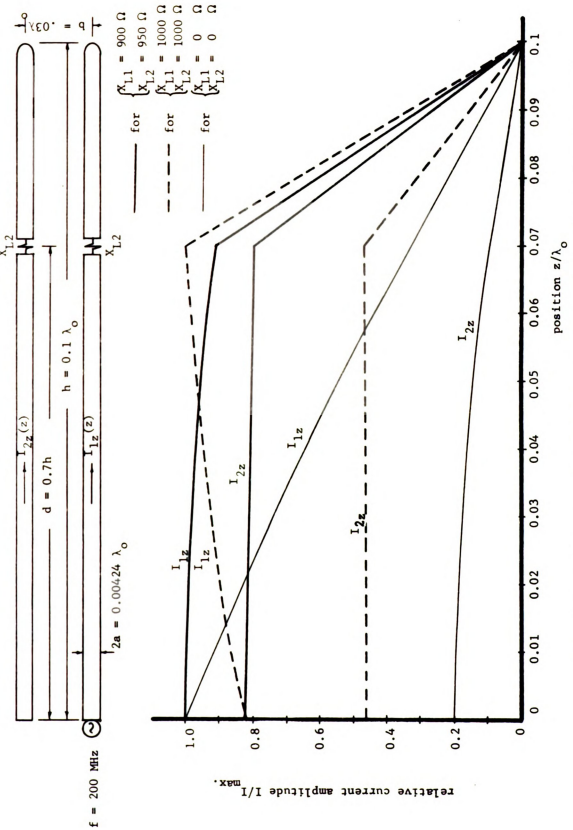
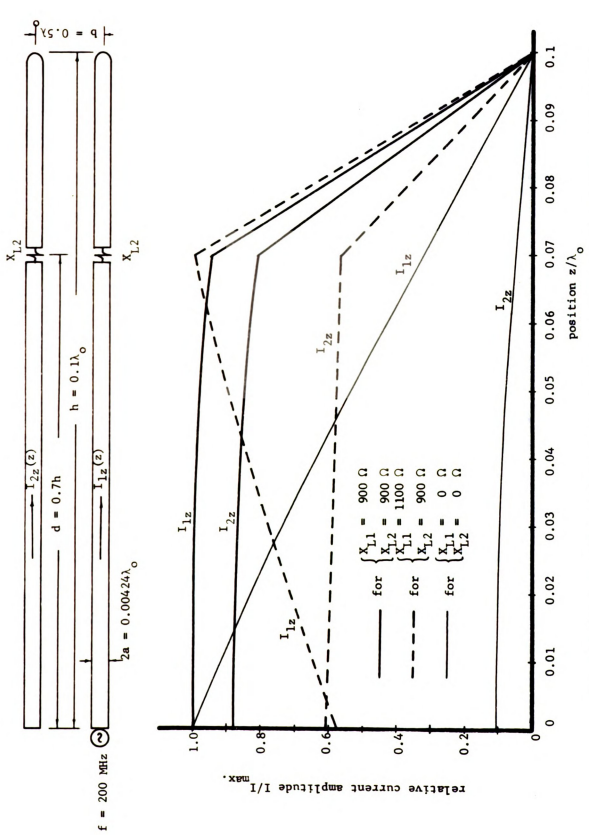


Fig. 5.4 Theoretical Current Distributions on Doubly Loaded Coupled Antennas Corresponding to Enhanced Radiation Condition Compared with that of Other Loadings (b = 0.03 λ_0).



Theoretical Current Distributions on Doubly Loaded Coupled Antennas Corresponding to Enhanced Radiation Condition Compared with that of Other Loadings (b = 0.05 λ_0).

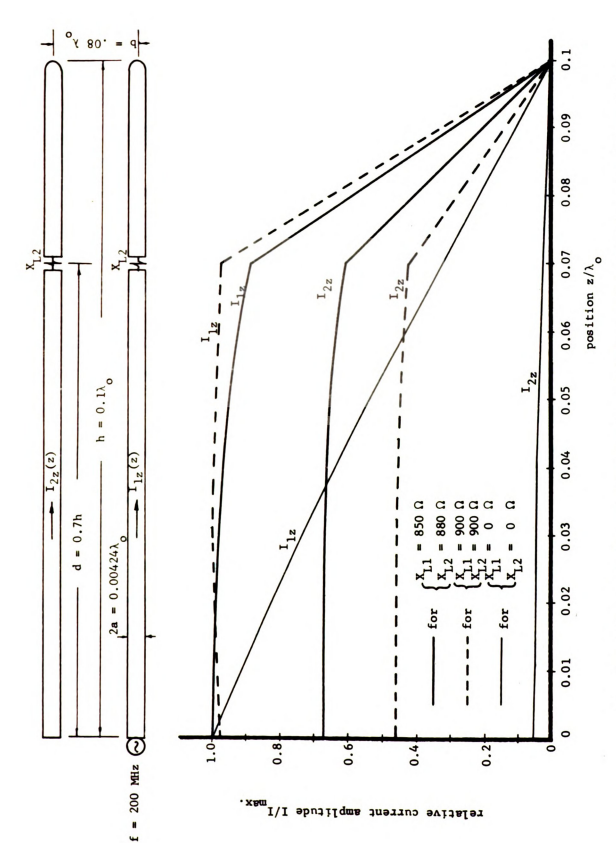


Fig. 5.6 Theoretical Current Distribution on Doubly Loaded Coupled Antennas Corresponding to Enhanced Radiation Condition Compared with that of Other Loadings (b = 0.08).

the loading points. Under the optimum condition of enhanced radiation, the shapes of $I_{1z}(z)$ and $I_{2z}(z)$ are quite similar and the phase difference between them is minimum as shown in Fig. 5.1. Thus, the radiated power under this condition can be enhanced to about four times that of an isolated antenna.

The input impedances of the driven antenna coupled to a parasitic element, both loaded with the optimum reactances, are determined from eq. (5.53) and shown in Table 5.1. It is indicated that under the optimum condition of enhanced radiation the input resistance is increased and the input reactance is reduced as compared with the case of an isolated loaded antenna.

5.8 Improved Directivity:

For simplicity, only the case of $\frac{D}{C} = \frac{A}{B}$ is considered in this section. Under this condition, eq. (5.61) can be expressed as

$$F(\beta_0h,\theta,\phi) \stackrel{!}{=} Sin\theta(1-K_1Cos^2\theta)[1+K_3e^{j\alpha}(1+j\beta_0bCos\phi Sin\theta)] \quad (5.66)$$
 since $e^{j\beta_0bCos\phi Sin\theta}$ since $e^{j\beta_0bCos\phi Sin\theta}$ for $\beta_0b \ll 1$. If $\frac{C}{B} = K_3e^{j\alpha}$ is not close to -1, the radiation pattern is similar to that of a single doubly loaded antenna for improved directivity as discussed in Chapter 4 and no further discussion is needed. However, if $C = -B$ can be implemented eq. (5.66) becomes

$$F(\beta_0 h, \theta, \phi) = j \beta_0 b(1 - K_1 \cos^2 \theta) \cos \phi \sin^2 \theta.$$
 (5.67)

The radiation patterns in the plane of ϕ = 0 are plotted in Fig. 5.7 for various values of K_1 . The directivity and beamwidth are also indicated in the same figure. By comparing with the

Table 5.1. Input Impedances of Driven Antenna Coupled with Loaded Parasitic Element and Phase Difference Between $\, I_{12} \, (z) \,$ and $\, I_{22} \, (z) \,$

	$z_{in} = R_{in} + j x_{in}$	Xin	-353.98	-128.05	444.62	-448.91	- 21.36	252.65	-402.94	37.02	698.57	-467.27	2.74	31 10
$a = 0.00212\lambda_0$, $h = 0.1\lambda_0$ and $d = 0.7h$.		R _{in}		1.22 -13	106.34 44	4.93	99.99	64.57 25	6.33 -40	89.69	137.3 69	7.28 -46	46.85	03 17
		(phase difference between I _{1z} & I _{2z})	1780	09	9.50	1750	130	23.50	1700	230	260	160°	o ⁰⁷	000
	۵	(spacing between ant. 1 & ant. 2)	0.01 λ _ο	0.01 λ	0.01 λ _ο	0.03 λ _ο	0.03 λ	0.03 λο	0.05 λ _ο	0.05 λ _ο	ο.05 λ	0.08 λ	0.08 λ	. 00 0
	x _{L2}	(0)	0	1050	1100	0	950	1000	0	006	006	0	880	000
f = 200 MHz,	x _{1,1}	(0)	0	950	1100	0	006	1000	0	006	1100	0	850	

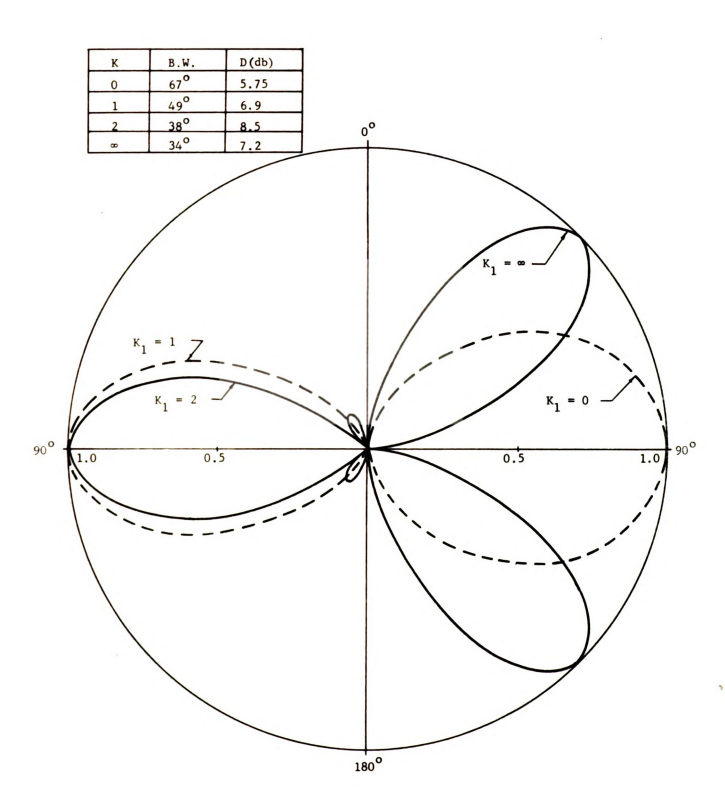


Fig. 5.7 Theoretical Radiation Patterns of Coupled Short Antennas with κ_1 = 0, 1, 2 and ∞ under Conditions of κ_1 = κ_2 , κ_3 = 1 and α = π . (ϕ = o)

radiation patterns shown in Chapter 4, it is observed that the doubly loaded coupled array has a higher directivity than that of a corresponding single antenna if the condition of $\int_0^h I_{1z}(z')dz' = -\int_0^h I_{2z}(z')dz'$ is met.

5.9 Discussion:

The approximate theory developed in this chapter for the doubly loaded coupled antennas has been checked by the existing theories [5] for the case of $Z_{L1} = Z_{L2} = o$. When $Z_{L1} = Z_{L2}$, the theory is still quite accurate, however, the accuracy of the theory starts to decrease when the difference between Z_{L1} and Z_{L2} increases. The reason for this discrepancy is due to the completely different current distributions on the antennas when Z_{L1} is greatly different from Z_{L2} .

CHAPTER 6

EXPERIMENTAL STUDY OF SHORT ANTENNA WITH HIGH DIRECTIVITY OR ENHANCED RADIATION

An experimental study of doubly loaded short antennas (both for single and coupled antennas) is presented in this chapter. In order to compare these experimental results with the theoretical results presented in the previous chapters, an antenna of particular dimensions, a = 0.125 inch and h = 15 cm, which was used in numerical calculation is used in the following experiments. The current distributions and input impedances of an antenna with different optimum impedance loadings at proper positions along the antenna are measured and are compared directly with the corresponding theoretical results. The excitation frequency is usually fixed at 200 MHz. In addition to the doubly loaded antennas, experiments have also been conducted to study the cases of an end-loaded antenna and an antenna with double impedance and end loadings.

6.1 Experimental Setup:

The experimental setup for measuring the current distributions and input impedances of the antennas is shown schematically in Fig. 6.1. Photographs of the inside and outside views of the anechoic chamber are shown in Fig. 6.2 and Fig. 6.3.

An 8' wide, 6' high, 6' long anechoic chamber was constructed with wooden frames enclosed completely with an aluminum ground plane on one wall and B.F. Goodrich type VHP-8 microwave absorbers covering the remaining five walls. A driven linear antenna (monopole) and

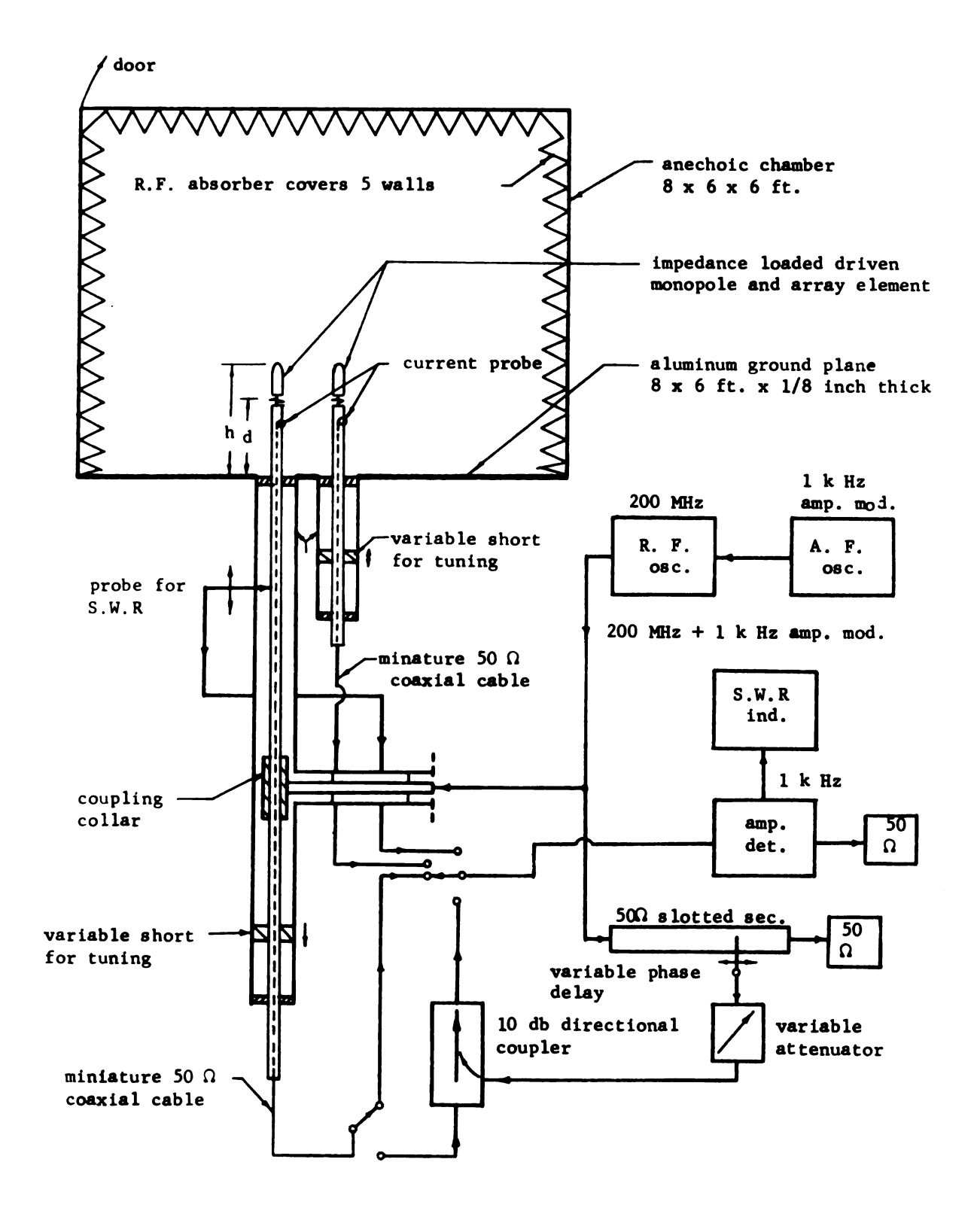


Fig. 6.1 Experimental Setup

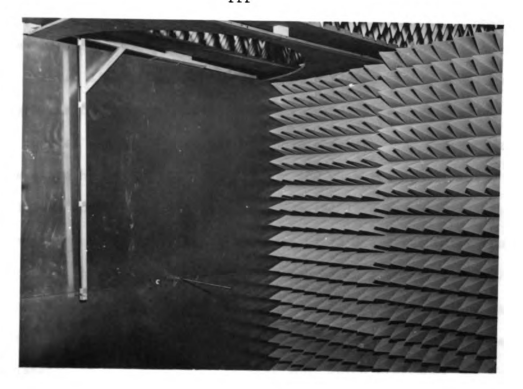


Fig. 6.2 The Inside View of Anechoic Chamber

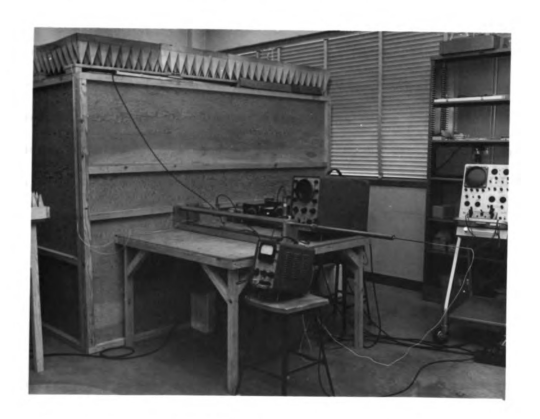
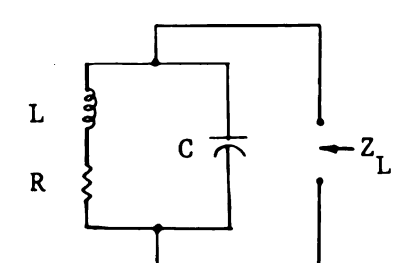


Fig. 6.3 The Outside View of Anechoic Chamber

array element are simply the extensions of the movable centerwires of the coaxial lines connected to the ground plane. Thus, the antenna length can be adjusted freely by sliding the centerwires inside of the coaxial lines and into the anechoic chamber. The driven antenna is excited by an R.F. OSC. at 200 MHz and with the square wave amplitude modulation of 1 KHz. The coaxial line which excites the antenna has a characteristic impedance of 75 Ω and its outer conductor has physical dimensions of 1 inch outer diameter and 0.875 inch inner diameter. The outer conductor of the coaxial line is directly connected to the ground plane. The center conductor has a diameter of 0.25 inch and its free end, which protrudes the ground plane, serves as the antenna.

The lumped impedance is mounted on the antenna as indicated in Fig. 6.4. Since the antenna is separated by a piece of insulating material at the loading position, the loading impedance is actually the parallel combination of the externally mounted inductor L (non-ideal inductor) and the unknown stray capacitance C existing at the loading location. The loading impedance may be determined from the following simple circuit. The impedance Z_L at angular exciting



frequency w is obtained as

$$Z_{L} = \frac{R + j \omega L}{1 + j \omega C(R + j \omega L)}$$

where
$$R = \frac{\omega L}{Q}$$
.

The frequency can be adjusted to make the current minimum at the loading point. At this frequency, the suceptance, $1/Z_{T}$ becomes

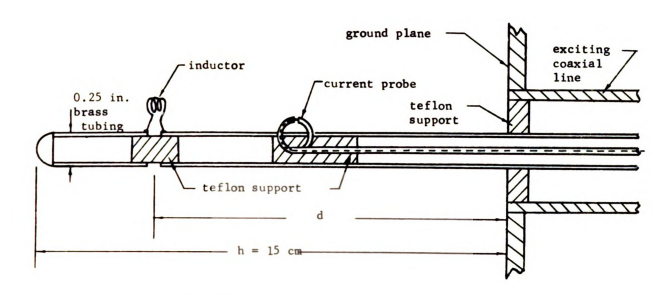


Fig. 6.4 Structure of Monopole Antenna

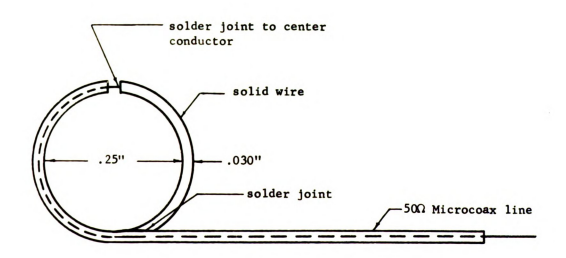


Fig. 6.5 Structure of Current Probe

zero. This critical frequency can be determined to be $\omega_0^2 = (L-R^2C)/L^2C$. The stray capacitance C can then be expressed as $C = L/(R^2 + \omega_0^2L^2)$ and Z_1 is determined as

$$Z_{L} = R_{L} + j X_{L} = \frac{(R + j\omega L) (R^{2} + \omega_{o}^{2}L^{2})}{R^{2} + L^{2}(\omega_{o}^{2} - \omega^{2}) + j\omega LR}.$$
 (6.1)

The current probe, which is connected to a flexible $50~\Omega$ coaxial line passing through the hollow center conductor of the excitating coaxial line to the instruments outside the chamber, is supported by a plastic guide in the antenna slot and can be moved freely between the driving point z = 0 (the point at the ground plane) and the loading point z = d. The detailed construction of the current probe is shown in Fig. 6.5. The relative amplitude of current can be measured by moving the current probe along the slotted antenna. The phase of antenna current is obtained by comparing the probe signal with the reference signal from the R.F. Oscillator.

A charge probe is inserted into the region between the outer and inner conductors of the exciting coaxial line. This probe is supported by a movable carriage and can be moved along the slotted outer conductor of the exciting coaxial line. The standing wave ratio and the phase shift of the wave pattern in the coaxial line can be measured by this charge probe. The input impedance of the antenna can then be determined as,

$$Z_{in} = \frac{1 - j S \tan \beta \ell_{min.}}{S - j \tan \beta \ell_{min.}} \times Z_{c}$$
 (6.2)

where S is the standing wave ratio and ℓ_{\min} is the distance between the first voltage minimum and the antenna driving point

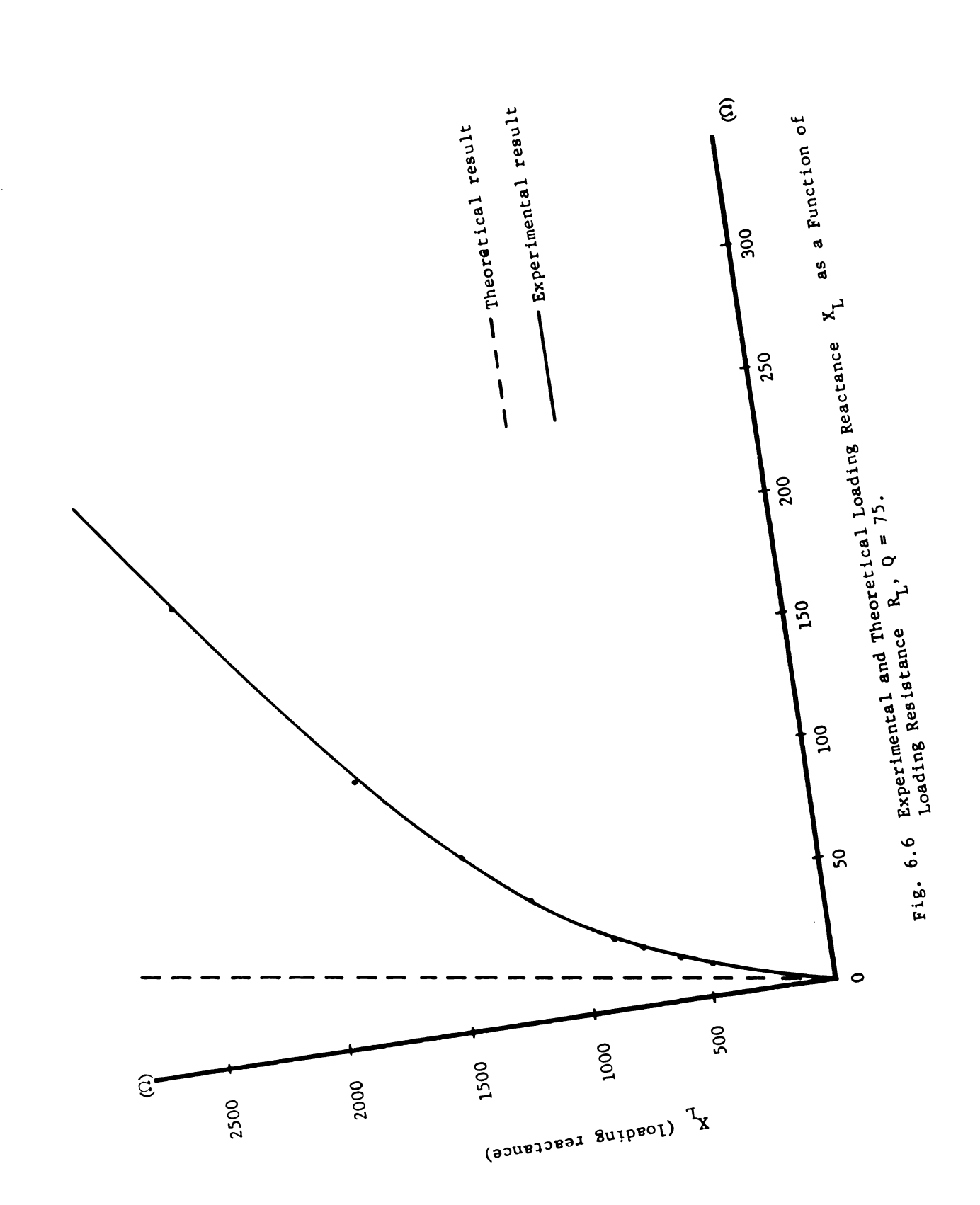
and Z is the characteristic impedance of coaxial line.

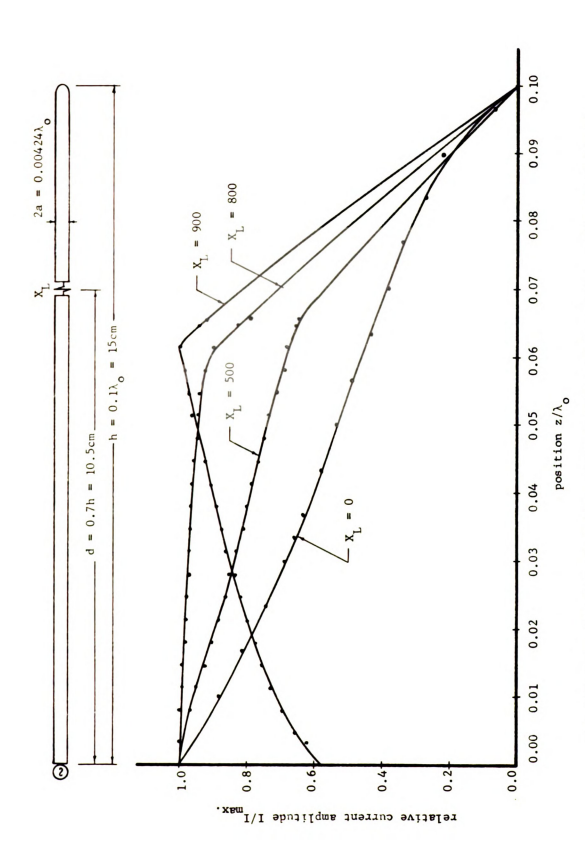
6.2 Doubly Loaded Short Antennas:

The experimental investigation of the current distribution and input impedance of an antenna both for enhanced radiation and improved directivity is presented in this section. An antenna, having the dimensions of a = 0.125 inch and h = 15 cm, is loaded with a reactance X_L of various values at d = 0.7h and excited at a frequency of 200 MHz. The loading impedance $Z_L = R_L + j X_L$, determined from eq. (6.1), is plotted in Fig. 6.6 in such a way that X_L is expressed as a function of R_L for the variance inductors L with the same Q = 75 at f = 200 MHz. The measured value is compared with the theoretical value. From here on, the reactive part of Z_L , X_L , will be used as the equivalent loading reactance in the following sections and R_L will be omitted in the expression of the loading impedance Z_L

6.2.1 Enhanced Radiation Case

In Sec. 3.3 of Chapter 3, it has been shown that the typical current distribution of an antenna with optimum loading reactance $\begin{bmatrix} X_L \end{bmatrix}_{op}$ at the position of z=d for enhanced radiation is a uniform distribution between the loading points which decreases to zero between the loading points and the extremities of the antenna. Under this condition, the input resistance is increased to two to three times that of an unloaded antenna and input reactance is tuned to zero. The experimental results for the antenna current distributions with various loading reactances of $X_L=0$, 500, 800 and 900 Ω , at d=0.7h, are plotted in Fig. 6.7. By examining these curves and





Experimental Antenna Current Distributions Corresponding to Enhanced Radiation Condition. Fig. 6.7

comparing with the theoretical results shown in Fig. 3.3, it is found that the experimental result for $X_T = 800 \Omega$ is correlated to that of the theoretical results for $X_{T} = 850 \Omega$. This gives a quite satisfactory agreement between theory and experiment. As the loading reactance is increased to 900 Ω , the current distribution becomes similar to the case discussed in Sec. 3.4. The experimental input impedance of the antenna, determined from eq. (6.2), is plotted in Fig. 6.8 as a function of X_{τ} , which is calculated from eq. (6.1). This experimental result is compared with the theoretical results of eq. (2.26) for an inductor with Q = 75 and $Q = \infty$. It is observed that the experimental results compare well with the theoretical results for the case of Q = 75. The higher experimental input resistance is mainly contributed by the loading resistance R_T present at the loading points (z = +d), since it is indicated in Fig. 6.6 that the loading resistance R_{τ} determined by eq. (6.1) has a value greater than that of the theoretical one. The higher input resistance is therefore expected.

6.2.2 Improved Directivity Case

In Sec. 4.4 of Chapter 4, it has been indicated that the typical current distribution along an antenna optimumly loaded for improved directivity has a phase reversal between the loading points $(z = \pm d)$ and the driving point (z = 0). At the point of phase reversal, the antenna current goes to zero. The total area under the current distribution along the antenna is, therefore, almost equal to zero. As a result, the input impedance has a small input resistance and a very large input reactance. By examining the experimental results of the current distributions shown in Fig. 6.9

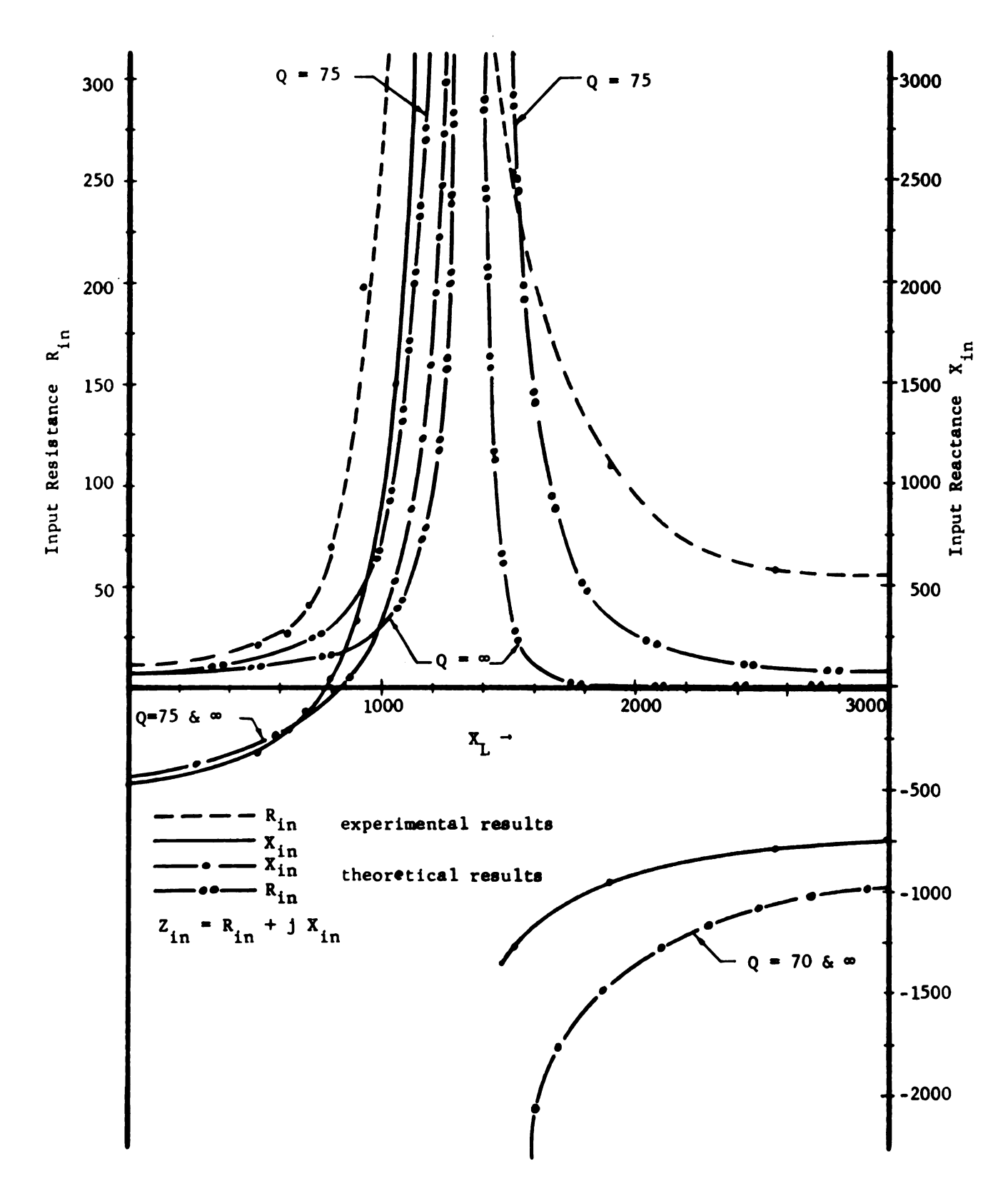
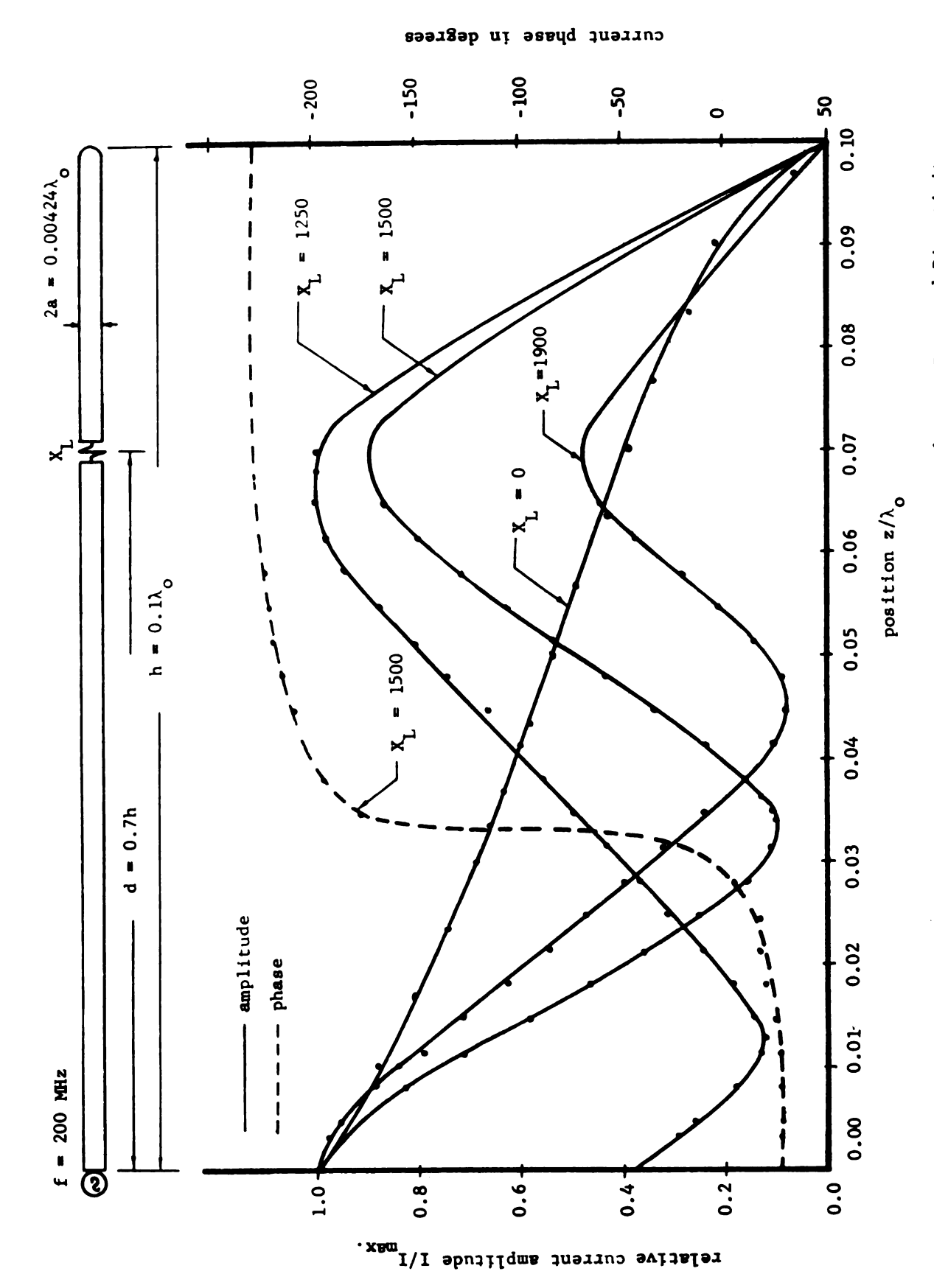


Fig. 6.8 Theoretical and Experimental Input Impedances of a Short Antenna as Functions of Loading Reactance X_L for the Cases of Q = 100 and Q = ∞ .



Experimental Antenna Current Distributions Corresponding to Improved Directivity Condition. Fig. 6.9

for $X_L = 0$, 1250, 1500 and 1900 Ω , it is observed that the optimum reactance X_L for high directivity is around 1900 Ω . This result is in agreement with the theoretical result shown in Fig. 4.9. In Fig. 6.8, it is shown that the input resistance for $X_L = 1900$ is 110 Ω while the theoretical value is 35 Ω . The deviation is mainly attributed to the difference in the experimental and theoretical values of the loading resistance as shown in Fig. 6.6.

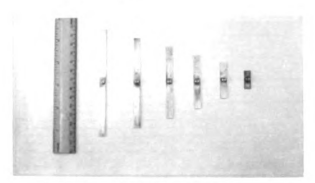
6.3 End-Loaded Short Antennas:

The current distributions and input impedances of an antenna loaded with various types of end loadings are experimentally investigated in this section. The end loadings include circular plates, rectangular bars, cylindrical bars, and helixes of various diameters and lengths. The antenna has the same dimensions and excitating frequency as that of the antenna used in the previous section (Sec. 6.2). The photographs of various end loadings are shown in Fig. 6.10.

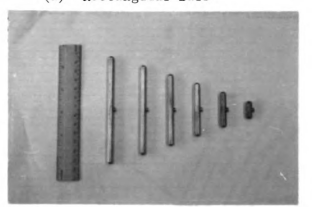
6.3.1 Current Distributions on the Antenna

The current distributions along the antenna with various types of end loadings are plotted in Fig. 6.11 through Fig. 6.15.

It is indicated in Figs. 6.11 and 6.12 that the current distributions on an antenna with rectangular and cylindrical bar loadings are almost the same as long as the lengths of bars are the same. It is also shown in Figs. 6.13 to 6.15 that the current distribution is a strong function of the diameters of circular plates and helixes used as end loadings. In Fig. 6.13, the current approaches a uniform distribution as the diameter of the circular plate is increased to



(a) Rectangular Bars



(b) Cylindrical Bars



(c) Circular Plates



(d) Helixes

Fig. 6.10 Various End Loadings.

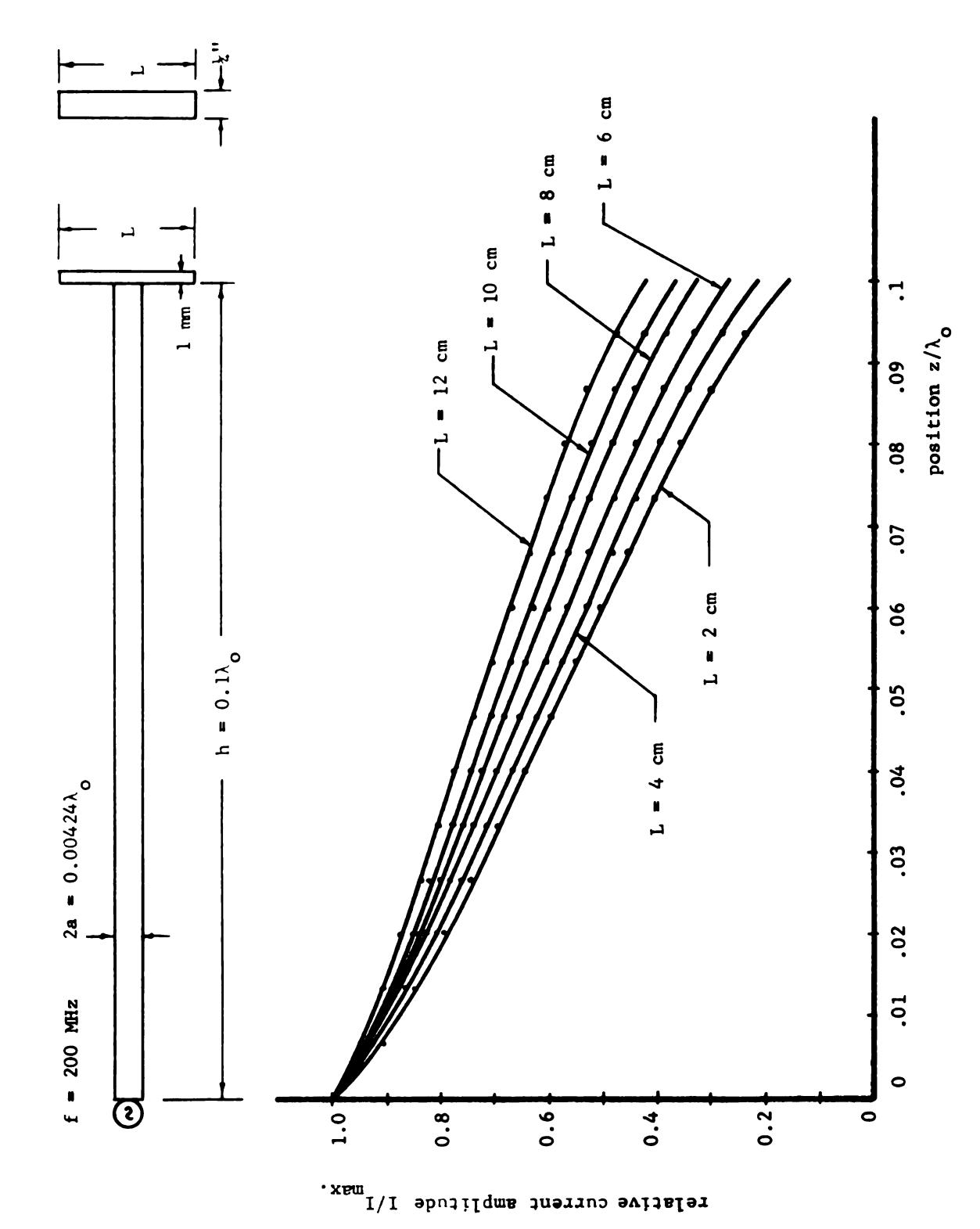
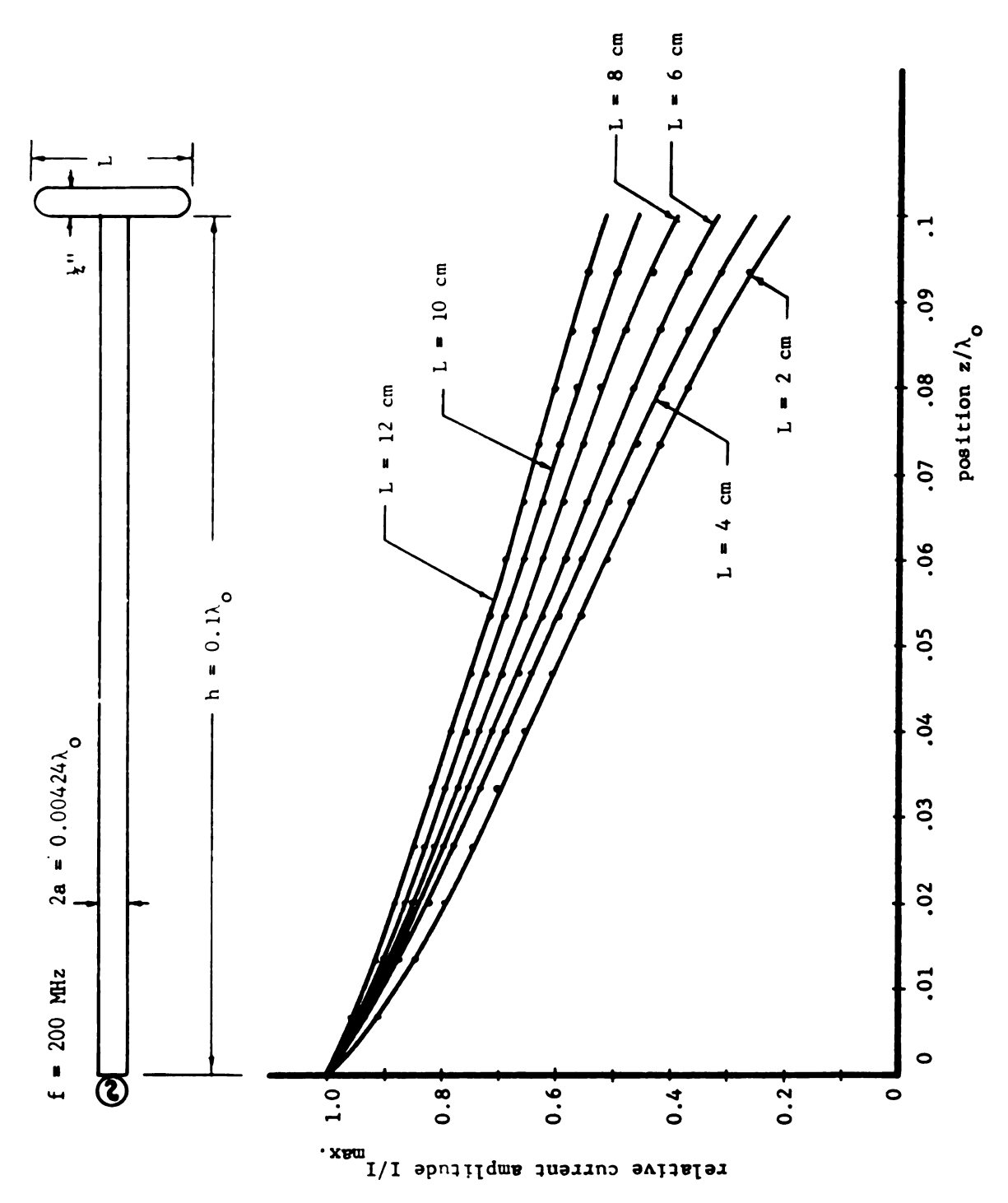
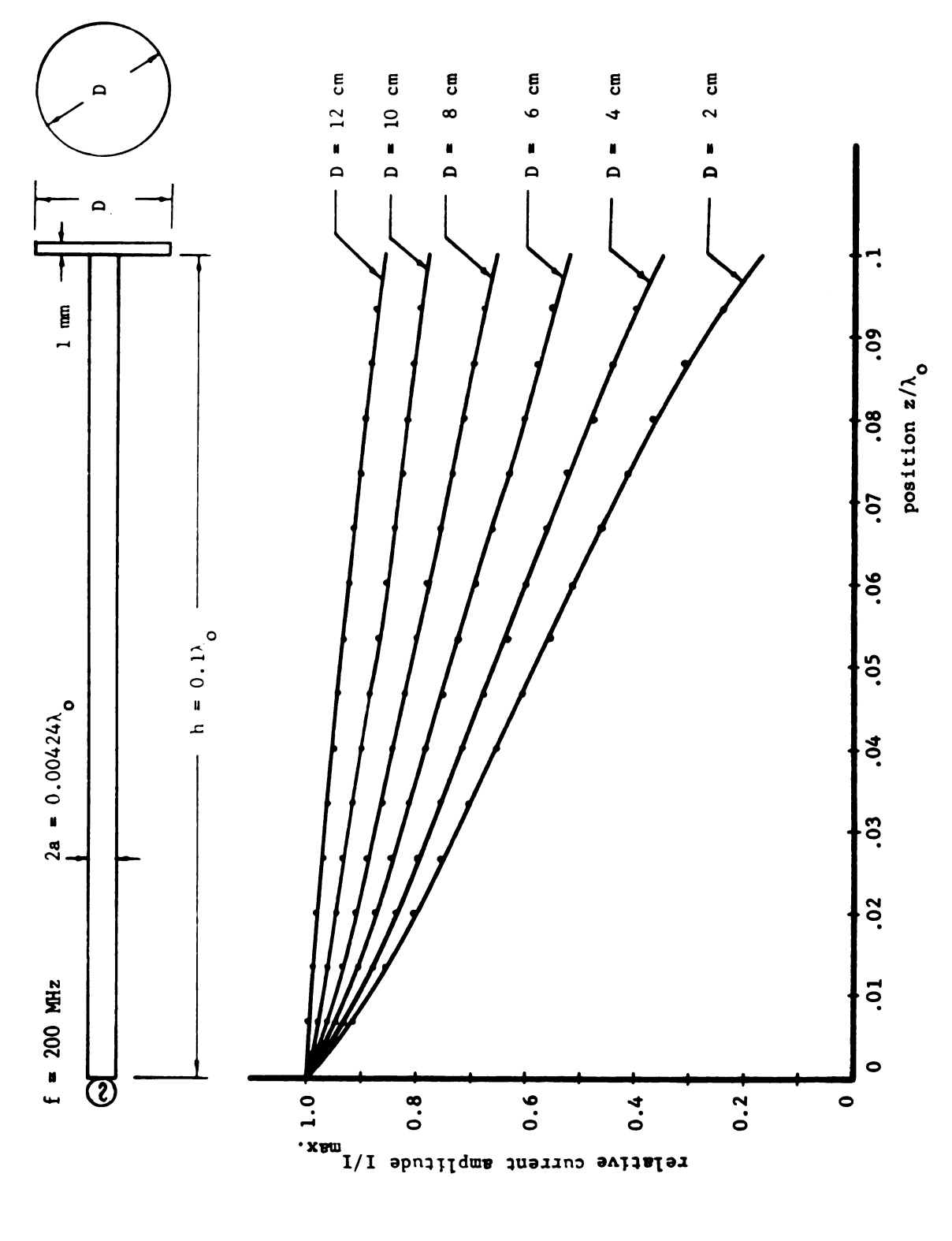


Fig. 6.11 Experimental Current Distributions on an Antenna End-Loaded with Rectangular Bars of Various Sizes (L x ξ " x 1 mm thich).



Experimental Current Distributions on an Antenna End-Loaded with Cylindrical Bars of Various Sizes $(D=\frac{1}{2}")$. Fig. 6.12



Experimental Current Distributions on an Antenna End-Loaded with Circular Plates of Various Diameters. Fig. 6.13

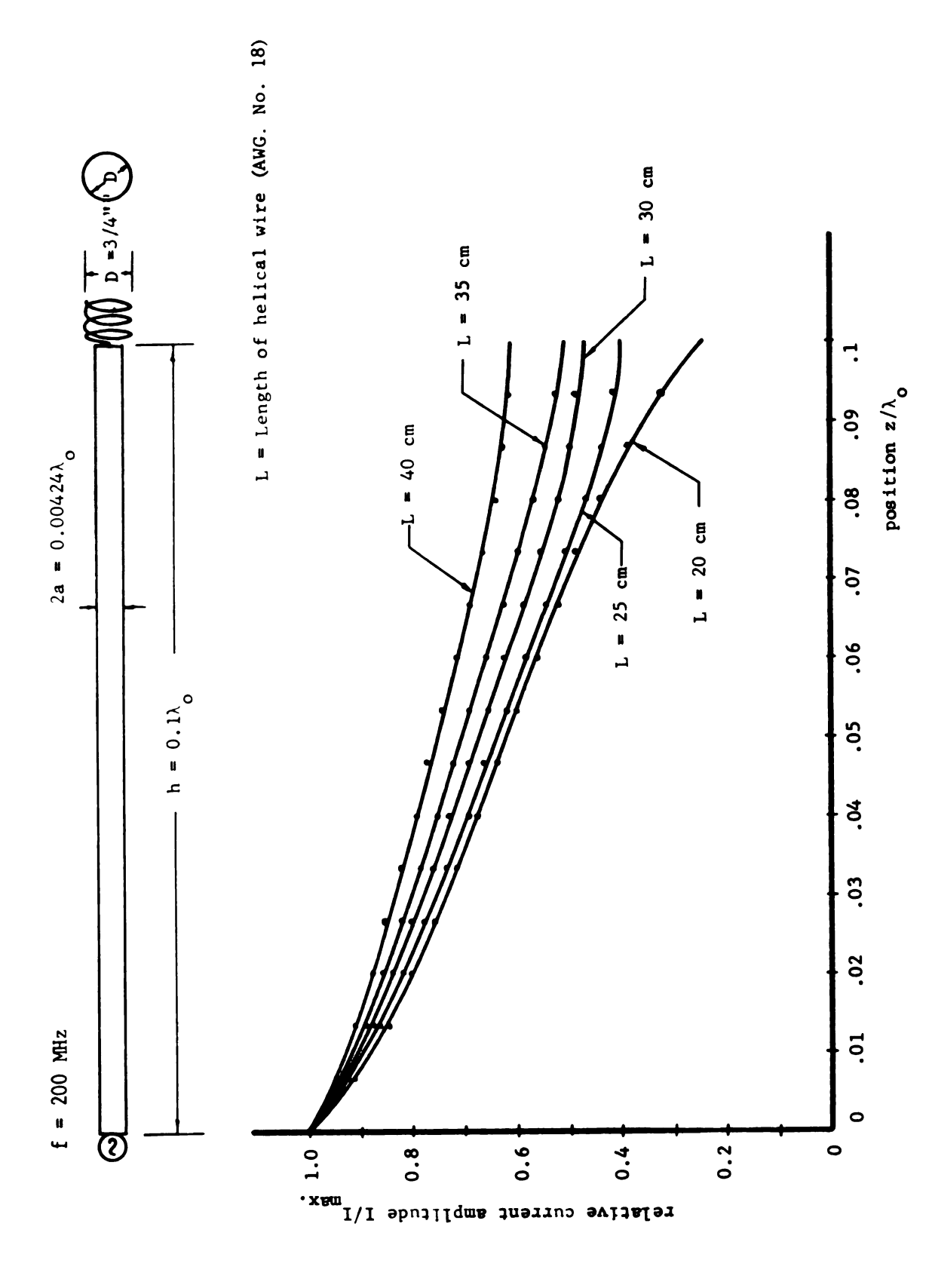


Fig. 6.14 Experimental Current Distributions on an Antenna End-Loaded with Helixes of Various Lengths (D = 3/4").

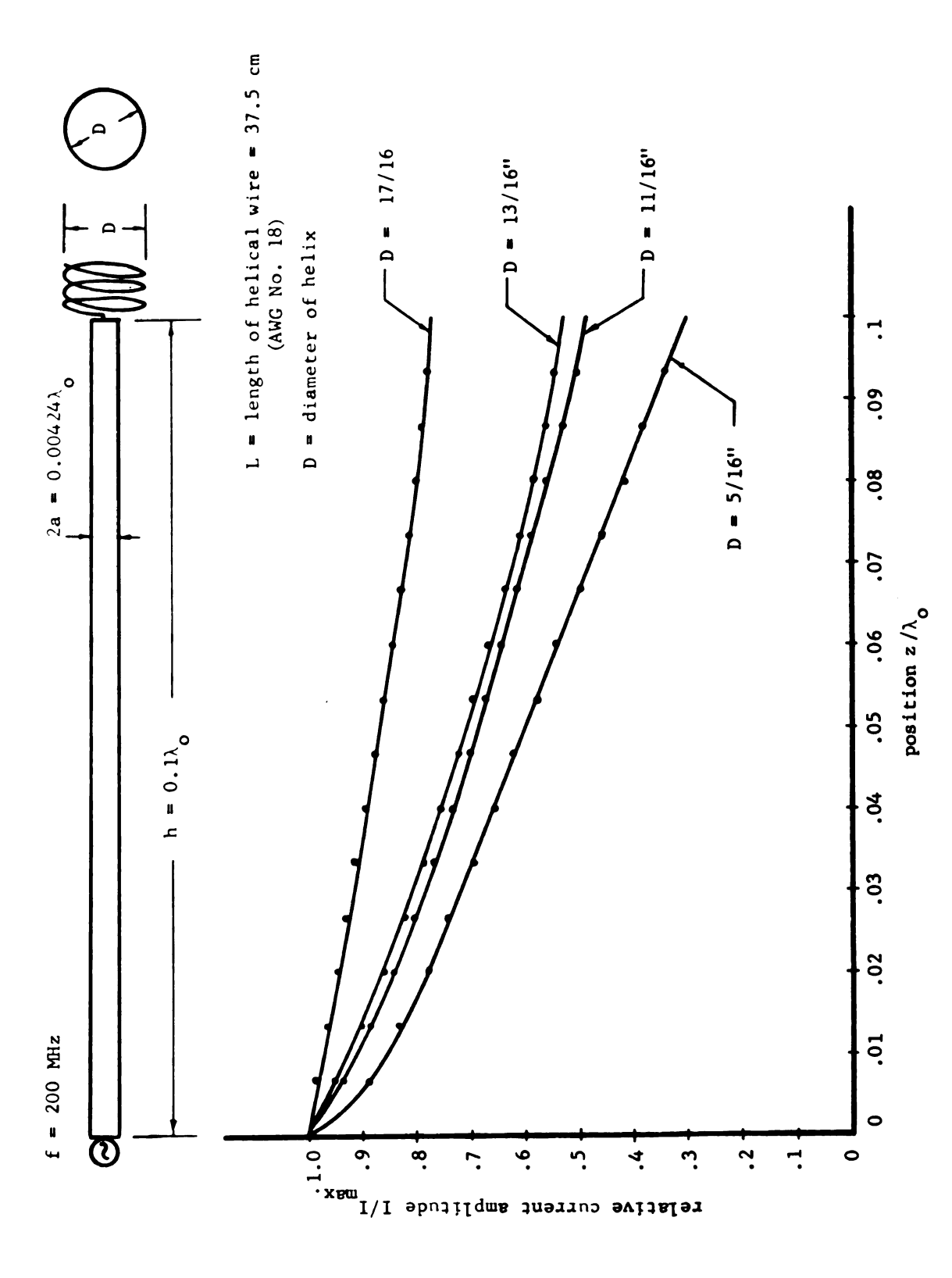


Fig. 6.15 Experimental Current Distributions on an Antenna End-Loaded with Helixes of Various Diameters (L = 37.5 cm).

12 cm. In Figs. 6.15 and 6.16, it is shown that when the helix diameter is approximately the same as that of the antenna, the current distribution resembles that of the unloaded antenna with an equivalent half length of $h' = h + h_1$, where h is the antenna length and h_1 is the height of the helix. As the diameter of the helix is increased to four or five times that of the antenna, the current distribution becomes nearly uniform along the antenna. In Chapter 3, it has been indicated that the power radiated by the antenna is approximately proportional to the square of the area under the current distribution on the antenna. Consequently, the circular plates and helixes are desirable end loadings for obtaining enhanced radiation.

6.3.2 Input Impedances

The measured input impedances of antennas with various types of end loadings are listed in Table 6.1 through Table 6.5. It is indicated that the input resistance is increased and the input reactance simultaneously decreased as the length of the bar or the diameters of the helix and the circular plate are increased.

By examining the current distributions and input impedances, it is concluded that by using the end-loading techniques, the power radiated by the antenna may be enhanced by a factor of one to four compared with that of an unloaded antenna if the dimensions of the end loadings are appropriately chosen. However, an end-loading is not capable of reducing the input reactance to zero and cannot increase the input resistance by a factor larger than four. It is clear that the technique of doubly loading as discussed in Chapters 2 to 4 can accomplish more than the end loading technique.

Table 6.1 Input Impedances of a Short Antenna End-Loaded with Rectangular Bars of Various Sizes (L(cm) x ½" x 1 mm. thick).

 $a = 0.00212\lambda_{o}$ $h = 0.1\lambda_0$, f = 200 MHz $z_{in} = R_{in} + j X_{in} (\Omega)$ Length of Xin Rectangular Bar 9.336 -424.818 2 cm 10.941 -373 4 cm 6 cm 11.92 -336.5 11.86 -315 8 cm 10 cm 12.328 -278 14.306 12 cm -247

Table 6.2 Input Impedances of a Short Antenna End-Loaded with Cylindrical Bars of Various Sizes (2" in diameter).

 $a = 0.00212\lambda_{o}$ $h = 0.1\lambda_0$, f = 200 MHz $Z_{in} = R_{in} + j X_{in}$ (Ω) Length of x_{in} Cylindrical Bar 10.018 -408.352 2 cm 4 cm 11.09 -356.542 12.914 -318.338 6 cm -286.43 8 cm 13.42 10 cm 14.024 -254.2 15.32 -223 12 cm

Table 6.3 Input Impedances of a Short Antenna End-Loaded with Circular Plates (1 mm thick) of various diameters.

Diameter of	Z = R + j X in	
Circular Plate (cm)	R in	X _{in}
2 cm	6.172	-403.254
4 cm	10.11	-301.9
6 cm	12.552	-221.778
8 cm	14.538	-148.66
10 cm	13.076	- 88.634
12 cm	14.57	- 36.18

Table 6.4 Input Impedances of a Short Antenna End-Loaded with Helixes of Various Lengths (D = 3/4").

Length of	Z = R + j X in in in	
Helical Wire (cm)	R _{in}	X _{in}
25 cm	9.06	-348.4
30 cm	14.24	-318.34
35 cm	14.56	-292.2
40 cm	15.66	-246.92

Table 6.5 Input Impedances of a Short Antenna End-Loaded with Helixes of Various Diameters (L = 37.5 cm).

Diameter of	$z_{in} = R_{in} + j X_{in}$	
Helical (inch)	R _{in}	X _{in}
5/16 inch	4.756	-356.7
11/16 inch	13.473	-249.4
13/16 inch	14.870	-244.696
1 1/16 inch	22.848	-135.61

6.4 Short Antenna with Double Impedance and End Loadings:

A short antenna which is doubly loaded and also end-loaded by various loadings is discussed in this section. Since it is difficult to measure the current distribution between the loading point z = d and the end point z = h, only the current distribution between z = 0 and z = d is measured in this experiment. The current distribution between $d \le z \le h$ is assumed to take that same form as that on the antennas of the previous section.

6 4.1 Current Distribution

The current distributions of doubly loaded antennas having various types of end loadings at z=h and various loading reactances X_L at d=0.7h are plotted in Fig. 6.16 through Fig. 6.23. These figures indicate that the loaded antenna can have typical current distributions appropriate to improved directivity (see Fig. 4.7) or enhanced radiation (see Figs. 3.1 and 3.9) if the appropriate corresponding loading reactances X_L are mounted at z=d along with various end loadings at z=h. It is also indicated that the current distribution is mainly controlled by the loading reactance X_L .

6 4 2 Input Impedances

The input impedances of antennas with various loading implementations are listed in each figure for various loading reactances \mathbf{X}_{L} .

6.5 Doubly Loaded Coupled Antennas:

The experimental results for the current distributions and input impedances of coupled antennas doubly loaded by various reactances

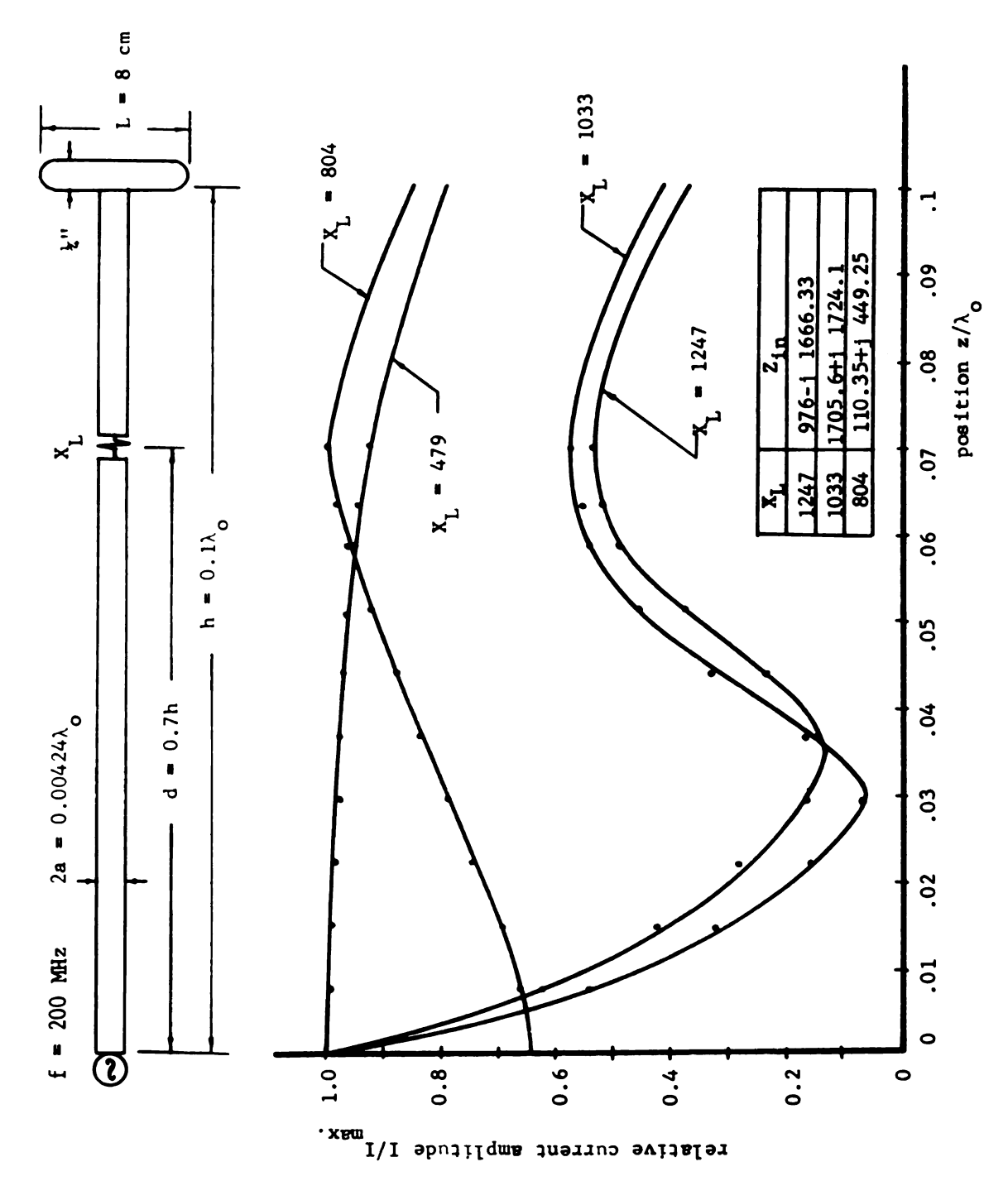
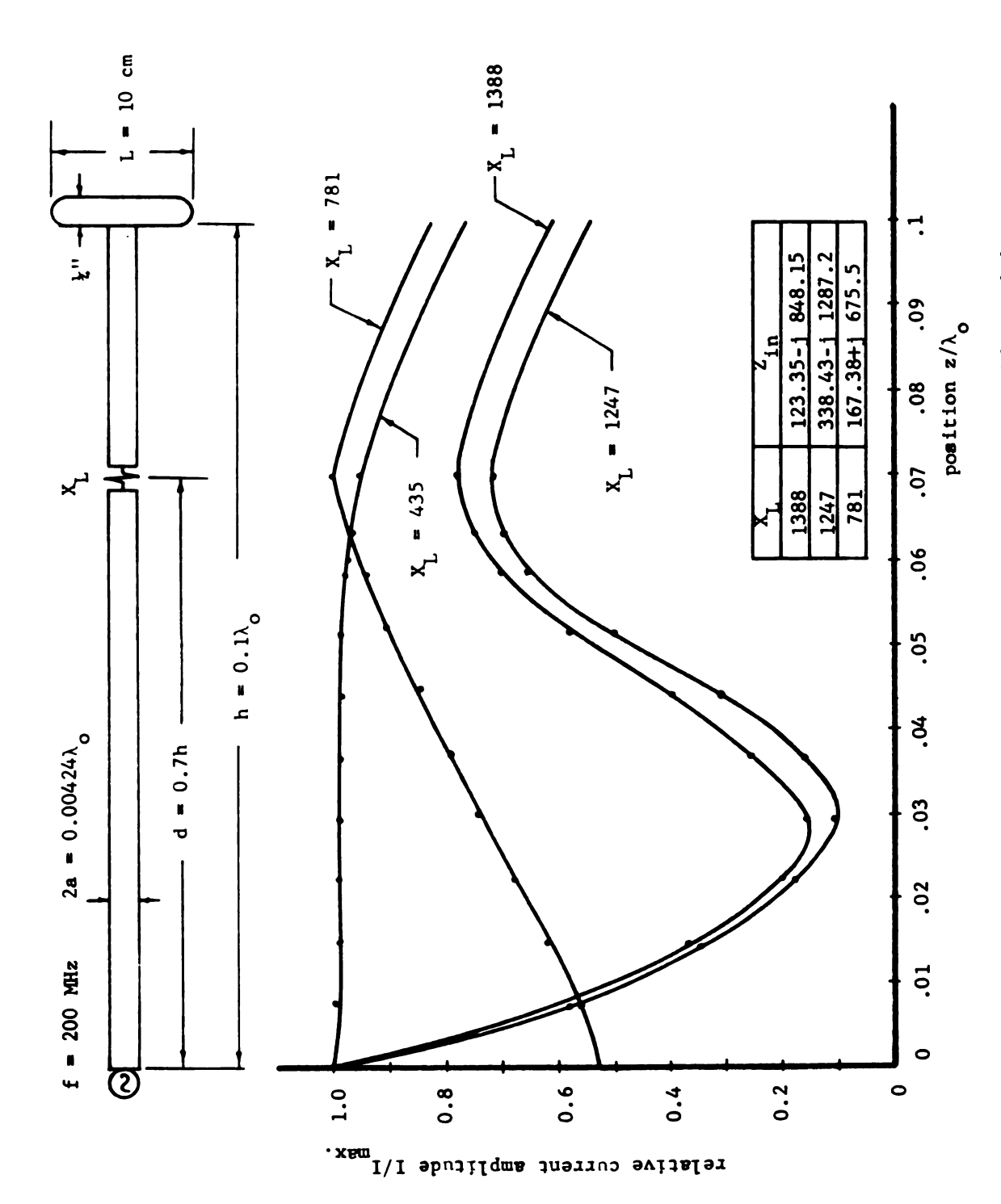


Fig. 6.16 Experimental Current Distribution on a Doubly Loaded Antenna End-Loaded by a Cylindrical Bar of 8 cm.



Experimental Current Distributions on a Doubly Loaded Antenna End-Loaded by a Cylindrical Bar of 10 cm. Fig. 6.17

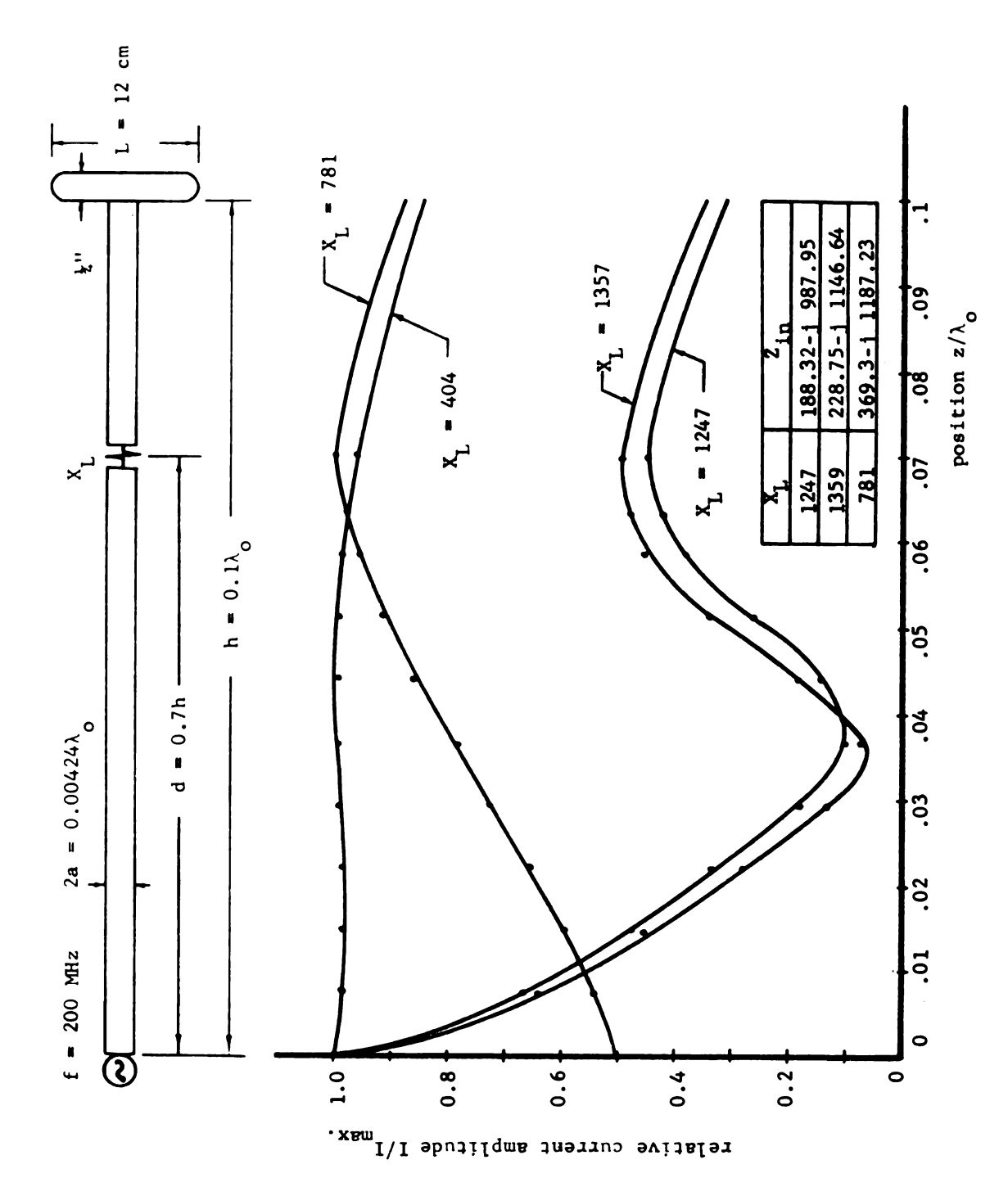


Fig. 6.18 Experimental Current Distributions on a Doubly Loaded Antenna End-Loaded by a Cylindrical Bar of 12 cm.

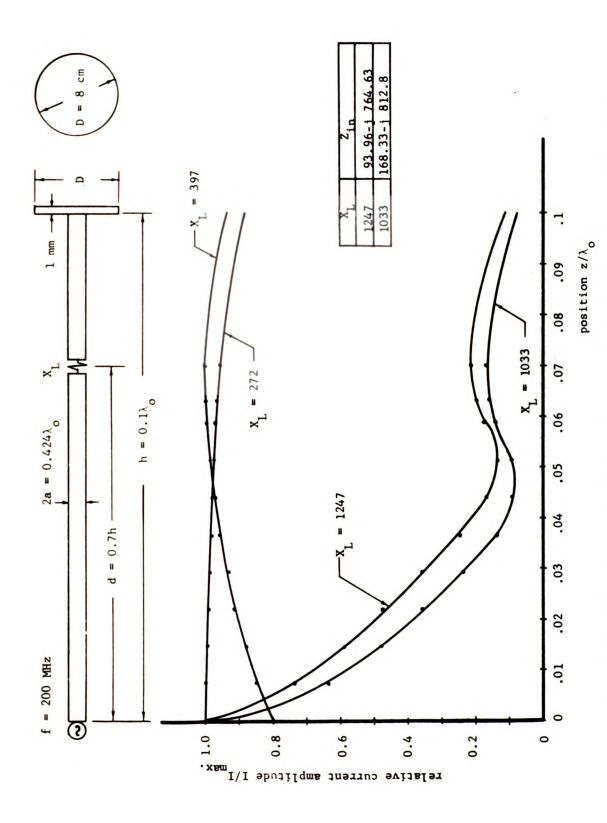


Fig. 6.19 Experimental Current Distributions on a Doubly Loaded Antenna End-Loaded by a Circular Plate of 8 cm diameter.

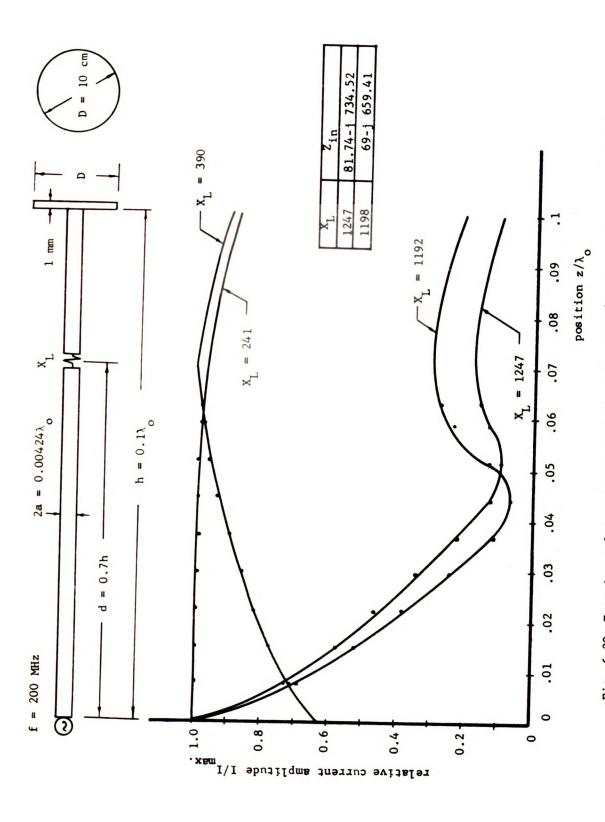
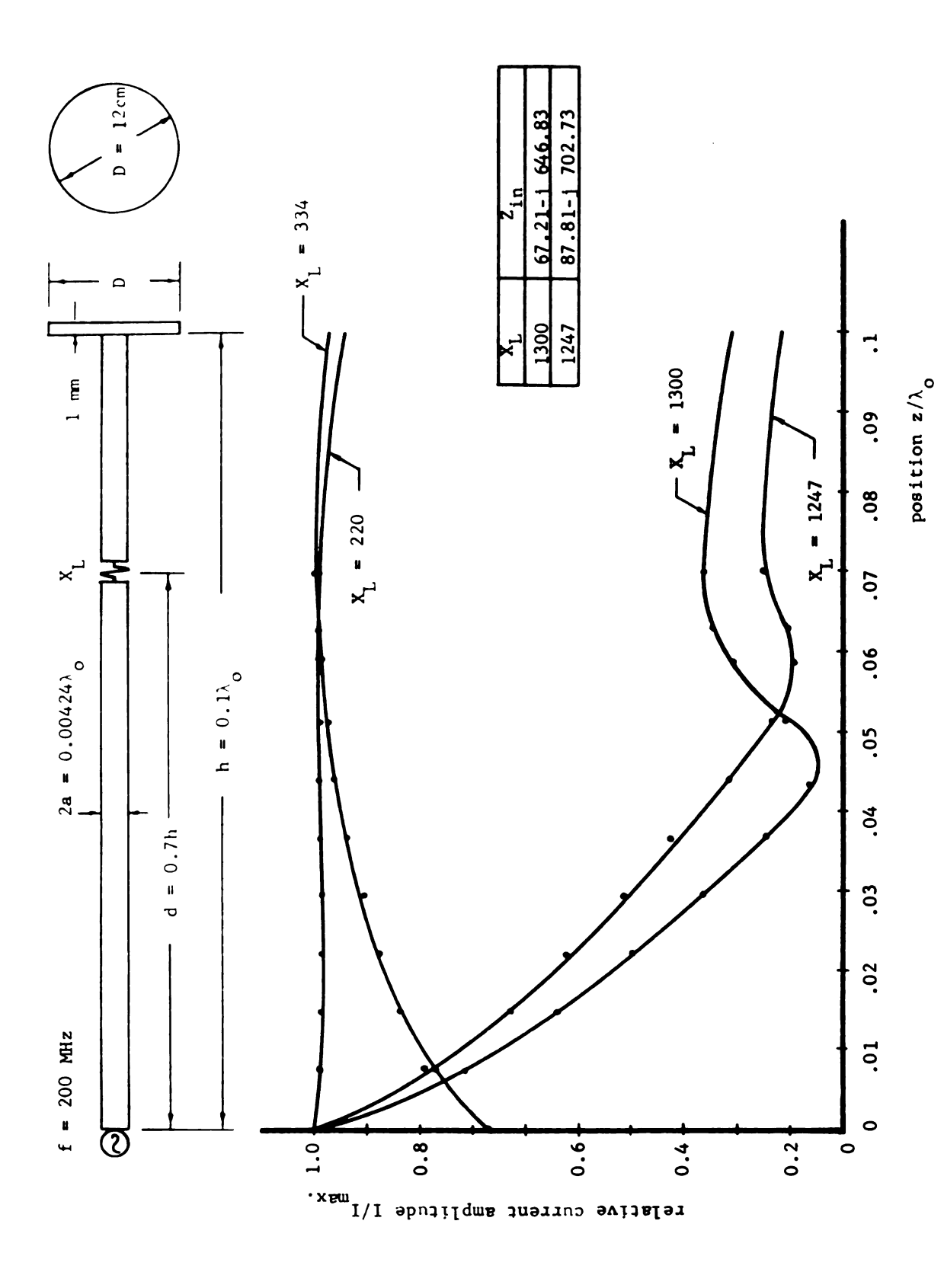
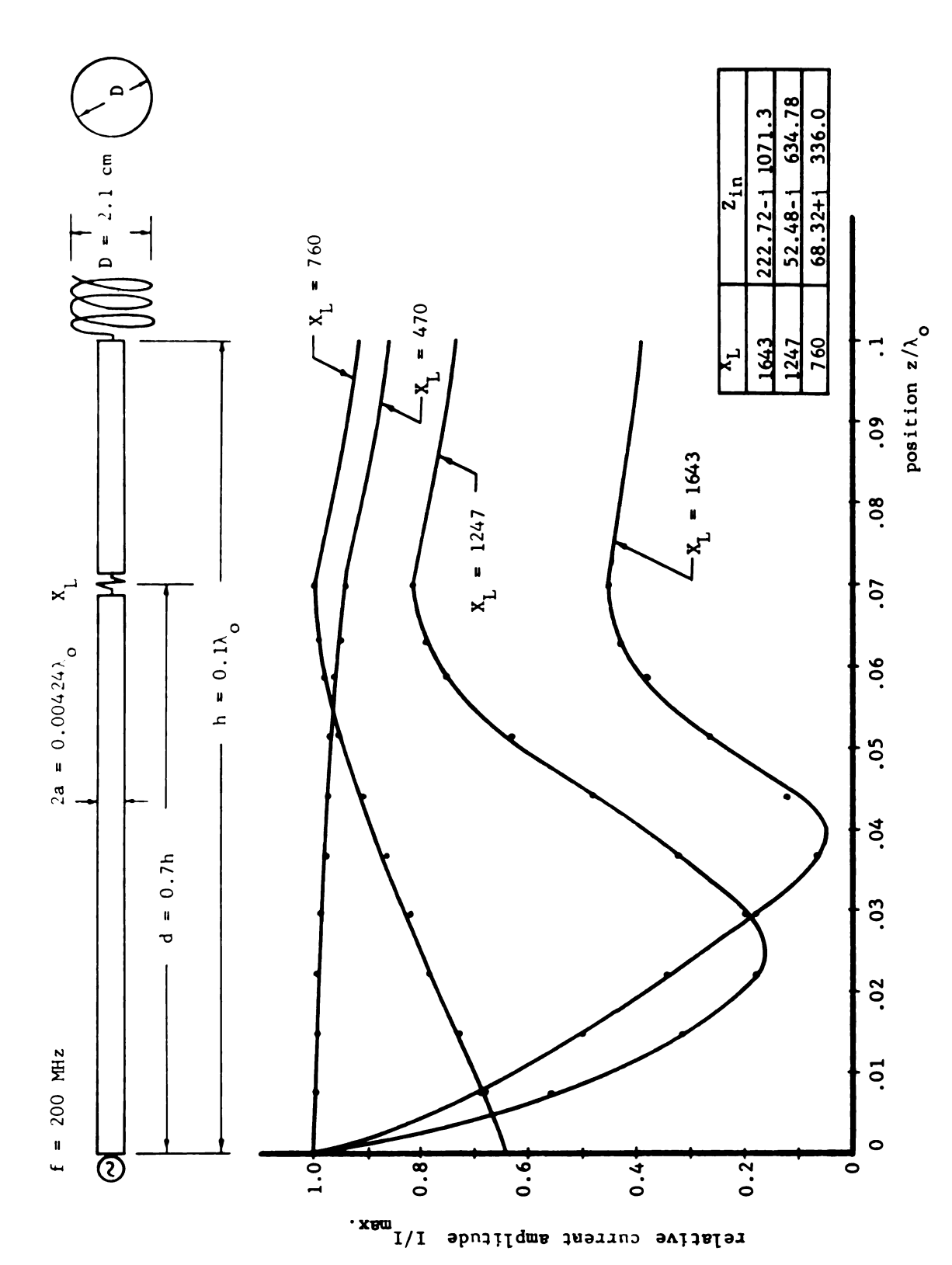


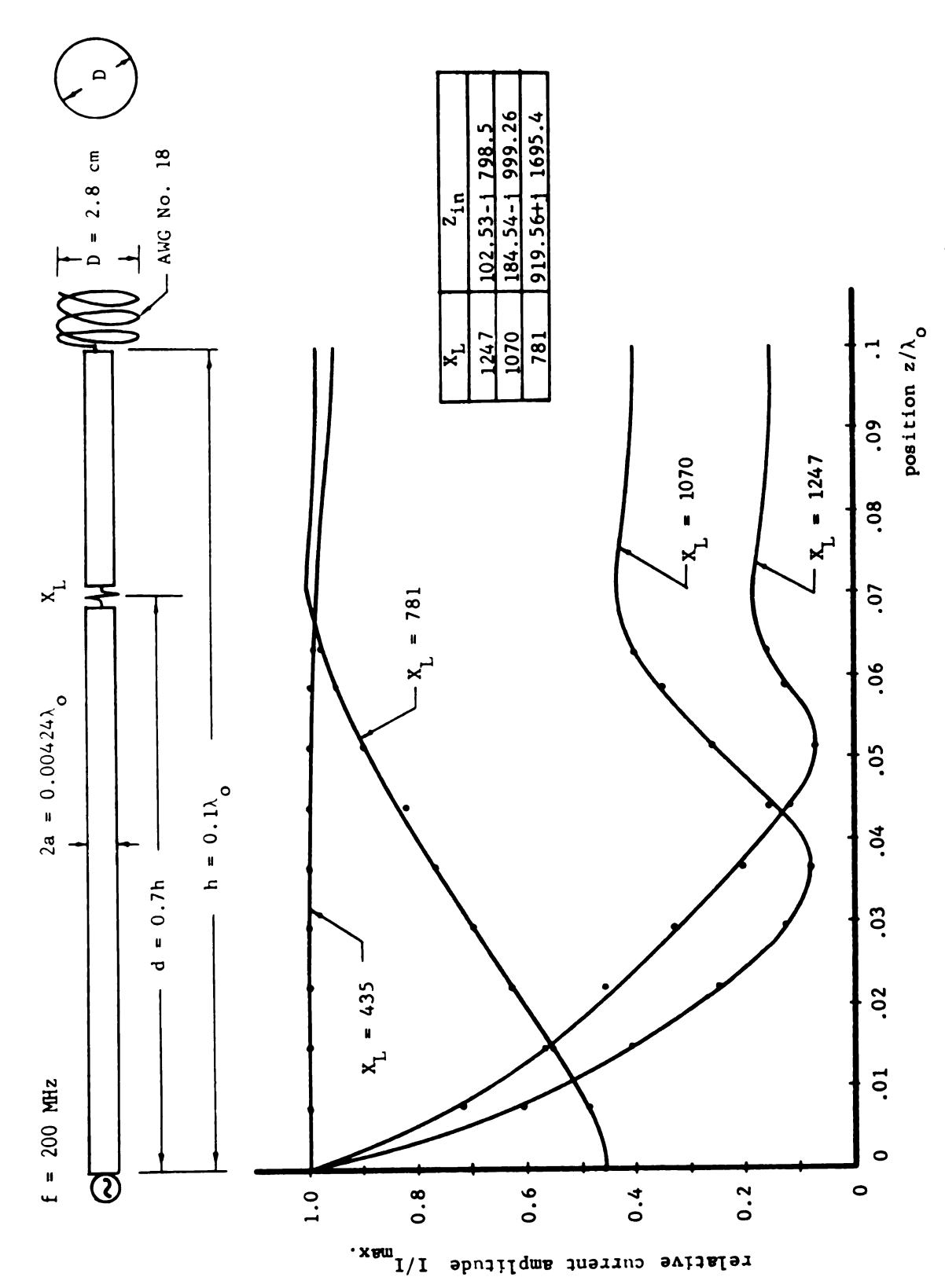
Fig. 6.20 Experimental Current Distributions on a Double Loaded Antenna End-Loaded by a Circular Plate of 10 cm diameter.



Experimental Current Distributions on a Doubly Loaded Antenna End-Loaded by a Circular Plate of 12 cm diameter. Fig. 6.21



Experimental Current Distribution on a Doubly Loaded Antenna End-Loaded by a Helix of 2.1 cm diameter. Fig. 6.22



Experimental Current Distributions on a Doubly Loaded Antenna End Loaded by a Helix of 2.8 cm diameter. Fig. 6.23

 ${\rm X_L}$ are shown in Fig. 6.24. By investigating these curves, it is observed that the coupled antennas doubly loaded with ${\rm X_{L1}}$ = 980 Ω on the driven antenna and ${\rm X_{L2}}$ = 1040 on the parasitic element have uniform current distributions between $0 \le z \le d$ on both antennas. The input resistance is greatly increased and the input reactance is decreased to a value much smaller than that of unloaded coupled antennas. These physical phenomenon observed are in good agreement with the theoretical prediction for enhanced radiation. This is evidenced by comparing Fig. 6.24 with Fig. 5.6 which shows graphically the corresponding theoretical results developed in Chapter 5.

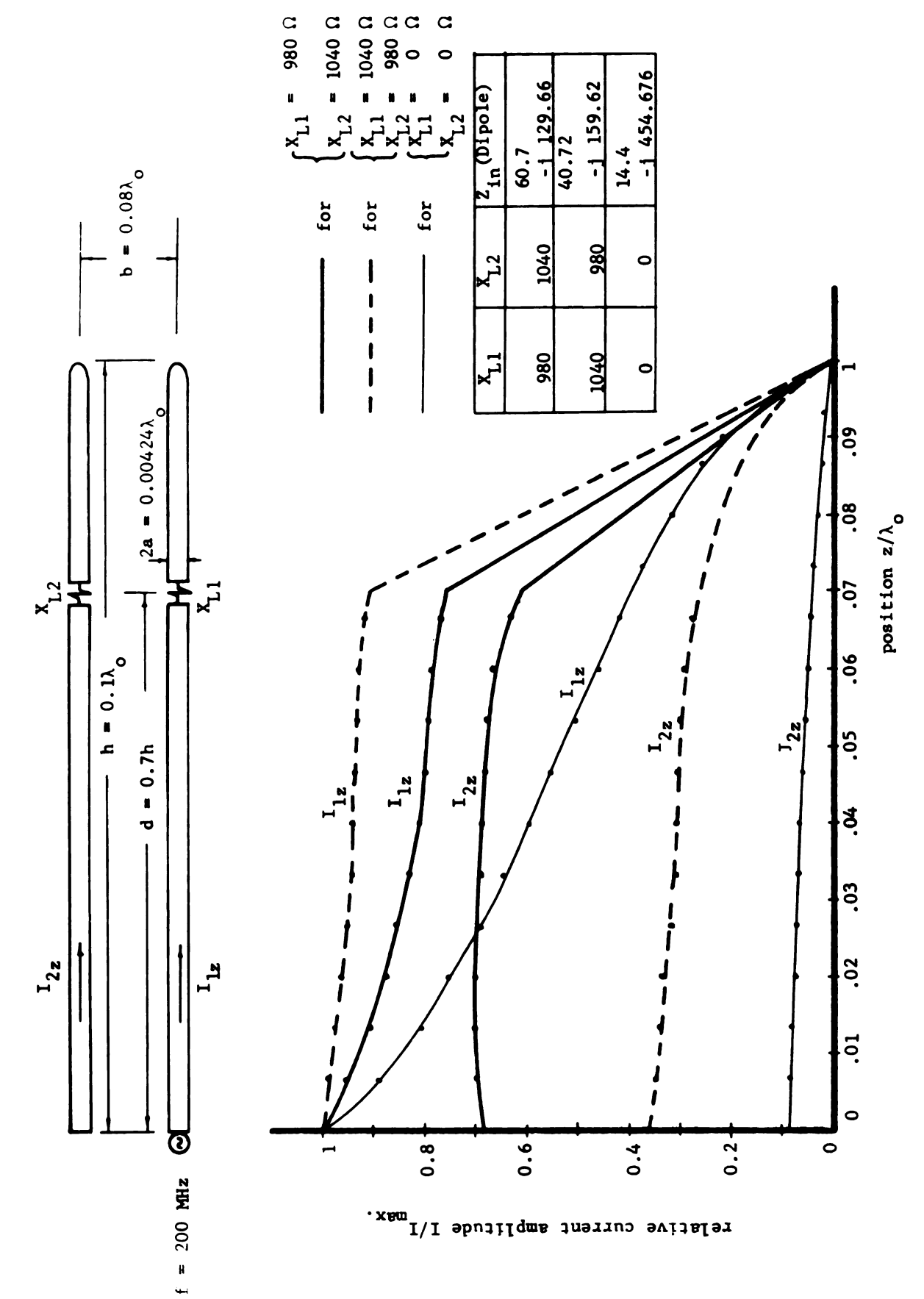


Fig. 6.24 Experimental Current Distributions on Doubly Loaded Coupled Antennas.

REFERENCES

- [1] C.W. Harrison, "Monopole with Inductance Loading," IEEE Trans. on Antennas and Propagation, AP-11, pp. 394-400, July 1961.
- [2] L. La Paz, and G.A. Miller, "Optimum Current Distributions on Vertical Antennas," Proc. IRE, 31, pp. 214-232, May 1943.
- [3] C.J. Bouwkamp, and D.N.G. De Bruijin, "The Problem of Optimum Antenna Current Distribution," Philips Research Reports, 1, pp. 135-158, 1945
- [4] H.J. Riblet, "Note on the Maximum Directivity of an Antenna," Proc. IRE, pp. 620-623, May 1948.
- [5] R.W.P. King, <u>The Theory of Linear Antennas</u>, Cambridge, Massachusetts: Harvard University Press, 1956.
- [6] R.W.P. King, and T.T. Wu, "Currents, Charges, and Near Fields of Cylindrical Antennas," Radio Science Journal of Research NBS/USNC-URSI, 69D, No. 3, pp. 429-446, March 1965.
- [7] R.W.P. King, <u>Fundamental</u> <u>Electromagnetic</u> <u>Theory</u>, Second Edition, Dover, New York, 1963.
- [8] E. Hallen, "Theoretical Investigations into the Transmitting and Receiving Qualities of Antennae," Nova Acta Rogiae Soc. Sci. Upsaliensis, 4, No. 2, pp. 1-44, 1938.
- [9] L.J. Chu, Physical Limitations of Omi-Directional Antennas," J. Appl. Phys., 19, pp. 1163-1175, December 1948.
- [10] R.W.P. King, and S.S. Sandler, "The Theory of Broadside Arrays," IEEE Trans. on Antennas and Propagation, AP-12, pp. 269-275, May 1964.